DISSERTATIONES
CHIMICAE
UNIVERSITATIS
TARTUENSIS
222

TÕNIS LAASFELD

Integrating Image Analysis and Quantitative Modeling for a Holistic View of GPCR Ligand Binding Dynamics

DISSERTATIONES CHIMICAE UNIVERSITATIS TARTUENSIS
222

DISSERTATIONES CHIMICAE UNIVERSITATIS TARTUENSIS
222

TÕNIS LAASFELD

Integrating Image Analysis and Quantitative Modeling for a Holistic View of GPCR Ligand Binding Dynamics

UNIVERSITY OF TARTU
Press
1632

Institute of Chemistry, Faculty of Science and Technology, University of Tartu, Estonia

The dissertation is accepted for the commencement of the degree of *Doctor Philosophiae* in Chemistry on June 22, 2023 by the Council of Institute of Chemistry, Faculty of Science and Technology, University of Tartu.

Supervisors: Professor Ago Rinken
Institute of Chemistry, University of Tartu, Estonia

Professor Leopold Parts
Institute of Computer science, University of Tartu, Estonia

Opponent: Professor Martin Lohse
ISAR Bioscience Institute, Germany

Commencement: 29.08.2023, at 14.15. Auditorium 1020, Ravila 14a, Tartu

The thesis at hand was financed by the Estonian Ministry of Education and Science (IUT20-17 and PSG230), the University of Tartu ASTRA Project PER ASPERA, NATO (SPS 985261), the European Union through the European Regional Development Fund (EU48695), the Enterprise Estonia Applied research programme 2021 and Ustus Agur stipend by Republic of Estonia Education and Youth Board and Estonian Association of Information Technology and Telecommunications. Furthermore, a large part of this work was made possible by the COST actions CM1207 GLISTEN, CA15124 NEUBIAS and CA18133 ERNEST.

This work has been supported by the Graduate School of Functional materials and technologies, receiving funding from the European Regional Development Fund in the University of Tartu, Estonia

ISSN 1406-0299 (print)
ISBN 978-9916-27-292-3 (print)
ISSN 2806-2159 (pdf)
ISBN 978-9916-27-293-0 (pdf)

University of Tartu Press
www.tyk.ee

CONTENTS

LIST OF ORIGINAL PUBLICATIONS

The thesis is based on seven original publications, referred to in the text by corresponding Roman numerals:

I. **Laasfeld, T**., Kopanchuk, S. and Rinken, A., 2017. Image-based cell-size estimation for baculovirus quantification. *Biotechniques*, *63*(4), pp.161–168.

II. Allikalt, A., **Laasfeld, T**., Ilisson, M., Kopanchuk, S. and Rinken, A., 2021. Quantitative analysis of fluorescent ligand binding to dopamine D3 receptors using live-cell microscopy. *The FEBS Journal*, *288*(5), pp. 1514–1532.

III. **Laasfeld, T**., Ehrminger, R., Tahk, M.J., Veiksina, S., Kolvart, K.R., Min, M., Kopanchuk, S. and Rinken, A., 2021. Budded baculoviruses as a receptor display system to quantify ligand binding with TIRF microscopy. *Nanoscale*, *13*(4), pp.2436–2447.

IV. Tahk, M.J., **Laasfeld, T.**, Meriste, E., Brea, J., Loza, M.I., Majellaro, M., Contino, M., Sotelo, E. and Rinken, A., 2023. Fluorescence based HTS-compatible ligand binding assays for dopamine D3 receptors in baculovirus preparations and live cells. *Frontiers in Molecular Biosciences*, *10*:, 1119157.

V. Grätz, L., **Laasfeld, T.**, Allikalt, A., Gruber, C.G., Pegoli, A., Tahk, M.J., Tsernant, M.L., Keller, M. and Rinken, A., 2021. BRET-and fluorescence anisotropy-based assays for real-time monitoring of ligand binding to M2 muscarinic acetylcholine receptors. *Biochimica et Biophysica Acta (BBA)-Molecular Cell Research*, *1868*(3): 118930.

VI. Tahk, M.J., Torp, J., Ali, M.A., Fishman, D., Parts, L., Grätz, L., Müller, C., Keller, M., Veiksina, S., **Laasfeld, T**. and Rinken, A., 2022. Live-cell microscopy or fluorescence anisotropy with budded baculoviruses—which way to go with measuring ligand binding to M4 muscarinic receptors?. *Open Biology*, *12*(6): 220019.

VII. Ali, M.A., Hollo, K., **Laasfeld, T**., Torp, J., Tahk, M.J., Rinken, A., Palo, K., Parts, L. and Fishman, D., 2022. ArtSeg—Artifact segmentation and removal in brightfield cell microscopy images without manual pixel-level annotations. *Scientific Reports*, *12*(1): 11404.

Author's contribution:

I. The author performed all the experiments, developed the software and wrote the manuscript.

II. The author developed the algorithms and software, wrote the manuscript and assisted with the experimental design.

III. The author designed the experiments, performed experiments, developed the software, analyzed the data and wrote the manuscript.

IV. The author developed the machine learning models, developed the experimental design and wrote the manuscript.

V. The author performed some of the experimental work and data analysis related to fluorescence anisotropy method, performed all global modeling and wrote parts of the manuscript.

VI. The author developed the data collection strategy and training of all the machine learning models, supervised the experimental work and wrote parts of the manuscript.

VII. The author prepared the M_4 receptor dataset, devised and carried out the machine learning model evaluation strategy and wrote parts of the manuscript.

ABBREVIATIONS

BBV	budded baculovirus
BRET	bioluminescence resonance energy transfer
cAMP	Cyclic adenosine monophosphate
CNN	convolutional neural network
DL	deep learning
D_3R	dopamine receptor D_3
FA	fluorescence anisotropy
FOV	field of view
FRET	Förster resonance energy transfer
GPCR	G protein-coupled receptor
GRK	G protein receptor kinase
GUI	graphical user interface
HEK293	human embryonic kidney 293 cells
HTS	high throughput screening
ICSE	Image-based Cell Size Estimation
IC_{50}	half maximal inhibitory concentration
K_d	dissociation equilibrium constant
K_i	inhibition equilibrium constant
k_{off}	dissociation rate constant
k_{on}	association rate constant
MIDAS	Minimum Information for Data Analysis in Systems Biology
ML	machine learning
MOI	multiplicity of infection
$M_{1,2,4}R$	muscarinic acetylcholine receptors M_1, M_2 and M_4
NAPS	N-(p-aminophenethyl)spiperone
NMS	N-methyl scopolamine
NPY	neuropeptide Y
ODE	ordinary differential equation
px	pixel
SB	systems biology
SD	standard deviation
Sf9	*Spodoptera frugiperda* clonal isolate 9 cell line
TIRF	total internal reflection fluorescence
TFI	total fluorescence intensity

INTRODUCTION

Humanity's understanding of biology has radically changed over time through scientific and technological progress, but it has developed hand-in-hand with medical sciences. Modern understanding of biology and pharmacology broadly acknowledges that life is a complex dynamic system which has led to widespread incorporation and employment of mathematical sciences such as systems theory, computer science and artificial intelligence in biology and given rise to new fields such as computational biology, systems biology, systems pharmacology, bio- and chemoinformatics and bioimage analysis among others. In turn, mathematical sciences have borrowed many concepts from biology and natural sciences, an idea known as biomimetics. This has led to the development of global optimization algorithms such as the genetic algorithms and simulated annealing and inspiring the development of neural networks and deep learning. This shows an exciting and continued interplay and codevelopment of biological and mathematical sciences. In practice, such progress is heavily mediated by various kinds and large volumes of data and software as well as interdisciplinary collaboration helping to turn the data into information and knowledge.

This thesis focuses on applying this kind of interdisciplinary approach more narrowly to develop new tools including assays, software, systems biology and machine learning models to study the signaling processes of a class of proteins called G protein-coupled receptors (GPCRs). GPCRs are an extremely important class of receptors for fundamental biology, being involved in a large portion of all physiological signaling processes. Furthermore, GPCRs constitute the most drug-targeted class of all proteins meaning that fundamental discoveries often have a direct impact on drug development. In biochemical context, the term ligand is used instead of a drug to describe molecules that can bind to a specific receptor. Ligand binding can be viewed as the first and one of the most important steps in receptor signalling. As the number of different GPCRs is substantial with roughly 800 members represented in the human genome, the thesis concentrates on just a few of these, which serve as models for the more general approach of ligand binding assay development. The developed ligand binding assays cover both spectroscopic and microscopy based methods.

For the development of imaging based live-cell GPCR ligand binding assays, deep convolutional neural networks are employed. As many excellent neural network architectures already exist, special emphasis is put on the influence of machine learning models and their quality on the assay quality. As the imaging assays rely heavily on large volumes of raw data and accurate metadata, and requires employing the concepts of data standardization and organization, this thesis presents Aparecium software for handling these tasks. Finally, the systems biology approach and global fitting are used to develop mechanistic kinetic models of receptor-ligand binding based on the data acquired from the

developed assays as well as the influence of assay properties on the model discovery itself.

As pharmacology develops and transitions from drug discovery to drug design, mechanistic information about drug action becomes more critical for this design process. Any tools and theories, whether biochemical, chemical or computational which help with the drug design process are, therefore, crucial to address and overcome global health challenges. This thesis shows that the developed tools can provide deeper insight and better standardization of several critical processes of drug design.

1. LITERATURE OVERVIEW

1.1. G protein-coupled receptors and their signalling systems – function, evolution and importance

G protein-coupled receptors (GPCRs) form a large category of cell surface receptors. The generally accepted common feature of all GPCRs is their ability to couple to one or more types of G proteins. Such a definition is far from comprehensive as GPCRs are known to also extensively interact with other proteins such as β-arrestins and regulated by G protein-coupled receptor kinases (GRKs). To account for these interactions, there have been attempts to define GPCRs by their common tertiary structure instead leading to the alternative name of seven-transmembrane domain (7TMs) receptors and heptahelical receptors among others. Such a common structural feature among a large class of receptors is evidence of their early emergence during evolution indicating their importance for the development of complex life forms (de Mendoza et al., 2014) while simultaneously retaining extreme flexibility of the GPCR function within constrained structure. The flexibility allows GPCRs to achieve signaling specificity both in terms of the ability to bind different endogenous ligands leading to a variety of GPCR classes and families. In addition the flexibility gives different GPCRs the ability to modulate the downstream signaling system in different ways giving rise to GPCR subtypes within families. The possibility of such tunability of GPCR signalling has led to the evolution of a large number of different GPCRs of which around 800 are present in the human genome and which can respond to a wide variety of chemical and physical signals. The chemical signals include small molecules such as dopamine and acetylcholine, oligopeptides such as neuropeptide Y and α- and β-melanocyte-stimulating hormones or large hormones like human chorionic gonadotropin (hCG), follicule stimulating hormone (FSH) or luteinizing hormone (LH). Common physical signals include photons in the case of rhodopsins and mechanical force in the case of adhesion GPCRs while somewhat more exotic influencing parameters include for example the membrane curvature (Lin et al., 2022; Marullo et al., 2020; Rosholm et al., 2017).

It is worth mentioning that many GPCRs also exhibit constitutive activity, in some cases through employing extracellular N-terminus of the receptor as a ligand (Srinivasan et al., 2004). Furthermore, activation of GPCRs is highly dependent on the availability and interaction with G proteins as well as GTP and GDP explained by the concept of reciprocity. In essence, reciprocity simply states that if receptor-ligand binding event affects the binding process of a G protein, then the receptor-G protein complexation also affects the process of receptor-ligand binding. A more narrow but comprehensive explanation of reciprocity is given by Colquhoun (Colquhoun, 1998) who explained how ignoring this effect leads to misinterpretation of effects of mutations on ligand binding and receptor activation and adapted the concept from the study of

binding cooperativity in hemoglobin (Wyman Jr. & Allen, 1951). The concept of reciprocity is not unique to GPCRs or even biochemistry and is instead the application of extensions of the Hess law to biological systems. These examples clearly show that GPCRs are not simply passing on the signal from the extracellular to the intracellular space but have the capability to modulate and interpret the signal from the very first steps of the signal transduction process. This complexity is now widely acknowledged and even led to the comparison of GPCRs to microprocessors (Smith et al., 2018). Considering the wide variety of modulatory processes of GPCRs it is clear that the receptor signalling process is a complex system acting in unison with other signalling and metabolic systems of similar complexity meaning that a living cell can be considered a system of systems. As reductionist ideas and approaches have been unable to solve many of the pressing problems in this field, systems biology and systems pharmacology approaches have emerged to explain this complexity. Expectedly, no single master model exists so far and instead, many new models describing a part of the system have been and continue to be proposed (Carvalho et al., 2021). Despite the relatively diverse landscape of complex models describing GPCR signalling, some aspects of it are generally accepted although many of the details are hotly debated.

1.1.1. Receptor in the resting state – not just a sleeping beauty

At the onset of receptor research, the receptors were considered to act as switches that turn on and start signalling upon agonist binding but are otherwise inactive (Clark, 1926; Hill, 1910). However, it has become apparent that such a simple assumption does not always hold true as many GPCRs have been found to display constitutive activity – that is the ability to activate the signaling pathways even in the absence of the agonist with examples including melanocortin and cannabinoid receptor families as well as histamine H_3 and dopamine D_1 and D_5 receptors (Milligan, 2003). Furthermore, constitutive activity can be inhibited by a class of ligands termed inverse agonists (de Ligt et al., 2000). From the structural point of view, constitutive activity can be explained in simplified terms by the receptor assuming at least partially active conformation in the ligand free state while the inverse agonist stabilizes the inactive state conformation (Nagiri et al., 2019; Qin et al., 2022).

1.1.2. Ligand binding – the signalling cascade begins

Although a GPCR can be functionally active in the ligand free state, it can still be considered to be the basal state of the system. In this regard, the signalling systems have usually evolved to sense the signals in extracellular space with ligand binding starting the cascade. Already at this stage a substantial variability of ligand-receptor complex formation emerges. The rate at which ligand binding can induce different structural changes and functional responses variess by

several orders of magnitude starting with subpicosecond timescale of first steps of rhodopsin activtion and ending with subsecond level activation of GPCR mediated ion channel conductance (Lohse et al., 2014). The rate of ligand binding also has a meaning for the drug action as the ligand residence time can correlate with pharmacological outcomes such as off target effects (Hoffmann et al., 2015). Together with residence time, the ligand binding affinity plays a crucial role as in pharmacological systems the drugs usually compete with the endogenous agonist for the binding site. Therefore, affinity is often optimized during drug design to achieve both low required doses as well as selective binding over off target proteins (Kairys et al., 2019).

One of the most important and used classifications of ligands is based on their ability to activate the GPCR, a concept known as efficacy with endogenous agonist efficacy set to 100% and neutral antagonist efficacy at 0%. However, the landscape of ligands is much more diverse as partial agonists have efficacies between 0% and 100%, superagonists go beyond 100% while inverse agonists have negative efficacies. In addition, different types of allosteric modulators can alter the behaviour of the receptor-orthosteric ligand complex resulting in a highly tunable system (Jeffrey Conn et al., 2009; Slosky et al., 2021).

1.1.3. G protein activation – the first decision

Despite the ligand binding focusing on the binding part of the reaction, it would perhaps be better to call this process ligand-receptor complex formation, as the receptor-ligand complex populates a distinct region on the conformational landscape often different from receptor complexes with other ligands, even in cases of similar efficacies, as has been for example shown for muscarinic M_2 receptors (Xu et al., 2019). As each complex potentially shows distinct functional properties, it is sometimes useful to consider each receptor-ligand complex as a separate molecular entity. Possibly the most important of these properties is the ability to activate the heterotrimeric G protein, which then dissociates into the G_α and $G_{\beta\gamma}$ subunits. The activated G-proteins can further activate or inhibit several pathways with the main ones being the cyclic adenosine monophosphate (cAMP) pathway through stimulation or inhibition of adenylyl cyclase by G_s and G_i alpha subunits respectively and the phosphatidylinositol pathway where G_q alpha subunits activates phospholipase C. This leads to generation of diacyl glycerol and inositol triphosphate. Diacyl glycerol and inositol triphosphate in turn activates protein kinase C and release of intracellular Ca^{2+} respectively. In this step, the GPCR signalling pathway has the first significant branching point as there are 18 different G_α ,5 G_β and 12 G_γ subtypes (Syrovatkina et al., 2016). Classically, GPCRs were assumed to show coupling selectivity to a specific G_α subunit while nowadays mounting evidence appears to point out that instead of selectivity there is merely a preference for a specific type of G_α subunit (Hauser et al., 2022). Despite this, common logic would suggest that GPCR signalling must be very precise to support complex

life and, therefore, it is very unlikely that there is anything accidental happening in the GPCR G protein coupling system.

1.1.4. Action of arrestins – GPCR signalling stops but not really

Arrestins comprise four protein subtypes (Arrestin 1–4). The name arrestin was coined after the observation that arrestins, specifically the β-arrestin, desensitizes β-adrenergic receptor signalling (Lohse et al., 1990). The mechanism behind the desensitization is more general and explained by phosphorylation of the GPCR by GRKs or PKC (Kelly et al., 2008) sterically hindering the subsequent heterotrimeric G protein binding to GPCRs and further, recruitment of both clathrin and clathrin adaptor AP2 leading to the formation of the clathrin coated pit and endosomal internalization (Scheerer & Sommer, 2017). More recent discoveries expand the concept of arrested signalling as arrestin pathway activation itself has been shown to be a functional signalling pathway with evidence of continued endosomal signalling (Vilardaga et al., 2014). These findings indicate that the function and importance of arrestins is much more significant than the name suggests.

1.1.5. Biased signalling – an emergent property

As GPCRs can exhibit mainly two different behaviors, G protein activation and β-arrestin recruitment, naturally questions arise about how these two systems work together or interfere with one-another. From a drug design perspective the choice between the two pathways could be modulated somehow for pharmacological benefit. Certainly, the complete theory of biased signalling is much more complicated than a simple choice. Numerous studies have shown that GPCRs do not exhibit perfect G protein selectivity based on the G_{α} subunit (Avet et al., 2022; Hauser et al., 2022; Inoue et al., 2019). In reality, different GPCRs have received very variable attention in scientific literature with some less studied GPCRs such as Frizzled receptors having non-canonical pathways (Medina et al., 2000) possibly leading to, ironically, biased understanding of biased signaling.

The first evidence of biased signaling of serotonin receptors was systematized already more than three decades ago showing that the rank order of different ligands can depend on the signaling system (Roth & Chuang, 1987). Although biased signaling has recieved significant attention, there is still some confusion about even the most fundamental aspects of emergence of biased signaling. One common view is that biased signaling arises due to conformational selection with different agonists promoting either ternary complex formation with G-protein or phosphorylation and complex formation with arrestin (Gurevich & Gurevich, 2020). Other studies have suggested that biased signaling is instead at least partially determined by spatial and kinetic factors (Tóth et al., 2023). In general, this idea is supported by data showing the

heterogeneity of cell plasma membrane and its properties (Iversen et al., 2015; Sungkaworn et al., 2017).

Such complexity has led to the development of guidelines for reporting ligand bias including the recommendations for terminology as well as experimental design for different types of bias (Kolb et al., 2022). However, it remains to be seen how applicable such an attempt to separate different types of bias from one another is in practice as signalling is a complex system and the application of holistic systems approach seems to be unavoidable in the end.

1.1.6. Muscarinic, dopaminergic and neuropeptide Y receptors

In this thesis, three GPCR families namely muscarinic, dopaminergic and neuropeptide Y (NPY) receptors are used as biochemical model systems to exemplify how assay development and mechanistic modeling can be carried out. Still, all three receptor families are pharmacologically interesting targets in their own right.

Muscarinic acetylcholine receptors are among some of the most studied GPCRs to date with crystal structures available for all subtypes (M_1-M_5). Muscarinic receptors and their endogenous agonist acetylcholine play a critical role in functions such as cognitive function, memory formation, heart function, smooth muscle control and also control dopamine release (Eglen, 2005; Kudlak & Tadi, 2023) and recently identified as a target for alcohol use disorder (Walker et al., 2020). Several drugs for muscarinic receptors are in clinical use for example tiotropium for reduction of bronchospasms and asthma symptoms. One of the main restrictions of muscarinic receptor drug development is the evolutionary conservation of the orthosteric binding site meaning that subtype selectivity is difficult to achieve thus sparking the interest in the development of allosteric modulators for muscarinic receptors (Jakubík & El-Fakahany, 2010). From mechanistic modeling perspective, muscarinic receptors are quite interesting as there is mounting evidence of muscarinic receptor oligomerization (Marsango et al., 2018, 2022) but also kinetic models that describe complex kinetic properties of ligand binding to these receptors including aspects of dimerisation (Ilien et al., 2009; Jakubík et al., 2000) but there is still no holistic understanding of this process.

Similarly to muscarinic receptors, dopaminergic receptors and dopamine signaling are widely studied and targeted by existing drugs. Dopamine and dopaminergic receptors are involved in many physiological processes such as motivation and addiction and related to diseases such as Parkinson's disease and attention deficit and hyperactivity disorder (ADHD) with many drugs already available (Napier et al., 2020; Pozzi et al., 2020; Wise & Robble, 2020). Mechanistically, dopamine receptors show some interesting homo- and heterodimerization properties making it possible to design quite unique bivalent ligands to target dimers more specifically (Ullmann et al., 2021) while also showing endosomal signalling (Martinez et al., 2020) indicating a complex signaling pathway of these receptors.

Neuropeptide Y (NPY) receptors are in comparison to muscarinic and dopaminergic receptors somewhat less studied and as of now there are no approved drugs targeting NPY receptors. Despite this the therapeutic potential is substantial with main ideas for therapeutic applications include obesity, anxiety, depression and epilepsy (Brothers & Wahlestedt, 2010). NPY receptors also possess some interesting kinetic properties such as irreversible binding depending on receptor subtype, also indicating more complex binding mechanisms of these receptors (Dautzenberg & Neysari, 2005).

1.2. Systems biology and global analysis

As seen, the GPCR signalling cascade, even after simplification and generalization, is a true complex system and, therefore, studying it using the systems biology (SB) approach is highly beneficial. It is hard to define what SB is exactly but it has been described as an approach or way of thinking about biological problems rather than a separate field of science (Kohl et al., 2010). One of the most fundamental concepts of SB is acknowledging that organisms and other biological systems are, by nature, dynamic in time and, furthermore, can and will respond to changes both within the system and the environment. Therefore, models of biological systems which consider the temporal effects can provide a much more holistic picture of the system or process under study. Many SB concepts have influenced and been adopted to pharmacology and GPCR research, but only quantitative kinetic modeling and global analysis is considered in more detail here. There are many technical challenges to applying SB approach to GPCR research which have been identified already more than a decade ago, some of which have been solved while some problems such as need for data standardization and sharing have not received enough attention and remain problematic for GPCR data (Heitzler et al., 2009).

It can be argued that the first kinetic model for a chemical reaction was indeed already a systems biology model when Ludwig Wilhelmy proposed essentially the differential and integrated versions of law of mass action to explain acid catalysed hydrolysis of sucrose to fructose and glucose (Wilhelmy, 1850). However since the Hill equation and Clark's receptor theory (Clark, 1926; Hill, 1910) the kinetic aspects were overshadowed by equilibrium or steady-state models relying on empirical concepts for essentially a century and has only started to gain traction roughly at the same time as the emergence of SB (Hoare et al., 2018).

Perhaps one of the practical reasons for paying little attention to kinetics was the lack of computational power and algorithms required to explore more complex kinetic models. The main problem with complex kinetic models emerges from the sheer number of parameters which are combined in a non-linear way. The optimal parameters are then searched using a non-linear fitting process, but due to numerous local optima in the parameter-loss function space, specialized algorithms are required which can ignore the local optima and find the global one. Use of these algorithms for non-linear regression is called global

fitting. Many global optimization algorithms have been developed often inspired by processes in nature such as simulated annealing based on annealing of alloys (Nelder & Mead, 1965), genetic algorithm based on natural selection (Fraser, 1957) or particle swarms inspired by movement of groups such as schools of fish (Kennedy & Eberhart, 1995). Even though such global optimizers have been developed, they are still limited by what is known as the No Free Lunch theorem essentially stating that without prior knowledge, all optimization algorithms perform equally on average (Wolpert & Macready, 1997). This sets the focus on gaining and incorporating prior knowledge to global optimization problems. For example, prior knowledge can be incorporated into more dedicated loss functions compared to simple mean squared error loss or reasonable choice of initial parameter values.

Despite being conceptually quite simple, global fitting is not used as often in pharmacology as local fitting, probably in part due to many of the popular software such as GraphPad Prism software (https://www.graphpad.com/) does not support defining and fitting of ordinary differential equation (ODE) systems.

1.2.1. Classical GPCR ligand binding and activation models

Somewhat remarkably, the process of developing mathematical models for pharmacology has even been called quantitative pharmacology (Gesztelyi et al., 2012). This reflects that pharmacological thinking has considered mathematical models primarily as practical tools for ranking ligands and explaining isolated experimental observations rather than as descriptions of fundamental processes which have evolved to possess such quantitative properties due to their appropriateness. Such applied thinking led to many relatively simple models becoming popular containing empirical and abstract parameters with sometimes weak connections to known laws of chemistry.

Many different classical theories of receptor function have been proposed but the ones which continue to be used have the highest practical impact. The first, and probably most widely used quantitative model for describing ligand binding is the Hill equation describing the iconic sigmoidal binding and dose-response curves, often also called the hyperbolic function (Hill, 1910).

$$\theta = \frac{[L]^n}{K_d + [L]^n}$$

Here, θ is the fractional receptor occupancy, *[L]* is the ligand concentration, K_d is the dissociation constant and *n* is the Hill coefficient. However, interpretation of fitting results of the Hill equation to the experimental data is difficult as the Hill coefficient n is only an aggregation of deviations from the assumed simple reversible bimolecular reaction in case of one site model and rarely provides significant insight into the underlying mechanism. Furthermore, if the Hill slope

is equal or close to unity, it does not necessarily mean that the underlying process corresponds to the simple one-site binding model. Therefore, using the Hill equation as the theoretical basis of experimental design can lead to missing the experimental conditions space that reveals the deviations from the assumption.

The next interesting proposal is the Black-Leff operational model attempting to explain the different maximal effects of different agonists (Black & Leff, 1997). In the Black-Leff model, a new concept, the transducer ratio τ defined as

$$\tau = \frac{[R_0]}{K_E}$$

is introduced. Here $[R_0]$ is the total receptor concentration and K_E is the concentration of agonist-receptor complex required to achieve half-maximal effect. The Black-Leff model is a further development of a model proposed by Stephenson (Stephenson, 1956), but making the additional assumption that binding and receptor activation are independent, a mistake made also in other models and sharply criticized by Colquhoun as it leads to misinterpretation of structure-activity relationships in case of receptor mutation studies but probably in an even wider context (Colquhoun, 1998). Still, pointing out this model is worthwhile as currently, the Black-Leff model is one of only two methods explicitly brought out in the community standards for determining GPCR ligand bias (Kolb et al., 2022) and thus also one of the two represented in the Biased Signaling Atlas (https://biasedsignalingatlas.org/) as of now (Caroli et al., 2023).

The ternary complex model is the third widely used classical model assuming the formation of a ternary complex between an agonist, the receptor and the heterotrimeric G protein. This model replaces the somewhat abstract and obscure term “stimulus” with a real molecular interaction between GPCR and the G protein. One of the significant effects this model can explain is the often observed increase of agonist affinity when the GPCR is coupled with the heterotrimeric G protein. However, the proposition of the high stability of the ternary complex raises a paradox between thermodynamics and GPCR signalling logic. From the thermodynamics perspective, the energetically stable ternary complex should be slow to dissociate into free GPCR, G_α and $G_{\beta\gamma}$ units. From the signaling perspective, the heterotrimeric G protein dissociation should be fast in order for the signaling system to have a short lag phase to the change of agonist concentration. In practice, this raises a question whether the design of agonists which make the ternary complex very stable is always a suitable optimization target for drug design.

1.2.2. Systems biology models of GPCR ligand binding and function

Although the definitions and boundaries of SB models are slightly unclear, in a broad sense, the SB models aim to postulate the model based on real physical entities and known physical and chemical logic, attempting to remove empirical functions. For example, SB models are often based on the definition of chemical reactions and ODEs based on the law of mass action although other options and assumptions are also acceptable (Keating et al., 2020). This in turn drives the models to be more rigorous, reproducible and falsifiable. For example, it is easier to establish reasonable parameter boundaries (diffusion limitation, conservation of energy, mass, charge, number of atoms or Hess law depending on the situation). Such boundaries may be difficult or impossible to define for parameters in empirical models.

Even when considering these factors, it remains unclear which exact type of models are the most appropriate to describe GPCR signaling specifically, as many processes with obvious spatial organization can and often have been replaced by bulk effects as seen with many classical GPCR ligand binding models discussed earlier. This may be achieved by replacing the law of mass action with a different and more appropriate theory for defining ODEs in the spatially highly organized areas and considering these as separate compartments in bulk models. This is also supported by systems biology modeling language (SBML) (Hucka et al., 2003, 2008; Keating et al., 2020). It is most likely that several types and even mixtures of several types of models find application in different situations.

1.2.2.1. Bulk models

Bulk models, which ignore all spatial aspects of signalling and assume homogeneous and continuous processes allowing the use of ODEs are the most widely used type of models applied to different processes of GPCR signalling. Models for many processes have been proposed considering aspects of biased signalling, dimerisation and allosteric modulation extending the basic receptor-ligand interaction theory. For modelling ligand binding to muscarinic receptors, several kinetically complex models have been proposed. Ligand binding to M_1 and M_2 receptors has been previously studied using the tandem two-site model (Jakubík et al., 2000). In that case, the allowed reactions are ligand binding to the receptor, isomerization of the receptor-ligand complex and finally additional ligand binding to the isomerized complex. The same model has been found to explain kinetics of other systems such as melanocortin MC_4 receptor (Kopanchuk et al., 2006). To explain kinetic effects of pirenzepine binding to M_1 receptor, Ilien and coworkers developed a different three step binding model (Ilien et al., 2009). In this model the possible reactions include initial ligand binding to the receptor, followed by receptor-ligand complex isomerization and finally dimerization of two isomerized receptor-ligand complexes. In this study,

modeling relied heavily on global fitting of the data. Interestingly, the authors also explored the tandem two-site model and determined it to be inconsistent with their data. However, the authors did not quantitatively test the ability of the newly proposed model to explain previously obtained data supporting the tandemly arranged binding sites model only stating that the data was obtained using radioligand binding studies with membrane preparations and without sufficient temporal resolution.

Bulk models have also been developed to model the GPCR signal transduction process beyond ligand binding with an interesting example emphasizing the role of fractions and not absolute amount of ligand bound and unbound receptor in the so called carousel model (Bush et al., 2016). Interestingly, this model is associated with control of pheromone driven directional growth of yeasts, serving as an example of a case where a bulk model is used to explain spatial outcomes. Additionally, here the authors started with a model and parameter value first and only gathered experimental data specifically later designing the experiments with the hypothesis formulated as the model definition. Recently, another study was conducted attempting to explain the emergence of spatio-temporal bias in GPCR signalling considering a wide variety of processes with a total of 96 kinetic parameters and 43 molecules or processes (Tóth et al., 2023). Such a study serves as a good example of how complex models can become raising many problems in the space of experimental design, overfitting, over-parameterization and parameter identifiability. Similarly to the carousel model, spatial conclusions are pulled from bulk data.

Finally, ODE based bulk models can and have been developed specifically to consider and explore different assumptions for explaining GPCR signalling. For example, the ternary complex model is challenged by the collision coupling model (Tolkovsky & Levitzki, 1981) and shuttle model (Tolkovsky, 1983), which also consider the possibilities that there is not necessarily any pre coupling between GPCR and the G protein before ligand binding. The shuttle model takes it even further bringing in the influence of membrane fluidity and diffusivity and their impact on GPCR signalling, while still defining the model in terms of bulk concentrations.

1.2.2.2. Spatial models

Despite most of the proposed and used models are bulk models assuming homogeneous distribution of molecules, more evidence is gathering that GPCR signaling is spatially regulated. For example, there is evidence of formation of so-called GPCR interaction hot-spots as well as cAMP nanodomains which cause both spatial coupling and decoupling of signaling pathway components (Anton et al., 2022; Paolocci & Zaccolo, 2023; Sungkaworn et al., 2017). These aspects may help to untangle how the cells are able to distinguish between different signaling sources in the situation where the number of different GPCRs surpasses the number of secondary messengers by more than an order of magnitude. Even simplistically, the implications of the difference between bulk and spatial

models are substantial. For example, inhibition of phosphodiesterases would only lead to increased and sustained cAMP levels in bulk conditions while in the case of accounting for cAMP nanodomains, it would potentially lead to disappearance or modification of the nano-domains and likely lead to more cross signalling between different GPCR pathways. Furthermore, it may be that activation of a full agonist or a superagonist would lead to cAMP leaking out of the nanodomains while partial agonists or constitutive activity may lead to more independent nanodomains.

For spatial models, additional complexity and variability is created by the spatial scale, and its interplay with the temporal scale. These factors determine for example which types of averaging operations lead to gross errors and which ones can safely be applied. Spatial models also create possibilities for defining new emergent properties such as spatial waves and both positive and negative feedback driven by spatial factors. A well known spatial model is the Turing network famously developed by Alan Turing (Turing, 1952). This model has been for example applied to describe the formation of fingers during the embryo development (Raspopovic et al., 2014). Here, the Turing network is formed by Bmp, Sox9 and Wnt. Interestingly, it is not necessary to explicitly describe the system in terms of regular kinetic or equilibrium constants and a more abstract level system of partial differential equations is sufficient. These kinds of models serve both as examples how GPCR signalling systems are heavily influenced by spatial aspects while the spatial scale can have significant variations.

1.2.3. Analytical and numerical solutions to models

Formulating a theory or a model in mathematical terms is not necessarily a straightforward process with many possible choices, including how the model can be used and solved. In general, mathematical models can be solved in two broad ways – analytically or numerically. Analytical solutions, also called the closed form solutions, are exact solutions to the equations proposed by the model. Numerical solutions on the contrary do not reach the solution in a single step but instead rely on iterative global optimization algorithms. The deeper analysis of mathematical properties of the two types of solutions is beyond the scope of this thesis, but it is worth mentioning that many models may either fundamentally lack an analytical solution, the analytical solution may be unobtainable with known mathematical techniques or the solution may be a series of poorly converging terms (Gupta et al., 1985). Numerical solutions on the other hand can be obtained to a substantially larger and complex set of models with the only major drawbacks being the requirement fo computational power to arrive at the solution, the chance to converge to a local minimum or overfit the model resulting in parameter degeneracy. In practice, computational power required to solve many of the models is rarely the bottleneck of the modeling process. Instead, the complexity of the modeling process usually lies in the iterative process of modeling, experimental design, performing experiments and experimental data analysis. Therefore, an important requirement to

the models is to increase the speed and quality of the bottleneck processes of modeling considering both the fundamental, technical and human aspects of this process. Usually there is no one-size-fits all solution to all of these problems, so the choice depends on the situation and the importance of some of the advantages and disadvantages of both approaches.

Analytical models have advantages in situations where the model is relatively simple allowing the user to quickly comprehend and even memorize the entire equation. In addition, analytical models often allow an intuitive overview of which parameter values lead to trivial solutions or large variations in the measured parameter making the experimental design more intuitive. The analytical models are often also quite compact making these models easy to share and publish. Finally, calculating solutions for analytical models is fast making the fitting process usually faster too and therefore more scalable. However, if the theories and models become more complex, the analytical models start to become increasingly more complex with entanglement of multiple parameters in both numerators and denominators as sums or products. For example some receptor dimer models can lead to five addends present in multiple terms in both the numerator and the denominator (Kukkonen, 2021). Even with three parametric addends the attempt to find a value for a single parameter which would result in the sum equaling zero does not result in a single number but instead a line with the solution gaining more dimensions in case of even more addends. Therefore, even if a solution exists, using it may be prohibitively difficult or requires the help of symbolic math software diminishing most of the previously listed advantages. Finally, analytical equations can take many mathematically equivalent forms but it may be difficult to recognize this equivalency, for example linear or logarithmic versions of the same model. This has led to reinvention of essentially the same models two or even several times in different fields of science clearly hindering scientific progress.

Advantages and disadvantages of the numerical solving process are quite the opposite of analytical solutions. The numerical solving technique can be applied to practically any SB model, even the simple ones. As the solving process requires specific software in any case, then the process of numerical solving is more general and may be a better fit in the process of model development where analytically solvable problems evolve into unsolvable ones. The possibility of numerical solutions allows the representation of models as ODE systems which can be presented in a very structured manner without the parameter entanglement making large models easy to understand. The disadvantages of numerical ODE solving include the need for significant computational power especially during the global fitting process and particularly during uncertainty, sensitivity and identifiability analysis which requires the fitting procedure to be run multiple times. In some cases the speed of these operations can become somewhat of a bottleneck, but advancements in computer software, hardware, cloud computing and machine learning (ML) are likely to alleviate this problem in the future (Han et al., 2018; Lienen & Günnemann, 2023; Lu et al., 2021; Regazzoni et al., 2019). In a more abstract sense, analytical solutions provide exact

answers but often to simplified questions while numerical ODE or PDE solving provides somewhat uncertain answers to more exact questions.

1.2.4. Systems biology software ecosystem

As a field, SB often attempts to find more general theories and models compared to the conclusions of single experimental studies. Development of such generalizations depends heavily on the availability of high quality software and experimental data. There are several generations of open-source software packages for SB analysis for example SBToolbox2, Data2Dynamics and PyPESTO (Raue et al., 2015; Schälte et al., 2023; H. Schmidt & Jirstrand, 2006). Such SB software usually adheres to community standards with the Systems Biology Modeling Language (SBML) being the central format of model exchange with several versions developed over the years refining the idea further allowing for example spatial models (Hucka et al., 2003, 2008, 2019; Keating et al., 2020). The development of the SBML format is a significant advancement as it allows several critical problems to be solved, namely, it removes ambiguity from model definitions, allows sharing and reuse of even very complex models for scientific and educational purposes and also serves as a type of quality control allowing for reproducibility of the simulation results. To take the reproducibility aspect even further by introducing the Minimum Information About a Simulation Experiment (MIASE) (Waltemath et al., 2011). The central motivation and idea of the MIASE project is that the simulation is a computational experiment performed using a model. This is a quite critical aspect since complex models allow a significant number of different simulations to be run using different assumptions about boundary and starting conditions, time-scales and parameter values. In the light of the success of such standardization, the Minimum Information for Data Analysis in Systems biology (MIDAS) format was proposed as a part of DataRail software and also used in ImageRail software (Millard et al., 2011; Saez-Rodriguez et al., 2008). An alternative format for such standardization is the Biological Dynamics Markup Language (BDML) and the binary HDF5 (Hierarchical Data Format version 5) based BD5 format extension of it (Kyoda et al., 2015, 2020), but these formats are mainly aimed for use for image data for example using the Open Microscopy Environment (OME) systems such as OMERO server (Allan et al., 2012). In addition to the few standards mentioned here there is a large number of other standards documented in the Fairsharing database (fairsharing.org) (Sansone et al., 2019). However, the GPCR and perhaps pharmacology field in general has not widely adopted these standards making public datasets about GPCR activation or even ligand binding rare at the raw data level. Of course, databases collecting affinity and kinetic constants exist but considering the fact that GPCR signalling is much more complex than the classical era models can describe, the lack of detail and standardization is becoming an ever increasing obstacle for pharmacological sciences. In some cases lack of raw data has led to unorthodox methods such as reverse engineering raw data from published figures using

tools such as WebPlotDigitizer (https://automeris.io/WebPlotDigitizer/) (Kukkonen, 2021). Obviously, there is a substantial risk of loss of data accuracy and reproducibility when using such analog methods although as a tool of last resort it could be used (Drevon et al., 2017). Finally, some of the named software have quite shallow learning curves and are better suited to large institutions (Li et al., 2016).

1.3. GPCR ligand binding methods

Biochemistry and pharmacology rely heavily on a myriad of different assays designed to measure the behavior of *in vitro*, *ex vivo* or *in vivo* systems. For a long time most assays have relied on relatively simple optical outputs such as changes in absorbance or fluorescence and luminescence intensities or fluorescence anisotropy (FA) (Stoddart et al., 2015, 2016; Uri & Nonga, 2020). The great advantage of these assays is the relative simplicity in terms of both sample preparation and measurement equipment and usually also quite good robustness making them suitable for high-throughput screening (HTS) campaigns as well as for fundamental research. In addition, more advanced spectroscopy-like methods have been developed such as fluorescence correlation spectroscopy (FCS) or surface plasmon resonance (Rascol et al., 2021; Stoddart et al., 2022).

Of these, FA also called fluorescence polarization assays are particularly useful for high throughput applications. Fluorescence polarization assays rely on few key properties of light polarization and molecular mobility. In FA assays, the fluorophores are excited with polarized light which induces photoselection by preferentially exciting fluorophores with the excitation dipole oriented in the direction of light polarization. Next, the fluorophores can rotate in the excited state and emit a photon some time later determined by their fluorescence life-time. Depending on the extent of ensemble rotation, the fluorescence is partially or fully depolarized. It is possible to design fluorescent ligands where the fluorophore is conjugated to a pharmacophore. If such a fluorescent ligand binds to a protein then the rotational freedom of the fluorophore is hindered leading to less rotation and higher polarization of fluorescence, thereby allowing to assess the extent of binding based on polarization of the fluorescence (Rinken et al., 2018).

Besides spectroscopic assays, high content microscopy has gained popularity especially in recent years with the arrival of advanced automated plate-reader type microscopy systems. Some of these assays rely on average image intensity measurements while others employ image analysis algorithms for quantification (Gherbi et al., 2015; Stoddart et al., 2012). In case of microscopy the image intensity usually corresponds to the amount of bound ligand amount directly. However, assays relying on only fluorescence images have several drawbacks such as added noise since not all fields of view (FOVs) may contain the same number of cells or biased results toward bright structures if cell segmentation is performed from the same fluorescence channel that is used for quantification. A

better alternative is to use the bright-field channel for cell, cell contour or nuclei segmentation as it allows simultaneously to avoid photobleaching and phototoxicity during focusing, segmentation of several different features of the cells and does not require additional fluorescence labeling for cell segmentation making the assays more robust (Allikalt et al., 2021; Fishman et al., 2021).

1.4. Bioimage analysis and machine learning

For quantification of the imaging-based methods, bioimage analysis needs to be applied. Bioimage analysis is an interdisciplinary field utilizing a collection of practical techniques and approaches to tackle biological questions and aims to draw qualitative, semi-quantitative or quantitative conclusions about a biological sample, species, experiment or observation at mostly based on images. Bioimage analysis most commonly incorporates technologies and knowledge from several fields such as optics and design of image acquisition devices, most often microscopes, biology and biochemistry, software engineering, computer vision including machine learning, measurement science and data science. It is generally accepted among bioimage analysts that the analysis of bioimages is essentially an act of measurement and thus some common concepts such as uncertainty and measurement quality apply. Although, in case of deterministic algorithms the uncertainty introduced by the algorithms has no random component. One of the main applications for bioimage analysis was envisioned to be the development of high-throughput screening for applications such as SB (Pepperkok & Ellenberg, 2006). One of the main problems at that time was the lack of algorithms which could analyze such datasets with sufficient quality. It turns out that in a general case, many image analysis problems can be solved via machine learning and especially deep learning algorithms (Angermueller et al., 2016).

Several deep-learning based convolutional neural networks and transformers have proven to be the most feasible and high-quality option for common tasks such as cell detection, segmentation and classification. Although deep neural networks and convolutional neural networks were developed decades ago, the real benefit of these algorithms and models was heavily restricted by computational hardware. One of the earliest works showing the high quality combined with feasible application of deep neural networks for image analysis was the development of AlexNet (Krizhevsky et al., 2017). In light of the success of AlexNet, deep fully convolutional neural networks (CNNs) have been applied to the biomedical field with one of the most important steps being the autoencoder based U-Net architecture, which is commonly used to segment organelles, cells, organs and other which commonly appear in biological samples (Falk et al., 2019; Ronneberger et al., 2015). A large number of both variations and applications of U-Net type autoencoders and similar CNNs have been made over the past few years (Pachitariu & Stringer, 2022; U. Schmidt et al., 2018; Siddique et al., 2021; Stringer et al., 2021).

One of the most important aspects of reliable bioimage analysis is the quality control of the algorithms including validation, calibration and robustness tests. While reporting standards for machine learning models themselves have been developed (Walsh et al., 2021) it has not been so well generalized for bioimage analysis pipelines in general as there is significant variation in tasks. Perhaps one of the best attempts to provide some workflow standards is the BioImage Informatics Index (BIII) (http://biii.eu/) but it is still far from solving all problems at the current stage (Laine et al., 2021; Segebarth et al., 2020). Of course, the lack of community standards does not mean that there are no good isolated studies where some useful validation techniques have been used (Aguet et al., 2013; Sio et al., 2007).

2. AIMS OF THE STUDY

As described in the literature overview, GPCR signalling is a complex system but deeper understanding of it is required for drug design. Application of both image analysis and holistic kinetic modeling would potentially solve many of the current problems. Therefore, the general aim of this study is to develop new and improve existing tools for studying GPCRs in a more holistic way. This can be split into several subgoals.

1) Develop new ligand binding methods for GPCRs
2) Develop principles of data analysis for the developed assays
3) Develop principles of development and implementation of the image analysis pipelines and machine learning models for image based assays GPCR assays
4) Develop the software to support further development and use of comparable assays
5) Use these principles and software to propose mathematical models for explaining the experimental results of ligand binding.

3. MATERIALS AND METHODS

3.1. Production of M_2R displaying BBVs and use for FA experiments

Sf9 cell culture and BBV production was carried out as described in **Paper V**. Briefly, Spodoptera frugiperda (Sf9) cells (Invitrogen Life Technologies) were used for transfection and amplification of baculoviruses. The Sf9 cells were grown as a suspended culture in EX-CELL 420 Serum-Free Medium (Sigma-Aldrich) at 27 °C, atmospheric gas mixture and shaken at 110 rpm using a rotary shaker. Cell density was kept between one and four million cells/mL to maintain the logarithmic growth phase. Cell density was periodically measured using TC10 automated cell counter (Bio-Rad Laboratories AB) using 0.4% trypan blue (Sigma-Aldrich) for cell staining.

The cloning of the cDNA (Invitrogen) of the wild type human M_2 receptor to pFastBac1 vector restriction site had been previously done by Dr. Anni Allikalt. The initial M_2R-BBV stock was prepared as previously described (Veiksina et al., 2015).

For M_2R-BV amplification 110 mL of Sf9 cells at density of $1.5*10^6$ cells/mL was infected with 18 µL of M_2R stock of the initial passage with a final MOI of 0.01. For P3 (passage 3) production, 110 mL of Sf9 cell culture at density of $1.5*10^6$ cells/mL was infected with P2 baculovirus stock with MOI = 0.1. The produced baculovirus titration was performed using the ICSE assay (**Paper I**) (Laasfeld et al., 2017).

For budded baculovirus (BBV) production cells were infected at $2*10^6$ cells/mL with a high MOI = 1. The receptor preparation was monitored and collected when the viability dropped below 30%, usually 4–5 days post infection. The cell suspension was centrifuged at 1600g for 15 minutes to remove the cells. The supernatant was further centrifuged at 48 000g for 40 min to sediment the BBVs. The sediment was washed once using 500 µL of ice cold buffer (0.1% Pluronic F-127, 11 mM Na-HEPES (pH=7.4), 1 mM $MgCl_2$, 5 mM KCl, 1 mM $CaCl_2$, 135 mM NaCl and Complete EDTA-free Protease Inhibitor Cocktail) and then resuspended in the ice cold buffer. The sediments were pooled, suspended using a 1 mL syringe with 0.3 mm diameter needle (Sterican, Braun Melsungen AG) and aliquoted until further use. Sf9 cell culture and BBV production was performed together with Dr. Anni Allikalt and Dr. Maris-Johanna Tahk.

For FA experiments with both UR-MK342 and UR-CG072 the experiments were conducted as described in **Paper V**. Briefly, the assay buffer consisted of 0.1% Pluronic F-127, 11 mM Na-HEPES (pH = 7.4), 1 mM $MgCl_2$, 5 mM KCl, 1 mM $CaCl_2$, 135 mM NaCl and Complete EDTA-free Protease Inhibitor Cocktail. The M_2R-BBVs were thawed and homogenized using a syringe as described for BBV production. A concentration dilution series of M_2R-BBV using two fold dilutions was prepared starting from 40 µl. Two different con-

centrations of fluorescent ligands (0.5 nM and 2.5 nM in case of UR-CG072 and 1 nM and 8 nM in case of UR-MK342) were added to both total and non-specific binding wells. In non-specific binding wells, 8 μM atropine for UR-CG072 and 8 μM scopolamine was used as the non-specific ligand. The M_2R-BBVs were added as the last component to initialize the association. Time of the initialization was recorded and corrected for in the data analysis among other time-line corrections. After 90 min for UR-CG072 and 180 min for UR-MK342 the dissociation was initialized in the total binding wells using 8 μM atropine or 8 μM scopolamine respectively. Blank wells were prepared for BBV autofluorescence correction with no added fluorescent ligands.

3.1.1. Cell culture and microscopy of CELT-419 binding to HEK293-D_3R cells

HEK293-D3R cells were grown as described in **Paper IV** (Tahk et al., 2023). Briefly, HEK293 cell line with stable expression of wild-type human D_3 receptors was generated by Dr. Reet Reinart-Okugbeni previously (Reinart-Okugbeni et al., 2012). The cells were cultured as a single adherent layer on BioLite Petri dishes (Thermo Fisher Scientific) using DMEM high glucose medium (Sigma-Aldrich) with 9% fetal bovine serum, 400 μg/ml geneticin (Capricorn Scienific) and antibiotic antimycotic solution (0.25 μg/ml amphotericin B, 0.1 mg/ml streptomycin and 100 U/ml penicillin) (Sigma-Aldrich) supplements at 37 °C and 5% CO_2 in a humidified incubator.

For kinetic high-content imaging experiments 30 000 cells/well were seeded to μ-Plate 96 well Black well plates (Ibidi). Cells were preincubated for 5 h in cell medium. Before imaging, CELT-419 (Celtarys Research) solution was added to the cells with a final CELT-419 concentration of 1 nM. Into non-specific binding wells, 10 μM spiperone (Sigma-Aldrich) was added simultaneously with CELT-419. At multiple time points after association initiation, the dissociation was initiated by adding spiperone to the corresponding wells with a final concentration of 10 μM. Dissociation was started after 1, 2, 3, 4 and 5 h association time in corresponding wells keeping total binding wells as a control without dissociation initiation. All experimental conditions were measured as duplicates. Imaging was performed continuously for 12 h with approximately 20 min cycle time, paused briefly for addition of the dissociating ligand. Cytation 5 Imaging multi-mode plate reader (BioTek) was used for all measurements. Imaging was performed in both bright-field and Red fluorescent protein (RFP) fluorescence (531 (40) nm excitation and 593 (40) nm emission filters) channels obtaining four fields-of-view from each well with six different focal planes (Z-stack).

For higher resolution epifluorescence and TIRF microscopy imaging a custom built microscopy setup was used as described previously (Laasfeld et al., 2021; Müller et al., 2022; Nonga et al., 2021). Briefly, epifluorescence, bright-field and TIRF microscopy was performed with an inverted microscope assembled using the Till iMIC body (Till Photonics/FEI) using the TIRF APON

60x oil (NA 1.49) objective lens (Olympus Corp). A 515 nm PhoxX laser diode (Omicron-Laserage) in combination with SOLE-6 lights engine (Omicron-Laserage) was used for sample excitation. Images were captured with EM gain of 100, 40% laser power and with 50 ms exposure time. For all imaging modalities 200 image frames were captured with 50 ms intervals. The microscopy was performed by Dr. Sergei Kopanchuk.

The cells were seeded at a density of 20 000 cells per well into eight-well CG imaging chambers (Zell Kontakt GmbH). After 5 h of incubation, 0.5 nM CELT-419 in medium was added to the total binding and the association + dissociation wells and 0.5 nM CELT-419 and 5 µM spiperone was added to the non-specific binding samples. After 12 h of incubation, the medium was exchanged for HBSS buffer with different ligands present. 5 µM spiperone was added to the association + dissociation samples to initiate dissociation, CELT-419 with final concentration of 0.5 nM was added to the total binding samples and mixture of 0.5 nM CELT-419 and 5 µM spiperone was added to the non-specific binding wells. Imaging was carried out approximately 3 h after the medium exchange over 1 h period.

Vesicle tracking was performed using the TrackMate plug-in in Fiji software (Schindelin et al., 2012; Tinevez et al., 2017). Detection was performed using the Difference of Gaussians (DoG) detector with 1 µm estimated particle size, quality threshold of 200 and sub-pixel localization. Tracking was performed using the Simple LAP tracker with linking max distance and Gap-closing max distances both 1,0 µm and Gap-closing max frame gap of 4 frames. Confinement ratio was calculated for each track by dividing track displacement by total track length.

3.1.2. Global fitting of kinetic data

For global fitting of FA experiments of UR-MK342 binding to M_2R a set of MIDAS files was prepared with the events of association initiation, measurement start and dissociation initiation recorded. A modified version of IQMTools software (https://iqmtools.intiquan.com/) was used for the global fitting. For all cases, rough parameter values were chosen using manual parameter tuning. During the fitting, all model parameters were set free with minimum and maximum bounds being 100 fold smaller or larger than the initial value. As exceptions, intrinsic FA values of all forms were given an upper bound of 0.4 and all volume to receptor concentration conversion factors were set to be below 1, which would correspond to 100 nM concentration in stock. Parameter optimization was carried out using the simulated annealing algorithm (Kirkpatrick et al., 1983) combined with Nelder-Mead simplex (Nelder & Mead, 1965) using the following parameters: starting temperature 5000, temperature reduction factor of 0.2, end temperature of 0.1, maximum 5000 interactions for each temperature and 1000 at temperature 0 respectively. Here, the temperature refers to the algorithmic parameter of the simulated annealing algorithm which controls

the optimizer's step size and is not related to experimental temperatures. The iterator had 1000 maximum number of steps with absolute and relative tolerances both set to 10^{-6}. All experimental wells were fitted simultaneously while time series of each well, even of experimental replicates, were considered as separate series to avoid periodic fluctuations and their influence on derivative analysis. All other software parameters were kept at default values. Uncertainties were estimated based on fitting results of two independent experiments.

3.1.3. Development of Aparecium software

Core modules of Aparecium software were developed using MATLAB (MathWorks) software. The PlateSimulator module was developed using Java language and Eclipse IDE (https://www.eclipse.org/). Aparecium is distributed as open-source software under the GNU GPL v2 license and is available at https://gpcr.ut.ee/aparecium.html and https://github.com/laasfeld/Aparecium.

3.1.4. Open datasets

The raw data of fluorescence ligand binding to M_4R presented in **Paper VI** was published as four open datasets in the DataDOI repository (datadoi.ee) following FAIR principles (Tahk et al., 2022a, 2022b, 2022c, 2022d). The datasets include raw images, manual annotations of images, MIDAS files of measurement data, ML model files for cell segmentation. Ground truth annotations of microscopy images as well as training, test and validation set split metadata of **Paper VII** was also published in the DataDOI repository (Ali et al., 2022).

3.1.5. Statistical analysis

The Z' (Z prime) for fluorescence anisotropy assays was calculated as

$$Z' = 1 - \frac{3(\sigma_{\text{positive control}} + \sigma_{\text{negative control}})}{|\mu_{\text{positive control}} - \mu_{\text{negative control}}|}$$

Where σ is the standard deviation of the measured value of either positive or negative controls and μ is the average measured value of either positive and negative controls.

The image quality parameters were calculated as

$$recall = \frac{TP}{TP + FN}$$

$$precision = \frac{TP}{TP + FP}$$

$$F_1 = 2\frac{precision * recall}{precision + recall}$$

$$MCC = \frac{\mathrm{TP} * \mathrm{TN} - \mathrm{FP} * \mathrm{FN}}{\sqrt{(\mathrm{TP} + \mathrm{FP})(\mathrm{TP} + \mathrm{FN})(\mathrm{TN} + \mathrm{FP})(\mathrm{TN} + \mathrm{FN})}}$$

where *TP* is the number of true positive pixels, *TN* is the number of true negative pixels, *FP* is the number of false positive pixels and *FN* is the number of false negative pixels and *MCC* is the Mathews correlation coefficient.

4. RESULTS AND DISCUSSION

To fulfill the set goals, this thesis presents the Aparecium data analysis software which is specifically designed to support the development and use of biokinetic and microscopy based assays. Next, Aparecium software is applied for the development of new FA based assays for studying GPCR ligand binding process. These assays are reviewed in meta analysis style to generalize common properties of these assays including aspects of assay quality control and data analysis principles. The case of ligand binding to M_2R is analyzed using ODE systems based kinetic models as an example of proposing a more holistic view of the ligand binding process.

The principles of assay development are further generalized by including both live-cell imaging based assays and budded baculovirus immobilization based TIRFM assay while bringing out specific problems of image analysis based assay development. These are mainly related to the quality and uncertainty of ML models and image analysis pipelines.

Throughout the discussion, the obtained results are contrasted with commonly used and often oversimplified data analysis methods to show when and how such simplifications can lead to missing interesting effects, skew the assay quality parameters and lead to misinterpretation of the gathered data.

4.1. Aparecium software

"*Truth emerges more readily from error than from confusion.*"
-Francis Bacon

Bioimage analysis, global fitting of kinetic data and experimental metadata management are all important tasks often undertaken for the development and application of kinetic biochemical assays. Furthermore, it is beneficial if all of these different types of data are handled by a single software or a set of tightly integrated or interfaced software to avoid problems associated with different data formats, standards and versioning as well as with more user related problems such as installation and learning. In addition, as the assays are almost always developed and applied iteratively in a research setting, the same software should be able to handle both the more exploratory optimization stage and the more routine application phase. Furthermore, scientific software should aim to place as few unnecessary restrictions to the experimental design as possible while still promoting best practices and acknowledging that a single software should not attempt to solve every possible problem. It is also important to take into account that experimental data in biochemistry often does not confirm the initial hypothesis. The reasons can be broadly divided into two categories: faults in the experimental design or in the execution technique and applying oversimplified or otherwise inadequate theory for hypothesis postulation. In both cases, these kinds of experiments are often the most valuable while group effort

may be necessary, potentially over an extended period of time, to overcome the discovered problems. In practical terms such group effort is enhanced thanks to dedicated and standardized software, data formats and processes. If correctly applied, such tools should allow more systematic and rigorous hypothesis testing, mining previously gathered published and unpublished experimental data and applied revision of data analysis techniques. Very broadly speaking, FAIR (Findability, Accessibility, Interoperability and Reuse) principles should be applied not only in public datasets but also for private data inside research groups (Sansone et al., 2019). With these general requirements in mind a data and metadata organization and standardization software Aparecium was created.

4.1.1. Aparecium software architecture

To move from the set general objectives to specific solutions it was necessary to obtain a good understanding of the design and application processes of the assays that should be supported by Aparecium software. One of the best approaches to requirements engineering is to either have first hand experience in the problem space or have the possibility to get constant and high-quality feedback from the users. For Aparecium software requirements engineering both approaches were used as the assays, presented in later chapters, were developed in parallel with the software.

The main requirements which set the software scope were:

- Ability to import experimental data generated by multi-mode plate readers
- Ability to import microscopy images in OME-TIFF format along with relevant metadata
- Allow to extract information from the images using image analysis algorithms including deep learning (DL) models.
- Merge experimental data and metadata into a single data structure – a MIDAS file and allow saving, retrieval and merger of these files.
- Allow to group and subgroup replicate microplate wells or similarly formatted samples to allow the definition of correct data organization and calculations including blanking against measurements of other samples or other time-points of the same wells.
- Allow restructuring the data and metadata as an input for different SB or global fitting software.
- Provide default settings and possibility to save new default definitions for specific assays or projects.
- Provide a user-friendly and intuitive GUIs for allowing to perform all the aforementioned tasks.
- Provide sufficient modularity such that new types of input and output formats could be integrated with the system especially for adding support for new types of assays.

To fulfill these requirements a general architecture of the system was used (**Figure 1**). To demonstrate the suitability of this approach, several data-analysis

pipelines of different developed assays were built on top of Aparecium architecture, namely pipeline for single particle analysis from TIRF microscopy (**Paper III**) using the SPOTNIC module, pipelines supporting FA based assays using Gen5Tools (**Papers III, IV and V**) or BMGTools (Veiksina et al., 2021) and pipelines supporting live-cell based assays ligand binding assays (**Papers II, IV and VI**) using MembraneTools and also an assay for baculovirus titrations (**Paper I**) using ICSETools.

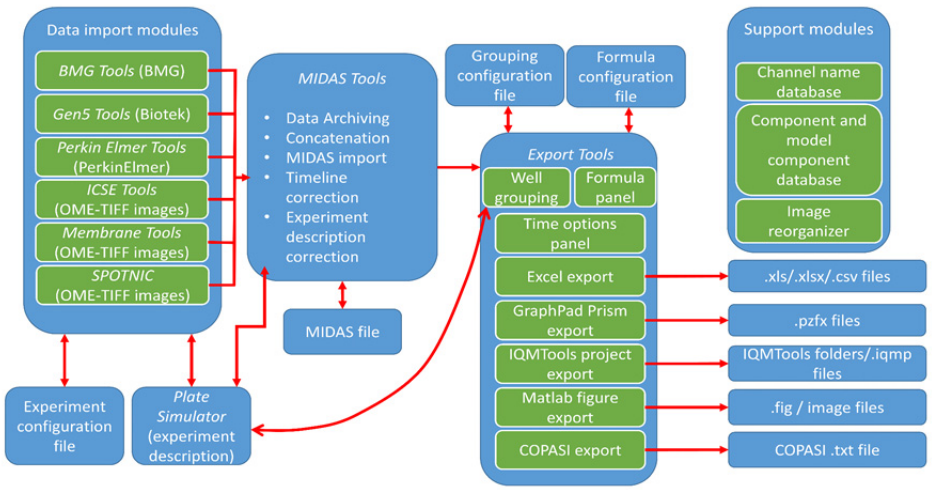

Figure 1. Schematic architecture of Aparecium software. Aparecium is divided into four modules: Data import modules, MIDAS file curation module MIDAS Tools, Data export modules in Export Tools and Support modules. Aparecium can import and export a number of data, metadata or hybrid file formats depending on the data source or next component in the data analysis pipeline.

4.1.2. MIDAS files and MIDAS Tools module

A substantial problem with applying SB methods for kinetic GPCR modeling has been the lack of a universal data format which contains all the necessary information needed for kinetic modeling while allowing for sufficient flexibility in experimental design and interoperability with different software (Heitzler et al., 2009; Saez-Rodriguez et al., 2008). The shortfall of some simple file formats is the inability to describe non-continuous situations which usually correspond to events such as addition or removal of specific assay components, although kinetic assay designs use such events quite regularly.

Aparecium solves both problems by employing MIDAS files which follows the general philosophy of other minimum information formats (Saez-Rodriguez et al., 2008; Taylor et al., 2008). MIDAS files are tabular files which allow simultaneously storing both measurement data and experimental metadata. This is achieved through considering rows to represent either of the two types of events – concentration change events and measurement events. Concentration

change events allow users to define non-continuous situations as previously described while measurement events are defined by the data export files created by the measurement equipment or previous analysis step, such as an image analysis pipeline. MIDAS files organize the data into a tabular format such that the file is both human and machine-readable making them quite easy to understand and integrate into other software. Another useful feature of MIDAS files is the possibility to store a separate timestamp for each measurement of each well. That makes it unnecessary to assume that all measurements in a single measurement cycle of the plate-reader happen at a single moment. This feature becomes particularly useful in case of measuring rapid kinetic processes where the plate-reader cycle time is comparable to the half-time of the process under observation. The importance of using this feature is further discussed in **Chapter 4.1.6**.

Aparecium provides a dedicated MIDAS Tools module for working with MIDAS files. The main functionalities match the common operations with MIDAS files. For example, these include making corrections to the treatment names or values in case an experimental mistake or miscalculation is discovered, unit conversion between logarithmic and linear scales and conversion of kinetically corrected (fast kinetics) type MIDAS files to slow kinetics files. The latter are required by some analysis software such as Graphpad Prism for equilibrium or empirical models in contrast to global fitting software such as IQMTools/SBToolbox2. MIDAS Tools also allows merging several MIDAS files together which may be necessary in cases where the plate-reader or image analysis software processes each kinetic phase e.g. association and dissociation phases separately and exports the data into separate files or database entries. It must be noted that MIDAS file is not the only possibility and support for equivalent formats such as BDML (Kyoda et al., 2015) could be added through modular design.

4.1.3. Data import module design

Aparecium consists of several data import modules which can read either the text or tabular output formats of plate-readers or microscopy images, combine the measurement data with experimental metadata and reorganize it into the standardized MIDAS format file. Modules for plate-reader format importers are relatively similar by design to reduce the learning curve between switching measurement equipment while remaining as separate modules to still allow adding equipment-specific features if necessary. Image analysis modules are somewhat more complicated and variable as different image analysis tasks have significantly more variability and may require parameter adjustments compared to plate-reader measurements. Currently implemented plate-reader import modules include *BMG Tools*, *Gen5 Tools* and *PerkinElmer Tools* for standardizing the output format of each measurement device. The image analysis modules include *ICSE Tools* (**Paper I**) for image analysis based baculovirus titration, Membrane Tools for analysis of live cell experiments (**Papers II, IV and VI**)

and *SPOTNIC* for analyzing TIRFM images of fluorescently labeled immobilized BBVs (**Paper III**).

The GUI components of a typical import module are shown using *Gen5 Tools* as an example (**Figure 2**). These include the main configuration window (**Figure 2, A**) and the plate simulator tabs for treatments (**Figure 2, B**) and events (**Figure 2, C**).

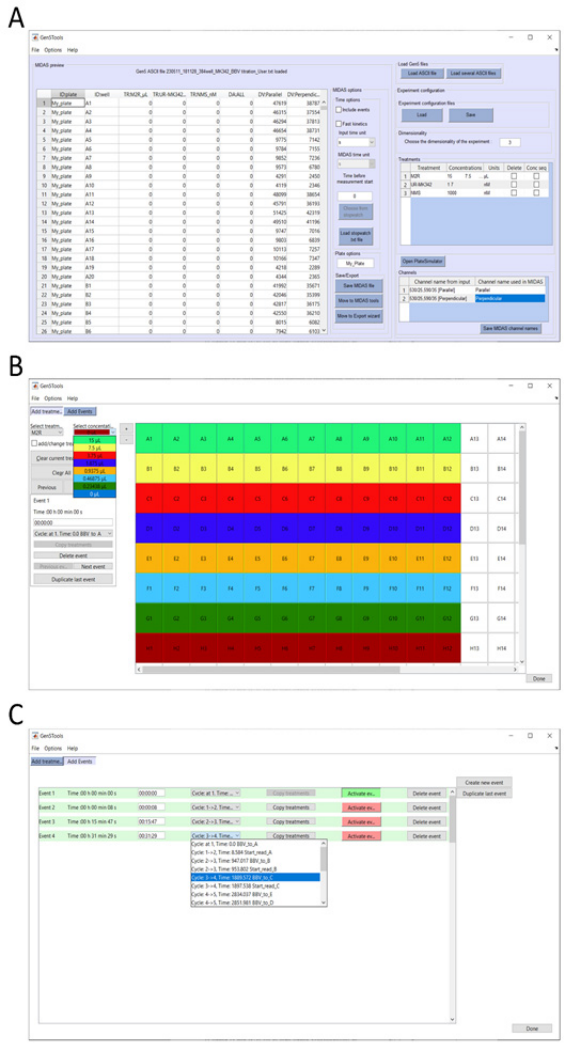

Figure 2. Graphical user interfaces of data import module Gen5 Tools. The main window of Gen5 Tools is shown (Panel A) with several visible panels such as MIDAS preview, Time options, Save/Export options, Experiment configuration panel and channels configurator. The Plate Simulator is accessible from the main window which consists of the Treatment tab (B) and Events tab (C). Treatment tab offers an intuitive way to add and remove treatments to or from the specific wells on the microplate while the Events tab allows to accurately describe the experiment time-line.

4.1.4. Export Tools module

The *Export Tools* module is the final tool necessary for data export to SB or other data analytics software. There are several important reasons to keep the data export separately from MIDAS file handling in *MIDAS Tools*. One critical aspect is that not all analyses utilize all the data available in a single MIDAS file. For example, only a subset of the wells or recorded measurements may be interesting for a particular analysis. The latter is especially common for imaging based assays where a large number of different image based measurements could be made initially with only some used for the routine analysis. For example, fluorescent spot analysis from TIRFM images using SPOTNIC module allows to calculate spot locations, sizes, spot counts, average and summed intensities of spots all of which were necessary during assay development but not all are needed for routine use (**Paper III**).

The main features of the *Export Tools* module include the possibility to group wells based on which data points they use as blank controls, add experimental replicates to subgroups, define formulae for data transformations, change the time units or choose a subset of time points for analysis and finally access and modify specific parameters unique to each of the export formats (**Figure 3, A**). The well grouping (**Figure 3, B**) can be performed using a GUI similar for adding treatments in the import modules (**Figure 2, B**). Formulae panel allows using both built-in as well as custom defined formulae. Export preview for IQMTools/SBToolbox 2 allows choosing which measured parameters to export, essentially allowing easy organization of data for multi-measurement fitting. For example simultaneous fitting of FA and total fluorescence intensity (TFI) is critical for correct interpretation of FA assay data in case of fluorophore quenching, bleaching or similar optical effects (**Paper V**). Finally, export to IQMTools also allows abstracting treatment names used in MIDAS files to be compatible with parameter names used in SB model definitions. Similar options exist for export to other software. The next chapters show in more detail how assays have been developed and used with the help of Aparecium software both for screening purposes and mechanistic modeling of GPCR ligand binding.

A

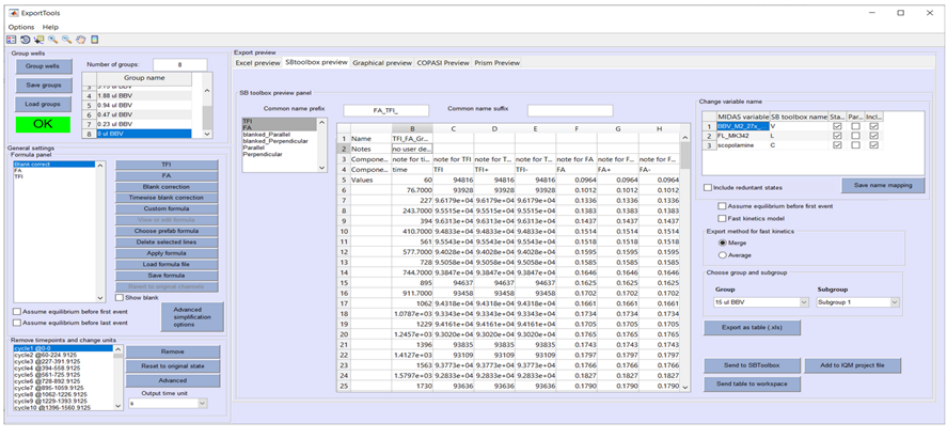

B

Figure 3. Graphical user interfaces of Export Tools module with IQMTools/ SBToolbox2 export preview and the grouping of a receptor concentration determination FA experiment. Export Tools main interface (A) allows to choose the number of groups and their names in the "Group wells" panel, enter calculation formulae in the "Formula panel", make adjustments to the experiment time-line in the "Remove timepoints and change units" panel and adjust SB software specific parameters in the "Export preview" panel (A). The grouping view of the Plate Simulator (B) allows to group and subgroup wells, set blank wells or set specific time-points or sets of time-points of wells as timewise blanks. Wells have specific color-based highlighting and tooltips based on the grouping, treatment and events to allow quick and accurate overview of the experiment and current grouping settings.

4.1.5. Analysis of event-based kinetic experiments

The most common plate-reader based assay formats rely on end-point measurements with a single mixing step in the beginning and a single measurement step at the end. Kinetic studies have much wider possibilities in terms of experimental design with the options to add or in some cases remove certain assay components potentially several times during a single experiment used for example for studying bivalent metal ion interactions with melanocortin MC_4 receptor (Link et al., 2020). These kinds of kinetic designs are beneficial as some biochemical reactions may be highly irreversible. The common assumption, often implicitly stated, that equilibrium can be reached during the measurement can be easily tested with kinetic events based assay designs by changing the time and order of mixing and concentrations of mixed components. As an example, event-based experimental design is applied for studying the ligand binding mechanism to muscarinic receptors in **Chapter 4.2.2** allowing to gain deeper insight compared to conventional equilibrium and exponential based kinetic models (**Paper V**). Sometimes, a more practical advantage of events based assay design is to save some valuable samples allowing to test several hypotheses in a single well. In cases where such experimental designs are used extensively, the structure of MIDAS files helps with both documentation of the experiment and modeling these results.

Aparecium supports describing these events by allowing a virtually unlimited number of events to be defined per experiment. Each event is described by time of occurrence relative to the experiment start time and changes in analytical concentration or quantity of each treatment defined in the experiment. From a practical perspective, Aparecium supports import of stopwatch files, which makes it possible to record sufficiently precise times of each event although manual possibilities for event time definitions are also available. Defining events in Aparecium is supported by several GUI convenience features. For example, event times can be quickly set by the prerecorded stopwatch timestamps, treatments can be copied from previous events, treatment values can be changed for a single or all events and events can be reordered. The overall set of features incentivizes the user to consider event-based experimental designs and to record all the necessary metadata.

4.1.6. Quality assurance in temporal measurements

Although event-based experimental design allows to reveal deeper kinetic mechanisms of ligand binding it requires careful consideration of the experimental data quality. The main concern with global fitting of ODE systems is the multidimensional nature of the independent and dependent parameter space. Usually the independent parameter space consists of the time dimension and one or several concentration or quantity dimensions. Here, it is crucial to reiterate that regression analysis assumes that all the measured values are independent and that the uncertainty in the dependent variable is much larger than in the independent variable. Fulfillment of these assumptions in global fitting of

kinetic data is not trivial in practice for plate-reader based measurements and is limited by some technical aspects.

Firstly, the individual measurements in the time dimension are not fully independent as required. A common example of this effect is caused by the uncertainty of concentration of an assay component, for example receptor or the ligand. This leads to all or a certain portion of the data points of the kinetic curve gathered from a single well in a kinetic binding experiment shifting in a systematic way. An apparently similar situation can be caused by difference in concentrations of an autofluorescent component in the measurement and blank wells. As blank wells are shared between multiple measurement wells, this can again introduce unwanted interdependence between individual data points.

Another assumption of the regression procedure is that there is no significant uncertainty in the independent variable. In case of plate-reader based measurements the risk of violating this assumption for the time dimension is substantial, especially in case of rapid kinetic processes. The cause of the problem is quite easy to understand – the time provided by the plate reader measurement output formats has no absolute connection to the experimental timeline even though the plate readers usually, in the lack of a better reference point, set the time point to zero when the measurement is initiated. From an experimental point of view the zero time point for a reaction is defined as the moment when the system components are mixed together or less strictly at any point in time where it can be assumed that equilibrium and analytical concentrations of components are equal. Furthermore, most plate readers also output the data in a tabular format outputting a single time value for the entire kinetic read. Finally, it must be taken into account that in microplate-based measurements the reaction can not be initiated at exactly the same time in every well. Usually, simultaneous addition to individual rows or columns can be achieved. Combination of all three effects lead to the so-called dead time being potentially different for each well and if ignored can lead to gross violation of regression assumptions and systematic errors towards apparently faster kinetics. Therefore, to avoid this problem, it is necessary to carefully correct the experiment time-line for these effects. Rather obviously, the influence of this effect is larger the faster the kinetic process under observation. Despite this concept being quite simple and the solution practically trivial, such corrections are not commonly used for plate-reader based kinetics measurements. Even worse, there is no standard for reporting if and how this effect has been accounted for in scientific literature with often just the general procedure and plate-reader model being reported. In some situations the effect is easy to identify. If several data points in a plate-reader based measurement are presented to have been made at exactly the same time point then it indicates ignoring the plate reader output format corrections. If the time between zero time point and first measurement point and subsequently between any two consecutive measurement points are the same, it indicates that the time shift between measurement start and reaction initiation has not been accounted for. This can of course only be used if the methodology suggests that the plate-reader cycle length was the limiting factor of measure-

ment frequency. A positive example where this effect seems to have been accounted for is a study of kinetic aspects of ligand bias of GPCR signalling (Hoare et al., 2020). Although more dedicated machinery or single well measurements could be used for precision kinetics measurements, these may not be viable options for HTS applications.

To illustrate the influence of this effect, the typical FA experiment for fluorescent ligand K_d, k_{on}, k_{off} and receptor stock concentration (R_{stock}) determination as demonstrated in several studies (**Papers IV, V and VI**), was simulated using the simple one-site binding model with and without taking into account the described time-shifts. Thereafter, the simulated data was fitted using global fitting with the same kinetic model used for the original simulation. This process was carried out using several combinations of K_d and k_{on} values (**Figure 4**). These results show that the timeline corrections are quite important at some parameter values and ignoring these causes substantial errors. As expected, the influence is larger the faster the association reaction. Also, lower affinity ligands seem to be affected more by this effect. The accuracy of k_{on} estimation is especially improved in two regions, firstly for ligands with k_{on} values around 0.1 to 1 $s^{-1}*nM^{-1}$ and around 0.1 nM K_d region and secondly for ligands with k_{on} values around 10^{-2} $s^{-1}*nM^{-1}$. In these regions k_{on} value overestimation (red) can be avoided (green) (**Figure 4**). Therefore, time corrections extend the measurement range of k_{on} by almost an order of magnitude. Such parameter values are also becoming more common, for example a set of high affinity NPY Y1 receptor fluorescent ligands have k_{on} and K_d values in the same range (Müller et al., 2022). Similarly large errors are expected in case of other plate-reader based kinetic measurements both for ligand binding and functional assays. Considering that $K_{d,kinetic}$ values are regularly reported with relative uncertainties around 10–20% or 0.04–0.1 Log_{10} units and then used later for statistical significance tests, then ignoring the systematic portion of the uncertainty can become a real problem for reproducibility. Furthermore, mechanistic kinetic models can be extremely sensitive to this kind of errors leading to poor fitting results and difficulties in differentiating between errors in data and errors in the model itself. These simulation results should not be taken as an absolute guideline of FA assay limitations as different assays may have different parameters such as levels of receptor expression, non-specific binding and fluorophore properties. Rather it serves as an example of the relative difference the time correction makes. Also, there is nothing particularly special about k_{on} and k_{off} as other kinetic parameters in different measurement setups would be affected similarly. The event based MIDAS format and Aparecium import modules effectively help to avoid this problem. These corrections have been systematically applied to data analysis for assays introduced in the next chapters.

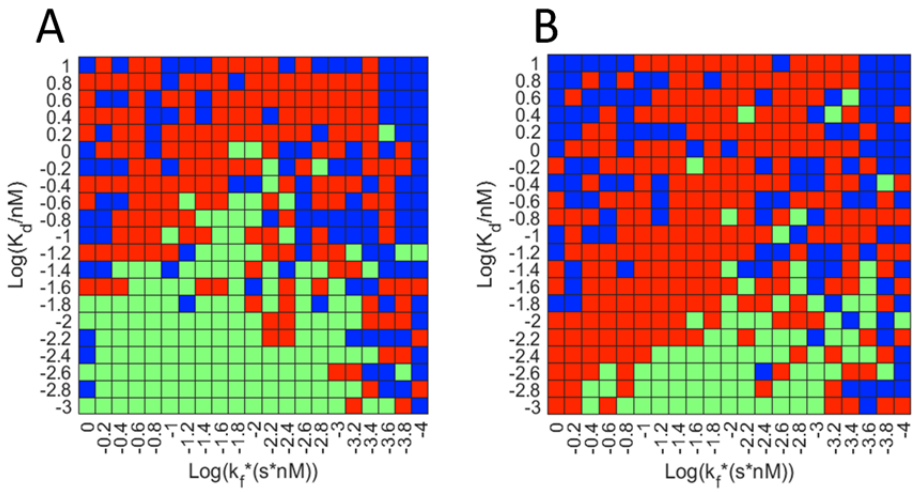

Figure 4. Theoretical dependence of second order association forward rate constant (k_f) estimation error on k_f and dissociation equilibrium constant (K_d) in case of all the described time-scale corrections applied (A) and in case of no corrections made to the time-scale (B). Green cells indicate conditions where the relative error was smaller than 10%, red cells show that the k_f value was overestimated by more than 10% and blue cells show that the k_f was underestimated by more than 10%. In ligand binding context k_f is equivalent to k_{on}. Limits of the simulation condition were chosen based on typical parameter range expected in the assays. A simple one-site binding model with non-specific binding possibility was used for both modeling and fitting.

4.2. Fluorescence anisotropy and budded baculovirus assays

In this thesis several BBV particle display system based fluorescence anisotropy ligand binding assays were developed. BBVs usually yield high concentration receptor preparations which are convenient to use for FA assays as it is possible to achieve the required ligand depletion to obtain changes in FA signal. Furthermore, BBV preparations are highly homogeneous in several ways. On one hand, BBV particles are sufficiently small to form a colloidal mixture meaning that problems such as sedimentation or concentration gradient formation are usually not an issue during the measurement. Although some evidence exists for aggregate formation in BBV samples, it is possible to combine filtration and mechanico-hydrodynamical disruption of the aggregates. This leaves only single BBV particles in the solution which do not further aggregate at experimental conditions as proven by TIRF microscopy (**Paper III**). In addition to short term stability, BBVs are stable for long periods at storage conditions. As BBV-s can be produced in large quantities at one time it is possible to perform a substantial number of experiments with the same production batch reducing the day-to-day variability of the results which may be more of a problem in case of live-cell experiments. The possibility to perform consistent experiments is further in-

creased by assay miniaturization to 20–30 µL total well volumes (**Papers III and IV**). Finally, BBVs also lack the down-stream cellular signaling and metabolic pathways meaning that the concept of chemical equilibrium instead of a steady-state can be applied to receptor-ligand binding reactions. Live cells, in comparison, require a much more careful approach, as the protein levels can vary from cell to cell and, furthermore, cells rely more on dynamic steady-state approximations than on true chemical equilibrium, which may complicate signal interpretation. These factors substantially simplify the data interpretation of BBV based FA assays allowing for better control of assay conditions for in-depth kinetic analysis.

In total, five different FA-based assays are considered in this thesis for M_1, M_2, M_4, D_3 and NPY Y1 receptors each with slightly different possibilities. With five FA assays available, the principles of meta-analysis can be applied to assess the similarities, differences and some emerging trends which helps to systematize the development process of such assays.

4.2.1. Similarities, differences and trends in FA assays

The main goals of FA assay development is to characterize the fluorescent ligand binding to the receptor source, BBVs in this case, and based on that assess how the probe and the assay could be used for investigation of GPCR ligand binding. This includes the determination of unlabeled ligand properties. The first and most critical requirement of the FA assay is the ability to discriminate between bound and free fluorescent ligand states. This is determined by the signal-to-noise ratio which depends on fundamental properties of the fluorophore such as effective molecular extinction coefficient (ε) and effective quantum yield (Φ), fluorescence lifetime (τ) and intrinsic anisotropy (r_0) in free and bound states as well as experimental parameters such as the concentration of the fluorophore in the free or bound state. While complete theoretical derivation of signal-to-noise ratios from these parameters is possible, some key properties can also be shown empirically (**Table 1**). As can be seen, the difference between replicates is the main driver of the noise with only a minor contribution from the signal fluctuation itself. The difference between replicates as well as standard deviation of the signal are quite constant across assays. What is interesting is that even for very small signal windows a considerable signal-to-noise ratio is achieved with very high predicted Z' showing that for many practical applications choosing the fluorophore based on maximum span (difference between upper and lower plateaus) is unnecessary giving space for optimizing other fluorescence ligand parameters such as affinity, kinetic properties, chemical and photostability, lipophilicity or usability across different methods. Based on current data, it would seem that spans of around FA 0.02 units are enough to achieve an excellent assay with Z' over 0.5.

Table 1. Sources of uncertainty and quality parameters of different FA assays.

Receptor	Ligand	Fluoro-phore	$\sigma(FA)_t$	$\sigma(FA)_{replicates}$	Span	Signal-to-Noise ratio	Esti-mated Z'
M_1R	UR-CG072	TAMRA	$6*10^{-4}$	$1.6*10^{-3}$	$1.5*10^{-2}$	4.88	0.79
M_1R	UR-MK342	TAMRA	$4*10^{-4}$	$1.7*10^{-3}$	$3.4*10^{-2}$	10.9	0.91
D_3R	CELT-419	Cy3B	$3*10^{-4}$	$1.5*10^{-3}$	$9.0*10^{-2}$	35	0.97

The $\sigma(FA)_t$ is calculated as the standard deviation of 10 subsequent measurement points at stable FA signal. $\sigma(FA)_{replicates}$ is calculated as the average standard deviation of between replicate wells calculated based on 10 pairs of experimental replicates.

The second-most important parameter determined by FA assays is the affinity of fluorescence ligand binding. As the developed assays allow determination of apparent K_d values assuming the one-site binding model using both the equilibrium and in some cases also using kinetic data, it becomes possible to compare the two analytical methods more systematically (**Table 2**). Here, it must be noted that during this phase of assay development the simple one-site binding model is assumed as even in the case of more complex binding models, the apparent K_d is a useful heuristic for further experimental design. What emerges from the comparison of multiple studies is that when the simple one-site binding model is able to describe both the equilibrium and kinetic features, the $K_{d,,equilibrium}$ and $K_{d,kinetic}$ values are in most cases comparable in magnitude. However, in all cases kinetic analysis results in a lower estimated affinity compared to equilibrium modeling. This appears to indicate that even after waiting for a substantial amount of time, the system does not achieve full equilibrium state. Furthermore, applying common rules of thumb of waiting for three to five reaction half times may be unreliable for FA assay analysis due to second order kinetic conditions for which association half times depend on receptor and ligand concentrations. Waiting for all experimental conditions to reach three to five half times may also take a substantial amount of time and in some cases lead to other problems connected with evaporation, bleaching or receptor degradation. In contrast, kinetic analysis is able to estimate equilibrium conditions from pre-equilibrium data which is likely to reduce systematic errors during analysis.

Table 2. Comparison of apparent pK_d values obtained using equilibrium modeling or kinetic modeling.

Receptor	Fluorescent ligand	$pK_{d,\ apparent}$, FA equilibrium	$pK_{d,\ apparent}$, FA kinetic	Source
M_2R	UR-MK342	9.30 ± 0.11	n/a.	**Paper V**
	UR-CG072	9.36 ± 0.02	9.12 ± 0.04	**Paper V**
M_4R	UR-MK342	8.9 ± 0.5	8.9 ± 0.4	**Paper VI**
	UR-CG072	8.4 ± 0.4	8.1 ± 0.1	**Paper VI**
D_3R	CELT-419	9.38 ± 0.15	9.2 ± 0.5	**Paper IV**
NPY Y1 receptor	UR-MC026	10.0 ± 0.7	10.0 ± 0.3	**Paper III**

In the context of mechanistic modeling, the K_d can be viewed as just a single parameter, although important, that can be used to describe receptor-ligand binding process, but it is far from a universal descriptor as many other models of ligand binding may apply for different GPCRs or even GPCR-ligand pairs (Carvalho et al., 2021; Ilien et al., 2009; Jakubík et al., 2000; Kopanchuk et al., 2006). In this regard, it is even more primary to validate if the applied binding model at all defines parameters such as K_d or it is only an apparent value that can be technically obtained through fitting but may have little to no real meaning and has much more limited applications. Apparent affinities may also be highly dependent on some aspect of experimental design. Therefore, the ability of the FA assays to discriminate between different binding models is a critical aspect to consider. In case of the developed assays, several receptor-fluorescent ligand pairs displayed a clear deviation from the commonly assumed single binding site model and in all cases the deviation is revealed by raw kinetic data. In other cases such as the UR-CG072 to M_2R binding, the effect of fluorescence quenching can be easily identified and also quantified (**Paper V**). In case of NPY Y1 and dopamine D_3 receptors (**Papers IV and III**) the single binding site model describes the experimental data reasonably well giving more confidence to the validity of the results. The physiological relevance of these different models remains, however, somewhat elusive as BBVs still constitute a somewhat artificial system and the transferability of these models to other expression systems is not comprehensively explored yet, but comparison with nanoBRET assay for M_2R (**Paper V**) or with live-cell microscopy assays in case of M_4R and D_3R (**Papers V and IV**) shows quite similar kinetic and equilibrium behaviour for the fluorescence ligands.

Finally, FA assays are mostly applied for screening for unlabeled compounds. All the developed assays excel at this task. In cases where the Z' analysis was carried out, it indicated that the assays have very strong statistical power for finding the ligand hits (**Table 3**). It must be noted, that Z' calculation was not carried out in all studies with one of the reasons being the clearly different binding behavior of some of the competitive ligands thereby leading to systematically different lower plateau levels in case of different ligands and the methodology for taking this effect into account was only developed for the later studies. Such a situation happens for example in case of M_1R when binding to UR-MK342 (Danková, 2020). In these situations the standard Z' calculation logic would not be correct as the cross substance distribution would be constructed from multiple but still a small number of individual Gaussian distributions with different means and small variances. This resultant mixture distribution is not Gaussian itself and, therefore, applying standard deviation calculation with assumption of Gaussian distribution would lead to erroneously large plateau standard deviation and underestimation of the Z'.

Table 3. Z prime values of different FA assays.

Receptor	Fluorescent ligand	Z'	Source
D_3R	CELT-419	0.71	**Paper IV**
M_4R	UR-MK342	0.67	**Paper VI**
M_4R	UR-CG072	0.52	**Paper VI**

Moving further to competition binding analysis, all the assays were also suitable for this task. In case of M_1R, M_2R, M_4R and D_3R receptors the obtained results were also correlated with radioligand binding data obtained from scientific literature. In all cases the correlation of K_i values obtained from FA assay and literature radioligand binding was high with R^2 ranging between 0.93 and 0.95 (**Table 4**). Interestingly, in all cases the intercept was negative while slope was larger than unity leading to underestimation of affinities of low affinity ligands which usually were also agonists. This is expected considering that the lack of G proteins in the BBVs used in all cases means that the ternary complex between the agonist, GPCR and heterotrimeric G protein can not be formed. Associating this effect with lack of G proteins is, however, also has some problems as previous studies with 5-HT_{1A} receptors did not reveal sufficiently large differences in ligand binding IC_{50} values depending on the presence or absence of added G-proteins (Tõntson et al., 2014). Based on the current data there are no strong quantitative trends in the slopes or intercepts and there are substantial variations between receptors and also between different reporter ligands for a single receptor in case of M_4R. Again, one part of the explanation may be that the estimated K_i is just an apparent K_{app} instead of a true model parameter similarly to the K_d determination. Unfortunately, more complex parameters have not been gathered with necessary systematicity in the scientific literature making the comparison of the mechanistic model parameters somewhat infeasible at this time. It is also clear that determination of the slope and intercept suffer mostly from large variability in literature data present for some ligands. Of course some part of the differences may also be caused by other effects such as differences in membrane composition, curvature, posttranslational modifications or differences in experimental conditions such as temperature, ionic strength etc. Overall, the used FA assay development strategy yields useful assays which can be effectively applied for characterizing ligand binding to different GPCRs.

Table 4. Correlation coefficients, slopes and intercepts between pK_d-s of unlabeled ligand determined in FA assay and radioligand binding data obtained from scientific literature.

Receptor	Fluorescent ligand	R^2	Slope	Intercept	Source
M_1R	UR-MK342	0.95	1.03 ± 0.09	-1.6 ± 0.7	(Danková, 2020)
M_2R	UR-CG072	0.94	1.29 ± 0.11	-3.6 ± 0.8	**Paper V**
M_4R	UR-MK342	0.93	1.01 ± 0.05	-0.7 ± 0.4	**Paper VI**
M_4R	UR-CG072	0.95	1.10 ± 0.05	-1.3 ± 0.4	**Paper VI**

4.2.2. Kinetic models of ligand binding to muscarinic M_2 receptors

As proven, FA assays can be quite successfully developed for screening purposes and also for basic characterization of fluorescent ligand binding to GPCRs. However, as FA can easily be measured in kinetic mode, a more in-depth SB style mechanistic analysis becomes possible. Here the M_2 receptor displayed in BBVs is used as an example of how this analysis could be carried out, but deviations from one-site behavior can also be seen for M_1 and M_4 receptors.

4.2.2.1. UR-MK342 and UR-CG072 binding to M_2 receptor

4.2.2.1.1. UR-CG072 binding to M_2 receptor

UR-MK342 and UR-CG072 binding to M_2 receptor in both FA and nanoBRET assays is extensively described in **Paper V**. Despite achieving generally good signal-to-noise ratios, some less common properties of this system became clear. One discovered problem was the quenching of UR-CG072 upon binding to M_2R (**Figure 5, A2, B3 and B4**). The fluorescence quenching was substantial with a decrease in fluorescence intensity by 27±2% upon binding to the M_2R displayed in BBVs. Direct measurement of quenching is quite challenging as the fluorophore remains in the solution as a mixture for free and bound states and it may be difficult to distinguish quenching from other effects such as bleaching. However, using global fitting of kinetic data of both FA and TFI in parallel for competition binding experiments it became possible to derive the extent of fluorescence quenching (**Figure 5**). One noteworthy advantage of this indirect approach is the possibility to test the hypothesis of quenching at variable time-points and with different competitive ligands thus allowing to rule out potential effects caused by experimental errors in single experiments or effects of different competitive ligands and also test if the quenching hypothesis remains true over time. Furthermore, the kinetic data allows following the dynamics of quenching by simultaneous fitting of FA and TFI values using a single set of kinetic parameters to show kinetic coupling between quenching and binding. From a technical point of view, it is also important to account for binding-induced quantum yield changes as ignoring it can systematically shift the apparent values of k_{on} and k_{off} and subsequently the K_d calculated from only FA data. The theoretical basis of this effect is explained by the following equation:

$$FA(t) = \frac{\sum_{i=1}^{n}\{FL_i\}_t * FA_i * FI_i}{\sum_{i=1}^{n}\{FL_i\}_t * FI_i}$$

Here, each fluorescent ligand state FL_i has its own characteristic intrinsic fluorescent anisotropy value FA_i and fluorescence intensity value FI_i which can be reduced by quenching while acting as the weight of the weighted average value. Therefore, quenching of the receptor-bound fluorescence ligand state leads to a

decreased predicted *FA(t)* at timepoint *t* value during association and can be misinterpreted as lower $[R_{bound}]/[R_{free}]$ ratio quenching is ignored. Of course, the quantum yield changes upon non-specific binding can also be taken into account within the same analysis.

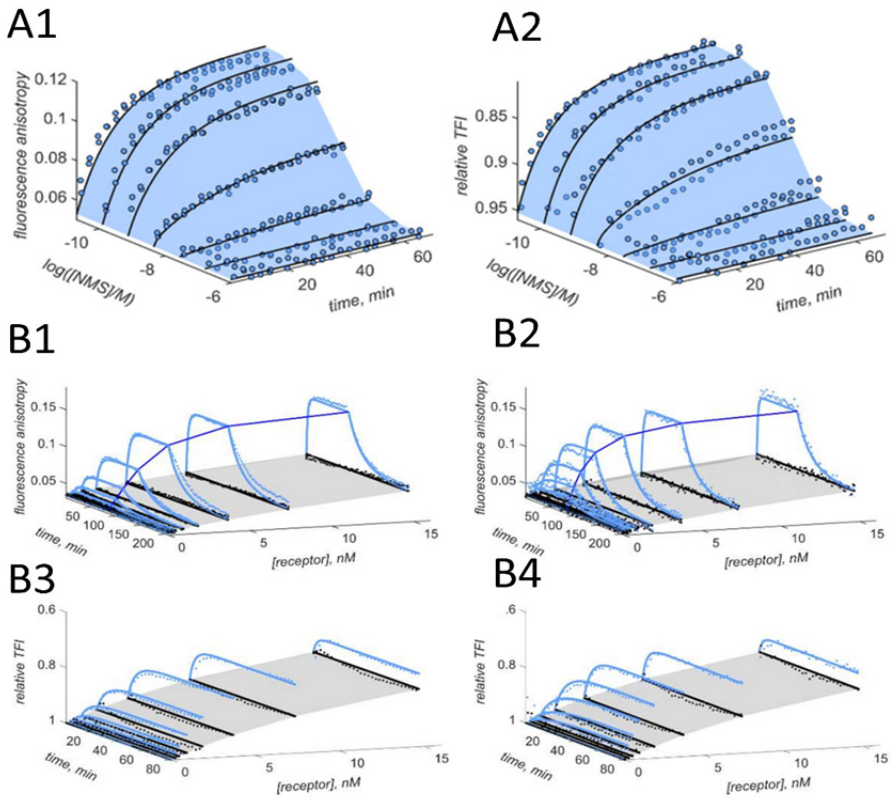

Figure 5. Global fitting of FA and TFI values in case of UR-CG072 binding to M_2R-BBVs. In competition binding type experiments, 1 nM UR-CG072 and NMS dilution series starting from 1 µM concentration was mixed with 10 µL of M_2R-BBV suspension. Both FA (A1) and relative TFI (A2) change was monitored in time. FA and TFI data was simultaneously fitted with a single ODE based model as described in **Paper V** assuming quantum yield change during binding and ligand depletion effects. Similar global fitting was carried out during saturation binding experiments (B). Again, FA (B1 and B2) and TFI (B3 and B4) were fitted simultaneously. In this case 2.5 nM (B1 and B3, blue dots and lines) or 0.5 nM (B3 and B4, blue dots and lines) UR-CG072 was used with a variable amount of M_2R present. The M_2R concentration was calculated from the BBV volume using the receptor stock concentration obtained from the fit. At 80 minutes, dissociation was initiated with 8 µM atropine. In non-specific binding samples (B1-B4, black points, lines and gray surface) 8 µM atropine was present in the wells. In all cases, reaction was initiated by the addition of M_2R-BBV.

Taking quenching into account allowed to determine the K_d, k_{on} and k_{off} of UR-CG072 binding to M_2R-BBVs which matched well with values obtained from nanoBRET assay (**Paper V** and **Table 2**). Additionally, it allowed to validate the use of this assay for competitive ligand binding screening. As an interesting coincidence, for determining affinities of competitive ligands, if both the 27% quantum yield decrease upon ligand binding and ligand depletion effects are ignored then the errors roughly cancel out. Therefore, K_i can be determined directly from IC_{50} values obtained from FA data only using Cheng-Prusoff equation (Cheng & Prusoff, 1973). It must be noted, that based on theoretical simulations (not shown), the 25–30% quenching is a "sweet spot" and such error cancellation does not work for other quenching values in which case the full global analysis accounting for quantum yield change is necessary to obtain accurate results.

4.2.2.1.2. UR-MK342 binding to M_2 receptor

As shown, solving the binding mechanism for UR-CG072 was possible by employing simultaneous modeling of FA and TFI values but still using the single binding site model. As it turned out, the binding of UR-MK342 to M_2R is a much more complex process with some interesting evidence as shown in **Paper V**. Firstly, equilibrium modeling of UR-MK342 and UR-CG072 binding to M_2R resulted in different concentration of total binding sites found namely 55 ± 7 nM for UR-MK342 and 35 ± 7 nM for UR-CG072. Secondly, two kinetic phases in both association and dissociation stages were found in both nano-BRET and FA experiments. Finding this two-phase behavior in two different expression systems, two different assay readouts and also similar behaviour of UR-CG072 in both assays makes it unlikely to be some kind of accidental pseudo effect of the binding assay. Taken together this evidence seems to indicate the existence of several distinct receptor binding-site pools. Furthermore, the disconnect between the proportions of slow and fast phases in association and dissociation stages (48% ± 2% fast binding in association vs 35% ± 3% in dissociation phase) suggest that the static and uncoupled existence of two binding site pools is unlikely to explain the obtained results, but no deeper insight could be gained using simple exponential fits for modeling this system.

To move towards solving this problem, additional kinetic FA data was included in the analysis (**Figure 7**). This data reveals several additional interesting features. Firstly, the presence of fast and slow dissociation phases is dependent on receptor total concentration with the fast phase only appearing in case of higher receptor concentrations. It is worth noting that only the bulk concentration of M_2R changes with changing BBV volume while the surface concentration of the receptor on BBVs remains constant. Secondly, the amount of M_2R-BBV required for the fast phase to appear depends on concentration of UR-MK342. A suitable model should be capable of reproducing these kinetic fingerprints at least qualitatively.

4.2.2.2. Tandemly arranged two binding site model

As the tandemly arranged two binding site model has been previously proposed for explaining kinetic effects of radiolabeled NMS and QNB binding this can be taken as a good starting point for this analysis (Jakubík et al., 2000; Kopanchuk et al., 2006). Although the original model for muscarinic receptor proposes two sites on a single receptor molecule, little proof was provided that the receptor is really a monomer with two binding sites. For melanocortin receptors the two tandemly arranged binding sites were already interpreted as the existence of dimers. Here, this model has to be modified to account for the specifics of FA assay. Namely, the fluorescent ligand *L* and competitive ligand *C* are considered as separate entities allowing to model all possible receptor-ligand complex combinations. Secondly, the BBV dependent non-specific binding of the fluorescence ligand is also considered. Thereby, system of following reactions is obtained.

Specific reactions:

R_R_ + L	⇄	RLR_	(Re1)
R_R_ + C	⇄	RCR_	(Re2)
R_RL + L	⇄	RLRL	(Re3)
R_RL + C	⇄	RCRL	(Re4)
RLR_	⇄	R_RL	(Re5)
RCR_	⇄	R_RC	(Re6)
R_RC + C	⇄	RCRC	(Re7)
R_RC + L	⇄	RLRC	(Re8)
R + L	⇄	RL	(Re9)
R + C	⇄	RC	(Re10)

and auxiliary reaction:

NBV + L	⇄	NBVL	(ARe1)

where *R_R_* is the receptor dimer with two free binding sites symbolized by the underscore (_), *R* is the receptor monomer, *L* is the fluorescent ligand, *C* is the competitive ligand, *RL* and *RC* are receptor monomer complexes with the fluorescent ligand and competitive ligand respectively and *NBV* and *NBVL* are free and bound non-specific BBV dependent binding sites respectively. The dimer is not symmetrical and in *RxRy*, *x* corresponds to the receptor-ligand being in the initial confirmation state and *y* corresponds to the isomerized state. The corresponding reaction scheme is presented on **Figure 6**. Although the existence of monomers is permitted in the general model, in this case the model converged to ignoring monomers and therefore, for simplicity, monomer variants are not included into further discussion.

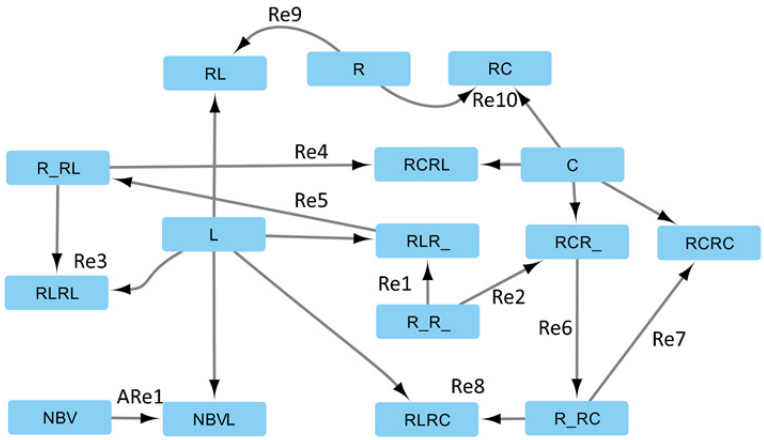

Figure 6. Visualization of the reaction scheme of tandemly arranged two-site model.

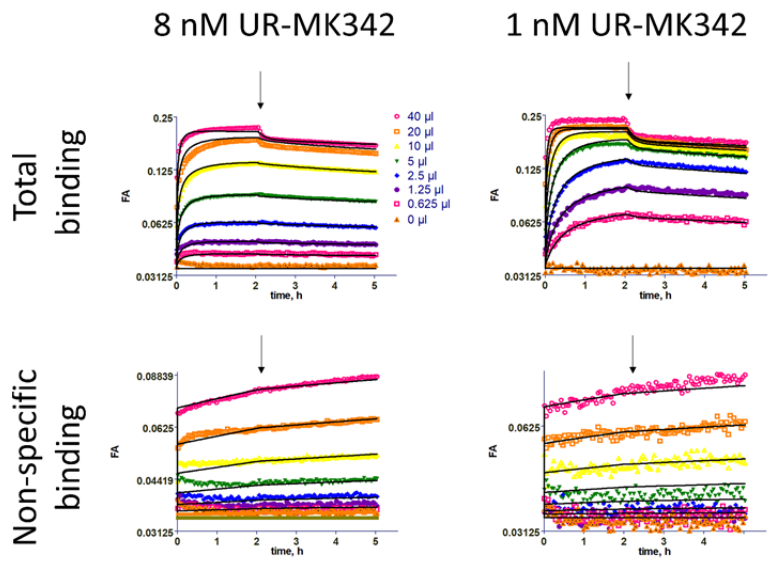

Figure 7. FA change in time of during association and dissociation phases of UR-MK342 binding to M_2R displayed on BBVs in case of total binding (top row) or non-specific binding (bottom row) and presence of 8 nM (left column) or 1 nM (right column) of UR-MK342 at variable amounts of used M_2R displaying BBVs. The arrow indicates the addition of 8 µM NMS. The Y axis is presented as logarithmic with base 2 for visualization purposes only. Global fitting was performed with the tandemly arranged two binding site model. Measurements were performed by Dr. Anni Allikalt.

The tandemly arranged two-site model gives a somewhat different explanation to the experimental observations compared to the equilibrium analysis (**Paper V**). This model is able to coherently describe several fingerprint behaviors (**Figure 7**). The first fingerprint effect is the appearance of a relatively fast FA decrease phase upon dissociation initiation followed by an extremely slow and practically linear decrease in FA for the remainder of the experiment in case of 40 µL of M_2R BBV and 8 nM UR-MK342 (**Figure 7, top row**). The second order fingerprint for this effect is that the fast phase completely disappears if the volume of M_2R BBV is reduced down to 10 µL. The third order fingerprint is that the same effects are visible in case of 1 nM UR-MK342, but the fast phase decrease has practically unchanged half-time but somewhat larger amplitude compared to 8 nM case. In addition, under these conditions the fast phase disappears between around 2.5 µL of M_2R-BBV, hinting that the loss of the fast phase seems to approximately depend on the M_2R-BBV to UR-MK342 ratio. The last fingerprint effect is the slow but steady rise in FA of the so called non-specific binding points, but the tempo of which depends on the volume of M_2R BBV stock present. It is also noteworthy, that true non-specific binding to BBV membranes is usually very fast and its kinetics can not be captured using a plate-reader. While the simplest explanation is that the non-specific binding is rising due to too low concentration of unlabeled ligand, it is not the case here as further addition of non-specific ligand does not reduce the FA increase rate at all. Finally, it should be clear that there are still clear disagreements between the model and the experimental data, especially at the higher volumes of M_2R BBV, and the nature of these effects remains unknown.

The parameter values of the best fit are given in **Table 5**. Firstly, the predicted $k_{fl} \pm$ SD is 0.0374 ± 0.0007 min^{-1} nM^{-1} which is in the similar range with the $k_{obs(slow)}$ of 0.048 ± 0.006 min^{-1} nM^{-1} and 0.052 ± 0.003 min^{-1} nM^{-1} determined for both UR-CG072 and UR-MK342 respectively in the nanoBRET assay in **Paper V** (Grätz et al., 2021). It is expected that these parameters are similar as the assays and the fluorescent ligand structures are quite similar (Table 1 of **Paper V**). The K_d for the first reaction (**Re1**) is 0.17 ± 0.01 nM which indicates much higher direct affinity towards the first binding site compared to the apparent K_d of 0.50 ± 0.15 nM obtained from equilibrium analysis. This difference is partially explained by the relatively high $K_{isomerizaton} = 6.9 \pm 0.5$ (**Re5**), which indicated that the isomerization itself is not an energetically favorable reaction, but it is necessary for the high-affinity binding of the second UR-MK342 molecule with a $K_{d,3}$ of 0.044 ± 0.005 nM (**Re3**). Therefore, the apparent K_d from equilibrium modeling is indeed expected to be somewhere between the initial tight binding affinity ($K_{d,1}$), effective affinity for the isomerized form ($K_{d,\ isomerized\ effective} = K_{d,1} * K_{isomerization} = 0.17$ nM $* 6.9 = 1.2$ nM) and binding of the second UR-MK342 molecule ($K_{d,3} = 0.044 \pm 0.005$ nM). A second quite important aspect explaining the difference is that the time of equilibrium modeling just before dissociation initiation does not represent the chemical equilibrium conditions according to this model as the concentrations of several components such as RLR_ and RLRL are still changing despite the fact

that both the modeled and measured FA values have remained stable for prolonged periods (**Figure 8**). While this conclusion is not unique to this system, it is still often assumed that signal stability reflects equilibrium and steady state without sufficient proof to this assumption.

Table 5. Best fit parameter values of the tandemly arranged two-site model

Parameter; unit		**Value**	**Uncertainty (SD)**
$k_{f,\ 1}$	$s^{-1}\ nM^{-1}$	$6.20*10^{-4}$	$1.1*10^{-5}$
$K_{d,\ 1}$	nM	$1.7*10^{-1}$	$1*10^{-2}$
$k_{f,\ 2}$	$s^{-1}\ nM^{-1}$	$1.98*10^{-4}$	$4*10^{-6}$
$K_{d,\ 2}$	nM	14.2	1.0
$k_{f,\ 3}$	$s^{-1}\ nM^{-1}$	$1.2*10^{-3}$	$1*10^{-4}$
$K_{d,\ 3}$	nM	$4.4*10^{-2}$	$5*10^{-3}$
$k_{f,\ 4}$	$s^{-1}\ nM^{-1}$	$1.8*10^{-6}$	$3*10^{-7}$
$K_{d,\ 4}$	nM	168	5
$k_{f,\ 5}$	s^{-1}	$9.1*10^{-3}$	$2*10^{-4}$
$K_{isomerization,\ 5}$	dimensionless	6.9	0.5
$k_{f,\ 6}$	s^{-1}	$1.09*10^{-6}$	$7*10^{-8}$
$K_{isomerization,\ 6}$	dimensionless	100	12
$k_{f,\ 7}$	$s^{-1}\ nM^{-1}$	$3.6*10^{-2}$	$5*10^{-3}$
$K_{d,\ 7}$	nM	11	1
$k_{f,\ 8}$	$s^{-1}\ nM^{-1}$	$1.6*10^{-4}$	$1*10^{-5}$
$K_{d,\ 8}$	nM	$1.8*10^{-2}$	$6*10^{-3}$
$k_{f,\ non\text{-}specific}$	$s^{-1}\ nM^{-1}$	37.7	$1*10^{-1}$
$K_{d,\ non\text{-}specific}$	nM	7700	400
$R_{stock,}$	nM	24.5	0.5
$Non\text{-}specific_{stock,}$	nM	80	1
FA_{free}	dimensionless	0.033	$2*10^{-3}$
$FA_{isomerized}$	dimensionless	0.184	$2*10^{-3}$
$FA_{shallow}$	dimensionless	0.218	$6*10^{-3}$
$FA_{Non\text{-}specific}$	dimensionless	0.164	$7*10^{-3}$

The table displays best fitted values of the parameters and using values obtained from independent experiments as well as expert knowledge and fit analysis for uncertainty estimation as for some parameters the instability and local minima of the fitting procedure itself cause the largest uncertainty.

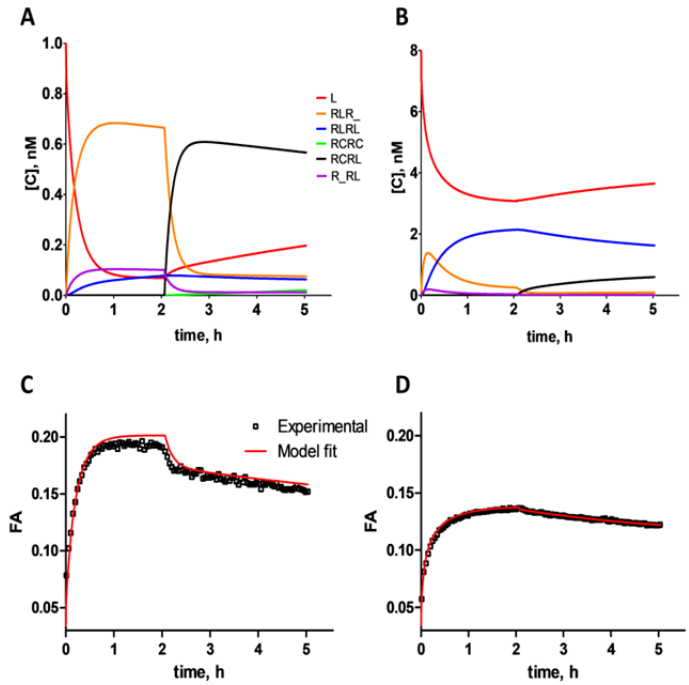

Figure 8. Simulation of concentrations of different receptor-ligand complex species during the association and dissociation type experiment using M_2R BBVs, UR-MK342 as the fluorescent ligand and NMS as the competitive ligand as described in **Figure 7**. Only the most dominant receptor-ligand species are shown (free fluorescent ligand L – red line; receptor dimer-fluorescent ligand complex before isomerization RLR_ – orange line; receptor dimer-fluorescence ligand complex isomerized form R_RL – purple line; receptor dimer-double bound fluorescence ligand complex RLRL – blue; receptor dimer – fluorescence ligand and competitor complex with the fluorescent ligand in the isomerized site RCRL – black line and receptor dimer- double bound competitive ligand complex RCRC – green line) (A and B). In parallel, the measured (black squares) and model predicted FA values (red line) are given (C and D). Two different experimental setups are shown namely mixture of 1 nM UR-MK342 and 10 µL of M_2R-BBVs mixed at time point 0 h (A and C) and mixture of 8 nM UR-MK342 and 10 µL of M_2R-BBVs (B and D). In both conditions, NMS with a final concentration of 8 µM was added at 2 h. 10 µL of M_2R-BBV corresponds to presence of approximately 2.4 nM receptor dimer and 4.8 nM total binding sites.

Secondly, it is interesting how the tandem two site model can explain the appearance of the fast and slow dissociation phases, and the disappearance of the fast phase if the UR-MK342 to M_2R-BBV concentration ratio increases beyond a specific level. In case of low ligand to receptor concentration ratio conditions (**Figure 8, A and C**), the RLR_ form dominates after the association phase but quickly disappears after dissociation initiation either by isomerization to R_RL form which in turn is quickly converted to RCRL or complete dissociation of

UR-MK342 from the receptor. The effect observed in FA is slightly amplified by the fact that the intrinsic FA of UR-MK342 in the isomerized binding pocket complex is lower compared to the predicted FA value in the non-isomerized case leading to larger drop in FA compared to the ratio of RLR_ converted to R_RL and amount of UR-MK342 dissociation from the RLR_ complex. Previously, the isomerized form of the binding pocket has been associated with a so-called deeper and higher affinity binding pocket (Jakubík et al., 2000). However, in this case, the unfavorable thermodynamics and lowered intrinsic FA both suggest that in the isomerized form the binding becomes somewhat looser instead allowing more rotational freedom to the fluorophore moiety. The slow phase of dissociation is then associated with the slow dissociation of the RLRL to form the R_RL complex and further inhibition of the dissociation of the second UR-MK342 molecule due to the rapid and stable formation of the RCRL complex driven by the high concentration of competitive ligand. In this situation the competitive ligand binding locks the UR-MK342 molecule into the isomerized binding pocket.

Conversely, when the ratio of UR-MK342 to M_2R-BBV is high, the equilibrium drives the system towards the formation of the RLRL complex due to the binding site depletion (**Figure 8, B and D**). This leads to the disappearance of the fast dissociation phase as the dissociation of the RLRL complex is very slow similarly to the previous conditions. The model also predicts that for a brief period after association initiation there is a period where substantial amounts of RLR_ complex is present and thus dissociation initiation in this time-window should again reveal the faster dissociation phase revealing another potentially interesting kinetic fingerprint region for this system and model. Unfortunately, some aspects of this model's validity remain unanswered as the effects would only become apparent after days of incubation, but carrying out such experiments requires more careful design as the combination of evaporation, protein degradation, and BBV conglomeration or sedimentation introduce additional effects which have to be into the measurements overshadowing the effects of this model. Therefore, other complementary methods and very specialized FA experiments are necessary for further exploration of this system. Additionally, it is also clear that the model is not able to explain all effects, such as the slower FA increase process in case of 8 nM UK-MK342 at 20 µL and 40 µL BBV concentrations. From this it can be concluded that there must be additional aspects to fully solve this system which the tandemly arranged two binding site model can not explain.

It is worth mentioning that there is no direct conflict between these results and the previous observation of the tandemly arranged two binding site model found in studies with radioligand binding studies using NMS and QNB (Jakubík et al., 2000). It is only expected that different ligands have different interaction profiles in such a complex situation and it is possible that the tandem arrangement of the binding sites can act with negative or positive cooperativity in case of different ligands or ligand combinations. However, an important difference from the previously proposed model is that the two binding sites are not present

on a single receptor molecule. One significant argument is that ligands such as UR-MK342 and UR-CG072 are quite large being composed of the pharmacophore, linker and the fluorophore making it extremely unlikely that sufficient free space remains anywhere close to the orthosteric binding pocket for the second ligand to bind. Of course, it is well known that muscarinic receptors possess a large allosteric vestibule, but based on the by-design bitopic nature of UR-MK342 and UR-CG072, most of the amino acid residues usually interacting with the allosteric ligand should also be either interacting with the fluorescent ligand or simply be sterically blocked. Finally, there are numerous studies suggesting the existence of M_2 receptor dimers in different systems making the dimer explanation more coherent with other findings (Marsango et al., 2018).

What is remarkable about the tandem arrangement of binding sites is that most evidence about the existence of this effect comes from kinetic binding data. However, the exact profile of the measured signal is highly dependent on the combination of model parameters making the fingerprint quite unique not only for the model itself but the exact parameters of the model. This, in turn, makes the recognition of this model quite difficult. However, as shown here, good data standardization practices provided by MIDAS files and Aparecium software can lower the barrier for attempting global modeling and such modeling an even more integral part of ligand binding studies.

From the pharmacological perspective if this behaviour would be extendable to live tissues, it could have interesting opportunities in terms of drug design. For example, such a cooperativity effect seems to lead to extremely slow dissociation rates which may allow the development of longer lasting drugs. In addition, it may be possible to design tetratopic ligands targeting the two orthosteric and two allosteric binding sites of a single receptor dimer simultaneously, potentially leading to unique pharmacology and extremely high affinities as well as improved muscarinic receptor subtype selectivity. Fortunately, some methods for studying these effects in tissues have recently been developed making the validation of these models feasible in more native systems (Marsango et al., 2022).

4.3. Imaging based live-cell assays

As shown, BBV based FA assays can be used for several useful applications. However, the questions of validity of the results in other GPCR expression systems remain. Therefore, a set of live-cell imaging based ligand binding assays were developed in parallel to cross validate both FA and live-cell imaging methods.

Dopamine D_3R has been in the focus of developing imaging based live-cell ligand binding assays both due to its physiological importance and simultaneously increased availability of potentially suitable fluorescent ligands. This opened up the opportunity to develop principally similar assays using several reporter ligands and subsequently directly compare the performances of the assays.

The first assay was developed using NAPS-Cy3B as the fluorescent reporter and using HEK293-D3 cell line (**Paper II**). Since similar assays had not been widely established at that time, the focus was on assay optimization and developing the optimization strategy. The assay setup required both more common and specific optimization steps. Critical ones included the cell density and incubation time allowed for cell attachment as well as cell culture technique. Automated imaging based assays set particularly high requirements for these parameters compared to regular plate-reader based spectroscopic assays such as FRET and BRET assays as systematic drifts in the dataset may significantly influence the performance of the entire assay. For example, cell aggregation, presence of overlapping cells and some detached cells may not significantly affect the performance of plate-reader based biosensor assays. Conversely, high-end imaging assays are usually not performed in fully automatic imaging modes and only a small number of cells, usually between a few to a few hundred cells are analyzed per data point. As the procedure for choosing which cells to analyze is often poorly described or even skipped in literature, it is not possible to say if cells were chosen randomly, completely hand-picked or something in between. Whether this should be considered cherry picking or not is highly dependent on the situation and is beyond the scope of this thesis. Nevertheless, manual procedures usually allow skipping cell aggregates or detached cells at the image acquisition phase, reducing the impact of such instances on the image analysis stage. Compared to plate-reader assays and high-end imaging methods, object segmentation based high-content imaging assays are much more sensitive to the quality of cell culture. The results of the optimization indicate that too high cell density leads to a substantial number of aggregates while too low density reduces the number of cells analyzed and therefore decreases the statistical power of the methods. In the end, 25 000 cells per well corresponding to roughly 15% confluency and 40 cells per FOV (area of 0.109 mm^2) was found to be suitable for the NAPS-Cy3B based HEK293-D3R assay. Choosing the correct incubation time after cell seeding is a somewhat more complex parameter. On one hand, the cell density increases due to cell division forming more aggregates but on the other hand, the total fluorescence signal window between the total and non-specific signal increases with time. The aggregate formation among other possible factors leads to heteroscedastic distribution of errors with increased intensity further complicating the situation (**Figure 9, A**). Therefore, the best incubation time was chosen based on the statistical significance between non-specific and total binding assay points. In this case, the 5 h incubation time point gave the largest statistical significance, but both 2 h and 24 h time points still resulted in sufficient statistically significant difference ($p << 0.01$) for a quantitatively strong assay.

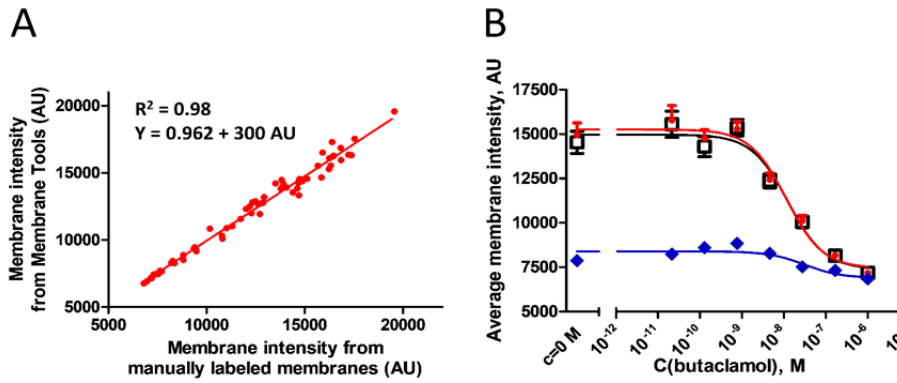

Figure 9. Comparison of average fluorescence intensities obtained by using manually annotated cell contours with random forest and morphological correction based cell contour prediction. HEK293-D3R cells were incubated with 1 nM NAPS-Cy3B and indicated concentration of (+)-butaclamol for 90 min. Different levels of intensity (A) were achieved by using different concentrations of competitive ligand (+)-butaclamol. Each data point represents the calculated cell contour intensity of a single FOV and the average pixel intensities of cell contours are presented as a.u. (Arbitrary fluorescence intensity units). The effect of different image analysis methods on estimating NAPS-Cy3B binding to D_3 receptors in competition binding experiment (B) as described in **Paper II**. Average membrane fluorescence intensities in a.u. (arbitrary fluorescence intensity units) were calculated: as average fluorescence intensity of the entire image (blue diamonds); as fluorescence intensity of manually detected cell membranes (red circles) and as fluorescence intensity of algorithm detected cell contours (black empty squares) and are presented as mean ± SEM. Average fluorescence intensity of the entire image and fluorescence intensity of algorithm detected cell membranes are representative experiments from three independent experiments. Manual detection of cell membranes was performed by three people for images from a single experiment. Data were fitted to the three-parameter logistic function.

For image analysis of the live-cell assay data the *MembraneTools* module of Aparecium was developed. *MembraneTools* has all the features of other Aparecium software import modules but also includes image-analysis specific features. These include the possibility to perform image quality control, use Ilastik (Berg et al., 2019) or Keras based ML and DL models for object segmentation and adjust some image-analysis pipeline parameters for example whether to correct the cell contour shape, use focused images or max-projection images for quantification and other similar options.

For NAPS-Cy3B HEK293-D3R binding studies, a random forest model in Ilastik was trained for cell contour segmentation which gave quite high quality results (**Figure 9**), although at the image analysis level metrics for the algorithm were not ideal achieving precision of 56.9% and recall of 45.6% (table 1 of **Paper II**). Such dissonance between assay quality and image level metrics can be explained by non-linear dependence between image level metrics and image

analysis pipeline contribution to assay uncertainty and is discussed more thoroughly in **Chapter 4.5.3**. Overall, the developed assay could be used both for saturation binding type assays for affinity determination in the classical radioligand binding setup as well as for competition binding with unlabeled ligands. The determined affinity for NAPS-Cy3B was 0.5 ± 0.4 nM which was in good agreement with the K_i of 0.7 ± 0.4 determined from radioligand binding assay using [^{3}H]raclopride. The only serious drawback of the assay was that HEK293 cells could not remain viable in the DPBS buffer for over four to five hours making kinetic measurements limited. The aspect of kinetic measurements was solved first for M_4R allowing for both association and dissociation kinetic measurements (**Paper VI**). Minor modifications to the assay setup were made such as using the cell medium (DMEM high glucose) allowing for longer measurements. The image analysis pipeline was also advanced further by replacing the Ilasik random forest for the Deep CNN U-Net model allowing to detect cells from single bright-field focal plane images rather than requiring a Z-stack and thus reducing the interval between sequential time-points. The same principles could be then applied again in **Paper IV** to validate a Cy3B labeled D_3R ligand CELT-419 by Celtarys Research for both FA and live cell assays. The modifications introduced for M_4R studies also allowed it to implement extended kinetic measurements for CELT-419 binding to HEK293-D3R (**Figure 10, A**) which allows it to gain more insight into the ligand binding process similarly to FA assays.

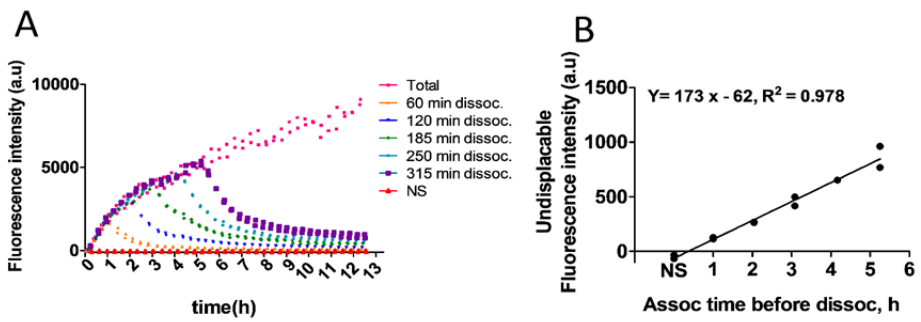

Figure 10. Time course of CELT-419 binding and internalization to HEK293-D3R cells. The fluorescence intensities were obtained as average detected cell pixel intensities of RFP channel images. Cell masks were obtained by cell segmentation of focused bright-field images using deep CNN U-Net model. The reaction was initiated at time point 0 min by adding 1 nM CELT-419 to 40 000 cells/well HEK293-D3R cells (A). After 60, 120,185, 250 and 315 min 10 µM spiperone was added to appropriate wells to initiate dissociation while total binding samples were kept as a control. In non-specific binding (NS) wells 10 µM spiperone was present from the start. Residual fluorescence intensity analysis was performed for each association + dissociation combination at 7 h post dissociation initiation (B). The residual intensity after different association time is described by a strong linear dependence with R^2 = 0.98. All wells were measured as duplicates with each replicate shown. The data is shown from a single representative experiment.

Kinetic study of CELT-419 binding in live cells indicated that an additional process besides ligand binding is occurring, albeit slowly, as some portion of the fluorescent ligand appears to have accumulated. The accumulation of undisplaceable CELT-419 is practically linearly dependent on the association time (**Figure 10, B**).

To confirm that CELT-419 is indeed internalizing to the cells, a higher resolution epifluorescence microscopy and TIRF microscopy was used. The results show that fluorescent puncta are clearly localized in the cell cytosol in case of total binding (**Figure 11, A2**) and in case of association followed by dissociation (**Figure 11, C2**) but no puncta are present in case of the non-specific binding (**Figure 11, B2**). Furthermore, the data shows that spiperone is only able to displace the fraction of CELT-419 in the plasma membrane (**Figure 11, D**). These conclusions are supported by TIRFM images where fluorescence is clearly localized to the basal membrane in case of total binding, but absent in the non-specific sample and in sample after dissociation (figure not shown). Videos of the internalized CELT-419 that the vesicles are being actively transported (**Figure 11, E**) as the movement is clearly directional with tracks showing high confinement ratios for some vesicles while some fraction of the vesicles also being stationary over 10 s time scale. Overall, the ability to quantitatively capture the internalization might have interesting future applications such as further development of image based HTS screening of GPCR internalization by using fluorescently labeled GPCRs even with lower end optical systems.

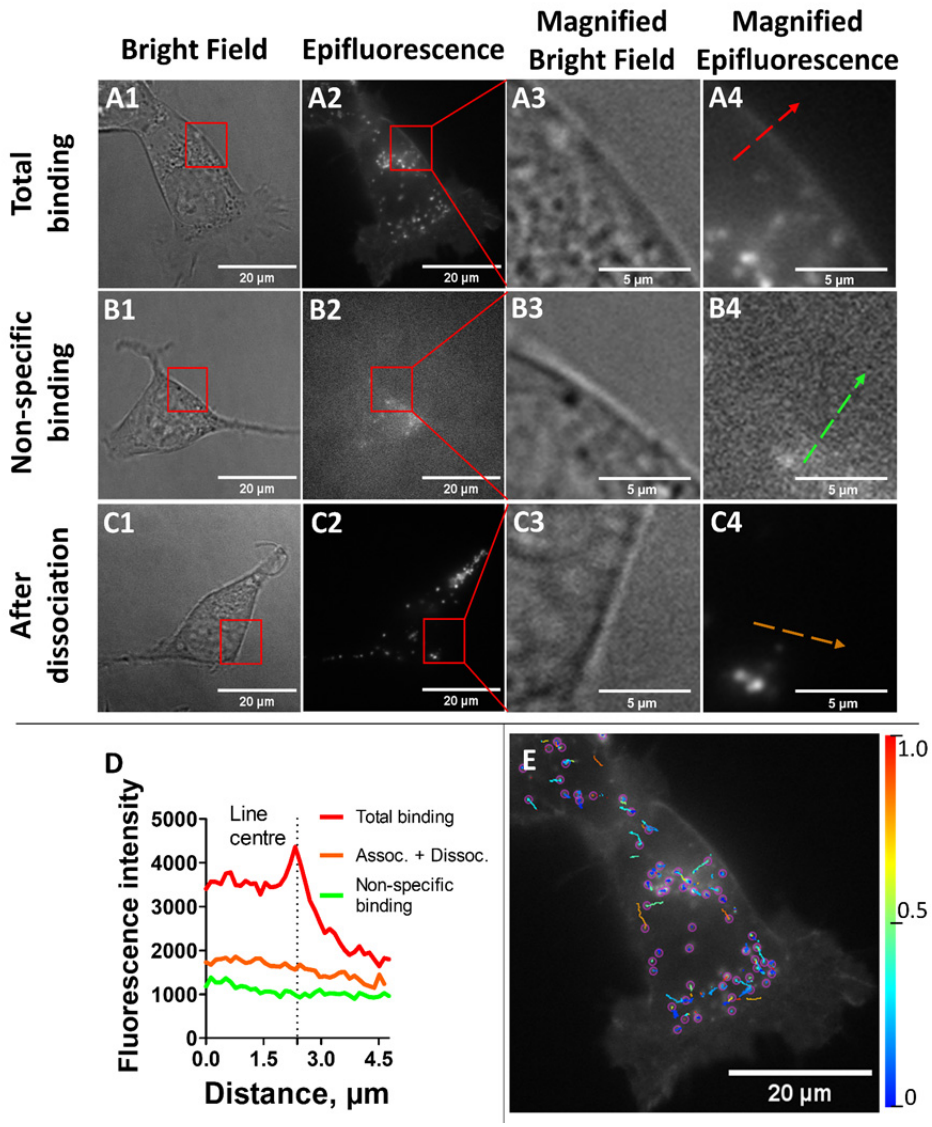

Figure 11. Bright-Field and epifluorescence microscopy images and spatial analysis of CELT-419 binding and internalization to HEK-D3R cells. Images of three different conditions are provided: Total binding (A1-A4), Non-specific binding (B1-B4) and association followed by dissociation (C1-C4). Bright-field (column 1), epifluorescence (column 2) and magnified views of areas within red squares of bright-field and epi-fluorescence images (columns 3 and 4 respectively). Line profile analysis was per-formed on the epifluorescence images (A4-C4) to assess the fluorescence intensity profile (D) of the lateral cell membrane. The line profile was centered on the lateral membrane and placed perpendicularly to the membrane based on the corresponding bright-field images. The extent and directions of the line profiles are indicated with arrows on magnified epifluorescence images (A4-C4). Particle tracking analysis results

of time-course of epifluorescence imaging (E). Tracking was performed over 200 frames lasting for 10.34 s. The image displays the last frame of the time-course with tracked particles labeled with a purple circle. Corresponding tracks are color coded based on the heat map and the value of the confinement ratio. Epifluorescence images corresponding to non-specific binding (B2 and B4) were contrast enhanced for visualization purposes only with the original quantitative values given by line profile analysis (D).

4.4. TIRF microscopy based ligand binding assay

FA assays and live cell microscopy are, as shown, powerful methods for ligand binding assay development, but have limitations for measuring binding of picomolar affinity range fluorescent ligands. To overcome this problem a total internal reflection microscopy (TIRFM) based assay using immobilized BBVs was developed.

TIRFM is a powerful microscopy technique and is particularly useful for ligand binding assay development. The principle of TIRF microscopy allows, similarly to the FA method, the photoselection of a subset of fluorophores. In TIRFM the photoselection process is based on the distance between the coverglass and the fluorophore with the probability of excitation being reduced exponentially with the distance from the coverglass surface. In practice, the excitation layer thickness remains usually in the range of 100–200 nm which results in approximately 10^6 improvement in photoselection over bulk solution measurement such as FA assays.

Applying TIRFM for immobilized nanoparticle imaging by using ultra-low non-specific binding pegylated coverglasses, it is possible to achieve single fluorophore detection and localization in situations when fluorophore spatial distribution is sparse enough. In this particular case, the developed TIRFM based method for studying ligand binding to NPY Y1 receptors utilizes immobilized BBV particles and a high affinity fluorescent TAMRA labeled ligand UR-MC026 (K_d = 100 pM) (**Paper III; Figure 12**). The BBVs are immobilized using the biotin-polyethylene glycol-cholesterol and neutravidin anchors to the pegylated coverglass with 2% of the PEG brush functionalized with biotin.

A unique aspect of the developed method is the generation and utilization of ultra low non-specific binding cover glasses (Figure 4 of **Paper III**), which in principle allow to push this assay to single molecule detection levels. However, as the size of BBV particles is around 50x50x200 nm, single molecule detection in this assay using BBVs is limited by the relatively high spatial density of the fluorophores on a single BBV particle and, therefore, it is more appropriate to consider the method to achieve single-particle detection and quantification. Nevertheless, for practical purposes, single particle detection resolution is sufficient for ligand binding assay development with appropriate data and image analysis techniques.

The developed assay allowed to simultaneously utilize multiple assay designs (Figure 5 of **Paper III**). For example, it became possible to perform saturation binding assays by varying either the concentration of the fluorescent ligand or the amount of BBVs similarly to radioligand binding assays. This is an advantage over FA assays where the fluorescent ligand concentration can only have small variations as in case of too low concentrations the fluorescence signal is hidden by the autofluorescence and scattering. Too high fluorescent ligand concentrations conversely induce too small changes in FA values. The situation with live-cell assays is the exact opposite. Fluorescent ligand concentration can be varied, but total receptor concentration level variation can´t be achieved with confluency variation while altering expression levels is often not that well controllable. The ability of TIRFM assay to cover both cases makes it a much more flexible method.

TIRF microscopy based ligand binding assay also has several advantages over FA assays in terms of suitable receptor systems themselves. One of the most important ones is that the TIRFM method only requires restriction of spatial diffusion of the fluorescent ligand upon receptor binding but not the restriction of rotational diffusion as is the case for FA assays. This is a significant advantage as the rotational freedom of the fluorophore moiety may change marginally or not at all in cases where the fluorophore is either not sterically locked upon binding, the fluorophore has very short fluorescence lifetime or the ligand itself is not a small molecule but rather a protein. The latter property is especially useful, as ligands of many GPCRs are large protein hormones such as hCG for LH receptor, Wnt protein for Frizzled receptors and follicle stimulating hormone (FSH) for FSH receptor. Conversely, fluorophores with very long fluorescence lifetimes may already depolarize the fluorescence even if the receptor is not bound to the receptor again leading to low signal-to-noise ratios. The developed TIRFM method may also be more suitable for more lipophilic labels thanks to the ultra low non-specific binding cover glasses (**Figure 12**).

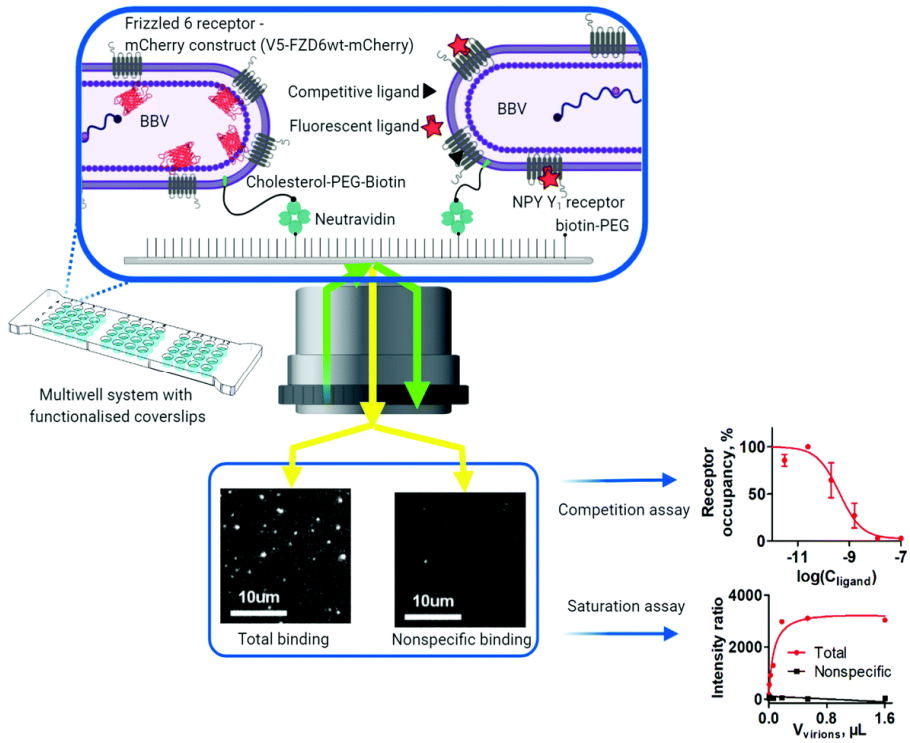

Figure 12. General principle of the TIRFM based assay for measuring ligand binding to NPY Y1 receptors displayed on immobilized BBVs. The BBVs are immobilized using the neutravidin and cholesterol-PEG-biotin anchors onto a biotin functionalized cover glass. As the fluorescent ligand binds to the receptor, the BBVs can be detected as fluorescent spots. Image analysis with SPOTNIC module of Aparecium software allows to measure fluorescent ligand binding to receptors as well as use the fluorescent ligand as a probe for measuring the binding of unlabeled ligands.

The developed assay may be developed further for kinetic assays. In this case the TIRFM could benefit from integrated microfluidic systems as further developments of the custom designed 48-well systems. Furthermore TIRFM potentially allows kinetic measurements by direct observation of ligand residence time but was not explored in this study. Of course, quantification of binding is not trivial in this case and for that the SPOTNIC module of Aparecium was developed for TIRFM image data analysis. The features of SPOTNIC module are presented later in **Chapter 4.5.2**. Overall, utilizing TIRFM in the displayed manner has some unique applications, less limitations compared to other assays and, therefore, has a unique niche among other ligand binding assays.

4.5. Development principles and quality control of image analysis pipelines

An approximate answer to the right problem is worth a good deal more than an exact answer to an approximate problem.
-John Tukey

Developing quantitative image-based assays have become increasingly practical as exemplified by the live-cell and TIRF microscopy based assays introduced in this thesis. Such practicality has been driven by the advancement of automated and more capable fluorescence microscopy systems, software, standards and to a large extent machine learning and especially deep learning algorithms. While powerful, these assays also present unique challenges regarding the quality control aspect which is an essential part of any quantitative analytical technique. There are several unique possibilities which are either unavailable or often impractical for other biochemical or molecular biology assays:

1) Images can be analyzed and reanalyzed several times with different algorithms often with negligible cost with all other sources of uncertainty being constant between different analyses.
2) Raw image data can be reanalyzed for a different purpose compared to the original purpose or combined with data from other sources. This is especially useful in the case of openly shared image datasets which helps the scientific community in development of more advanced algorithms.
3) Comparatively large amounts of data can be manually checked during result and data validation of the results as humans have very good visual capabilities at looking for trends, unexpected objects or other features which may not be readily or easily quantifiable. This essentially allows development of human-in-the-loop solutions where algorithms take care of most of the routine work while human analysts deal with the exceptional cases.

Some of the main challenges and questions during the development of a regular image-based microscopy assay are:

1) How to choose the best way to develop the image analysis pipeline?
2) Which samples can serve as a standard or control for microscopy based assay?
3) Which quality control measures should be taken to ensure the assay validity?
4) How to account for and estimate algorithmic uncertainty introduced by imperfect image analysis algorithms?
5) How to calibrate algorithms in case of drifts in the data?

Here, some general guidelines were derived from the developed assays. Although the developed principles may have many exception, they can serve as a good starting point.

4.5.1. Machine learning models for cell based assay development

4.5.1.1. Machine learning models for cell and cell contour detection

Computer vision has been a critical and irreplaceable method of cell based microscopy assays for decades, but before the development of powerful machine learning algorithms along with suitable software and computational hardware, many use-cases remained unfeasible due to the complexity and variability of image data. In this thesis a series of ML and DL models or image analysis pipelines were developed for segmentation of cells (**Papers I, IV and VI**), cell contours (**Paper II**) and microscopy artifacts (**Paper VII**).

While fundamental ML research is often concerned with developing new algorithms, ML architectures, loss functions and other similar topics, ML in this thesis was used in a relatively pragmatic and applied manner. The reason for this is twofold. Firstly, no matter the algorithm, a biased ground truth is likely to affect most naive algorithms. Secondly, it is well known that transfer learning is one of the most effective ways to adapt and calibrate existing ML models to new datasets (Zhuang et al., 2021). This relies on the users, most often a life scientist rather than a computer scientist, also being able to compose new datasets and carry out retraining and validation. Therefore, the goal was not to attempt to necessarily use the apparently best or most modern and often complex DL model architectures and techniques. Instead the focus was on finding user-friendly options in terms of both inference, training, robustness and data collection strategy which still contribute sufficiently small algorithmic uncertainty to the entire pipeline such that the down-stream application would not be impacted.

Several different tools were used as model training environments, namely Ilastik, Zero Cost DL For Microscopy (von Chamier et al., 2021) and also custom-built Jupyter notebooks.

Choosing the correct ML model and, therefore, the tool for the task is not trivial as it is *a priori* unknown which kind of relationship between image level metrics and algorithmic uncertainty contribution to assay uncertainty best describes the developed live-cell assays. The different options are outlined in **Chapter 4.5.3**. The first piece of information for establishing such relationships was based on the dopamine D_3R and NAPS-Cy3B live-cell binding assay in **Paper II**, where a random forest algorithm trained on manually annotated data for cell contour detection in Ilastik gives reasonably good results (**Figure 9**) although this technique is often considered to be inferior to many DL based CNN models such as U-Net. Therefore, in the next **Paper VI** for developing M_4R – UR-CG072 based assay, both the Ilastik pipeline and the more generic U-Net3 deep CNN model were both used and compared. The main difference from the initial assay developed for NAPS-Cy3B binding to HEK293-D3R cells was that in this case instead of segmenting the cell contour, the task was set to segment the entire cell body, which is a comparatively easier task. Somewhat surprisingly the image-level metrics for the two algorithms were quite different since the U-Net3 trained on the bright-field modality (U-Net3-BF-1) consis-

tently performing better in all used image-level metrics compared to Ilastik random forest model (RF-BF-2) while the assay level metrics were much more similar (**Table 6**). Furthermore, a second study based on the same dataset, discussed in more detail in the next chapter, studied the impact of anomaly removal on the quality of the assay. The results show quite clearly that the specific and direct anomaly removal strategy has much higher impact on the live cell assay quality compared to the assay level difference between the weaker random forest model and U-Net3 model.

Table 6. Image-level and assay-level quality metrics and binding parameters.

Metric	**U-Net3-FL-1**	**U-Net3-BF-1**	**RF-FL-1**	**RF-BF-2**
recall	0.94	0.86	0.91	0.72
precision	0.88	0.93	0.94	0.74
F_1 score	0.91	0.89	0.93	0.73
MCC	0.89	0.86	0.91	0.67
$R^2_{\text{competition binding}}$ (mean±SD)	N/A	0.93 ± 0.05	N/A	0.89 ± 0.09
$R^2_{\text{saturation binding}}$ (mean±SD)	N/A	0.87 ± 0.08	N/A	0.86 ± 0.13
$k_{on,UR\text{-}CG072}$, $s^{-1}*nM^{-1}$ (mean±SD)	N/A	$(3.4 \pm 1.4) * 10^{-4}$	N/A	$(4.8 \pm 1.7) * 10^{-4}$
$k_{off,UR\text{-}CG072}$, s^{-1} (mean±SD)	N/A	$(7.8 \pm 1.3) * 10^{-4}$	N/A	$(7.5 \pm 0.5) * 10^{-4}$
$K_{d\ kinetic,\ UR\text{-}CG072}$ (mean±SD)	N/A	2.6 ± 1.3 nM	N/A	1.7 ± 0.6 nM

The binding and image level model quality parameters were obtained using either the deep CNN U-Net3 or Ilastik based random forest (RF) algorithm on fluorescence images (FL) or bright-field images (BF). All values with uncertainty estimates are calculated considering each experiment as a single datapoint and uncertainties are given at the level of the standard deviation. Three experiments were used in case of R^2 saturation binding, k_{on}, k_{off} and K_d calculation. For competition binding R^2 values of 15 individual competition binding curves were pooled. Binding parameters were not calculated for U-Net3-FL-1 and RF-FL-1 as these models were trained to detect cells only for the generation of ground truth for the bright-field based models.

4.5.1.2. Anomaly detection and removal from live-cell imaging data using deep CNNs and weakly supervised approach

The greatest value of a picture is when it forces us to notice what we never expected to see.
-John Tukey

During the development of live-cell imaging assays described earlier it became apparent that several kinds of artifacts are often present in the bright-field and

fluorescence microscopy images. Closer inspection of these revealed that the ML models trained to perform the tasks of cell, cell contour or nuclei segmentation from bright-field images often tend to classify these objects as foreground objects instead of the background. This effect was not surprising as these artifacts on bright-field images share many common low-level image features with the cells and nuclei such as image edges and corners as well as some higher level features such as similar object size or overall contrast level. As an initial solution, a feature was added to the *Membrane Tools* module of Aparecium to manually annotate and remove these artifacts from analysis (**Paper II**). However, the manual annotation process is both restrictively slow with repeatability depending on human related factors which is far from ideal for quantitative assays. It is worth mentioning that the generation of artifacts can not always be avoided using laboratory techniques since the artifacts may include dead and detached cells, fragments of cell membranes, apoptotic bodies and other vesicles, microplate defects etc. Although some problems may be alleviated after substantial optimization and continuous validation of the cell culture, it would have a negative impact on the assay robustness. Despite the problem appearing to be significant enough to be addressed, hardly any research had been carried out to solve and explore this problem with only some classical CV techniques tried previously which usually do not generalize well to all situations, especially low contrast objects (Zhang et al., 2014). In parallel, reviewing datasets used for previous studies, the presence of artifacts was also discovered indicating that the problem is clearly not a specific feature of the particular assay system but a much more general one (Fishman et al., 2021). Considering these aspects, a technique for artifact detection and removal was developed and the impact of anomaly removal on assay quality was assessed (**Paper VII**).

The developed ArtSeg technique relies on a U-Net model specifically trained for segmentation of anomalies from bright-field images. The training technique of this U-Net model is, however, quite unique not necessarily requiring the manual annotation of the anomalies but instead relying on binary classification of training images into clean or anomalous images (**Figure 13, A**). Using such a technique of using image level labels for pixel level predictions is called weakly supervised learning. The transition between image-level labels and pixel-level labels takes place in a separate deep CNN model called Score-CAM (Wang et al., 2020). During the training phase of the Score-CAM model, a binary classifier is trained to attempt to classify images into the clear or the anomalous classes. However, instead of using the classification results, the activation maps of the network are used, which reveal the areas on the image which were most impactful for the network classification decision. The obtained activation maps are then binarised by thresholding the activation maps and used as the ground-truth for training the U-Net model.

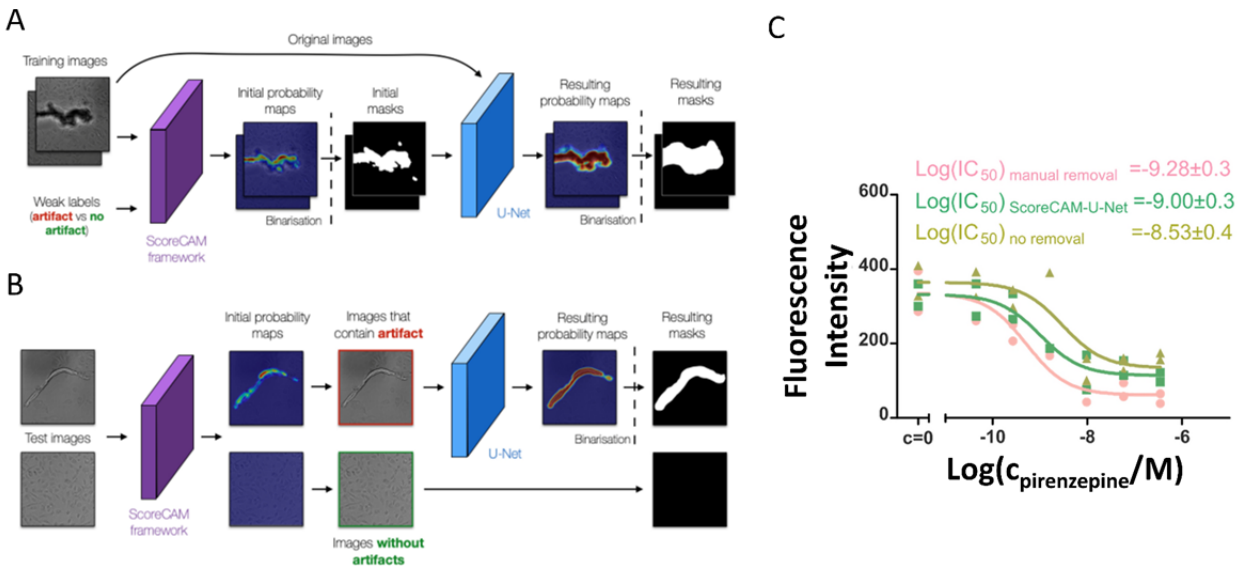

Figure 13. Principle and impact of artifact removal using ArtSeg technique (**Paper VII**). The model training pipeline (A) uses image level labels (weak labels) to train a ScoreCAM model and the ScoreCAM output is used directly as training input for the U-Net model. The inference pipeline (B) uses the trained ScoreCAM model for initial image classification and the U-Net model for artifact segmentation. In practice, the ScoreCAM model can be skipped during inference and only the U-Net model can be used. Competition binding curves (C) fitted using the Hill equation with Hill coefficient set to -1 of pirenzepine using 2 nM UR-CG072 as the reporter ligand in live-cell microscopy assay with CHO-M4 cells as described in **Paper VI** and **Paper VII**.

When applying this model (**Figure 13, B**) for anomaly removal from the microscopy images of CHO-M_4R cells, it turns out to be quite successful: manual anomaly removal, automatic anomaly removal and no anomaly removal yield average R^2 of 0.89, 0.86 and 0.74 respectively as average coefficients of correlation for competition binding curves (**Table 6 and Figure 13, C**). However, the segmentation intersection over union (IoU) scores remained only at the level of around 0.2, which is usually not considered excellent. Although a slightly different set of experiments was used for comparing U-Net3-BF-1 and RF-BF-2 models (**Table 6**) than the anomaly removal methods, it is clear that anomaly removal has a much higher impact on assay quality than switching from random forest based model to a U-Net model at least when quantifying whole cell fluorescence intensities based on cell segmentation from bright-field images. This also serves as an interesting case study for analysis of algorithmic uncertainty presented later.

4.5.2. SPOTNIC module for immobilized nanoparticle TIRFM image analysis

Similarly to live-cell binding assays, TIRFM assays rely heavily on appropriate software and algorithms for both data organization and image analysis. For spot detection and analysis with the developed experimental setup for NPY Y1 receptor ligand binding, application of ML models was not necessary, but questions about importance of image analysis pipeline quality are similar. During the design of Aparecium software SPOTNIC module, several options were considered as a number of spot detection algorithms and plug-ins have been implemented previously (Aguet et al., 2013; Albrecht et al., 2017; Mashanov & Molloy, 2007; Stein & Thiart, 2016). Attempting to establish and optimize an assay using only image-level metrics may result in biased assays, overstating the importance of the problem being solved or overlooking the real source of uncertainty. Therefore, the algorithm parameter optimization capability was prioritized along with the possibility to use assay level metrics as optimization target. This was most convenient with a custom software solution but using a previously published algorithm.

The used algorithm was based on 2D Gaussian approximation of the point spread function and subsequent sub-pixel localization (Aguet et al., 2013). In the context of this study the algorithm had two optimizable parameters: σ, corresponding to the expected radius of the spot in pixels and detection threshold. The optimization results showed that the quality of the algorithm is quite dependent on the choice of parameter values with a region of stability in terms of threshold around σ value of 2.1 px and the entire surface having a clear maximum (**Figure 14**). Anyhow, performing parameter optimization using assay quality metrics allows to find a more correct and absolute quality and impact of the image analysis pipeline compared to using image level metrics.

The found optimal value was used for the further analysis in the TIRF assay. It must be noted that although parameter optimization resulted in clear improve-

ment in the assay parameters, the R^2 remained quite far from unity pointing towards either the incapability of the used algorithm to achieve close to perfect quantification, remaining problems with the sample preparation, cover glass functionalization, the measurement process or combination of multiple of these factors. In either case, this algorithm was sufficient for the development of the assay as shown in **Paper III**.

This study has by now sparked new projects for example using different types of nanoparticle samples, building of a somewhat different TIRF microscope and optimizations of the coverglass functionalization process, all of which can reuse SPOTNIC module to repeat similar optimizations and TIRFM data analysis.

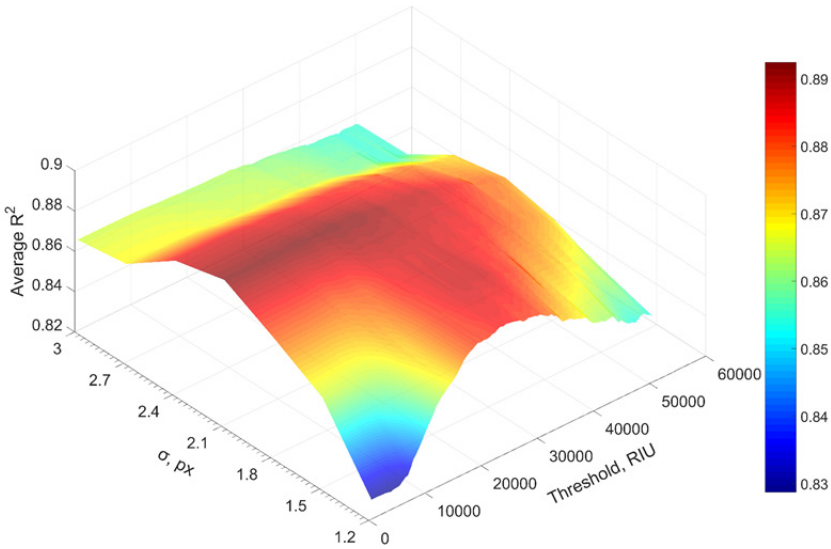

Figure 14. Dependence of average coefficient of determination (R^2) on spot detection algorithm parameters. The fluorescence image intensity threshold was varied in the range of 0 to 60 000 at 100 unit intervals and the expected spot intensity 2D Gaussian distribution standard deviation was varied between 1.2 to 3 px at 0.3 unit intervals. Each parameter pair combination was used to run the entire image analysis procedure of the entire dataset with three saturation binding experiments with UR-MC026 concentration variation, three saturation binding experiments with NPY Y1R concentration variation experiments and twelve competition binding experiments using MC-026 as the tracer ligand and UR-MK299, BIBO3304, pNPY and PYY as competitive ligands. The resulting average spot intensities were used to automatically fit appropriate non-linear regression models to the obtained data and the obtained R^2 of all experiments were pooled for that combination of parameter values.

4.5.3. Algorithmic uncertainty of image analysis pipelines

Reporting quality metrics for image-analysis pipelines or their subcomponents has become a standard and required step in validation of these pipelines. A vast majority of publications use a relatively small number of widely accepted metrics for quality assessment. Such metrics usually include precision, accuracy, recall, F1 score (Sorensen-Dice index), Jaccard index, Intersection over Union (IoU), Mathews correlation coefficient (MCC) or Area-under-curve (AUC). One common feature of all of these metrics is that the values depend on only the predicted and expected images (ground truth) as an input. On one hand, using these metrics it is quite a practical and universal solution, as this allows comparison of different algorithms or pipelines across a wide variety of datasets. In addition, numerous studies have been carried out developing methods for uncertainty estimation of ML and DL models, usually in terms of the same metrics (Abdar et al., 2021). However, much less attention is paid to the quality of ground-truth itself, especially to the systematic errors in it which may very well be the largest uncertainty component, potentially leading models to also learn and overfit to the biased ground truth data. On the other hand the few image level metrics may tell very little about the absolute uncertainty introduced into the assay result by employing a particular image analysis pipeline. The reason for this discrepancy is that these metrics are not always the best predictors of overall assay uncertainty. For example, in segmentation and detection tasks, not all pixels or objects are equally important for the final assay result. It can be easily imagined that the quality of carrying out tasks such as nuclei or more generally any object counting are quite robust against mask image erosion (making object segmentations slightly smaller) at least if the image objects are not touching. Conversely, adding salt-and-pepper noise to the masks would generate potentially a large error in the number of objects if counted by connected component analysis. Obviously, the image level metrics such as precision and recall would not change substantially in either case. Although this is an extreme situation of an oversimplified problem, the same conceptual situation happens in real problems too. Usually, this leads to a situation where the used metric or loss function merely correlates with the algorithmic uncertainty contribution to the final task and the shape of the resulting function may take a variety of forms (**Figure 15**). Essentially, the shown effect is a variation and concretisation of the well known GIGO (garbage in, garbage out) principle which itself is not very strictly defined. One approach to solve this problem is to use a trained model for image inference and calculate the value of the downstream assay level metrics and the corresponding uncertainty contribution of the image analysis pipeline. This would help to avoid choosing the best image-based model (BIM) according to image level metrics instead of the best downstream-based model (BDM) based on assay level metrics (**Figure 15 right panel**). Another risk that can be mitigated by using down-stream metrics is the use of systematically biased ground-truth data which could otherwise lead to a situation, where increasingly better models in terms of image-based metrics pass through

an optimal point and further increase of image-based metrics lead to worse models in terms of assay quality (**Figure 15, gray line**). Of course, the assay uncertainty estimation may also be systematically biased so choosing which type of ground-truth is more reliable is ambiguous in many situations and may require case-by-case analysis.

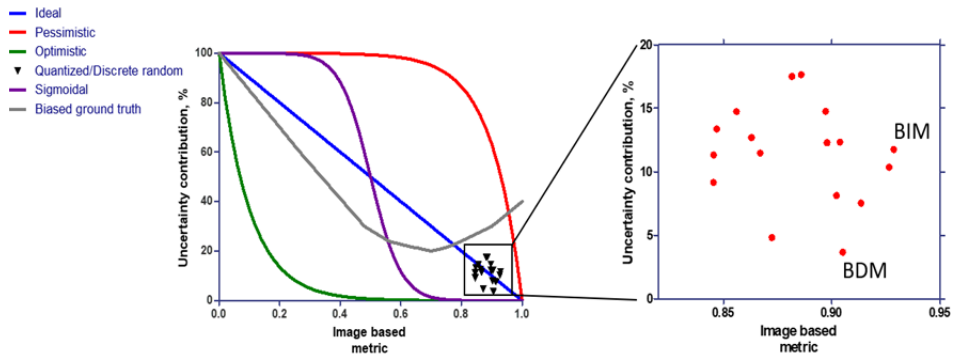

Figure 15. Simulations of different possible types of relationships between a hypothetical image based metric and the corresponding algorithmic uncertainty contribution to an imaging based biochemical or biological assay. Left panel shows the behavior of different situations over the entire range of image-based metric values. Ideal case (solid blue line) represents the situation, where the image based metric perfectly correlates with the algorithmic uncertainty. Pessimistic case (solid red line) represents the situation where the image based metric is good, but the uncertainty contribution remains high. Optimistic case (solid green line) represents the situation where even an image analysis algorithm with marginal quality results in a small or negligible contribution to uncertainty. Sigmoidal case (solid purple line) represents the situation where a small window of change in the image based metric results in a large change in uncertainty while a small or negligible uncertainty condition is achieved with a much lower image based metric than is considered to be good compared to state-of-the-art solution. Biased ground truth case (solid gray line) represents a situation where increase of the image based metric leads to systematic increase of uncertainty contribution due to the image-based ground-truth containing a systematic bias. A case representing real world scenario (black triangles, left panel and red circles, right panel) where a continuous line can´t be achieved and instead each data point represents the performance of a single trained model. BIM indicates the best image metric-based model, BDM indicates the best downstream metric based model.

There are several options on how to choose the down-stream metric. One option is to use an alternative or standardized assay in parallel with the assay being developed. Such an approach is often used for analytical methods and is most useful in situations where such a standard or alternative assay is available, but suffers from either limited useful range, cost, robustness, time to result, need for special equipment, poor portability or other similar factors. Such cross-validation approach was taken for developing an assay for baculovirus titration where two alternative assays were used for the validation of the Image-based Cell Size

Estimation (ICSE) assay (**Paper I**). A different, down-stream parameter based approach was taken in the case of developing a live-cell imaging based ligand binding assay for studying fluorescence ligand NAPS-Cy3B binding to dopamine D_3R (**Paper II**) introduced earlier. In that case, several different ways to assess the downstream assay quality were used. One option was the direct comparison of obtained fluorescence intensity via manual cell membrane segmentation and cell membrane segmentation employing a ML based algorithm (**Figure 9, A**). The second option was comparing the concentration response curves obtained using both approaches (**Figure 9, B**). The two downstream assay level metrics are complementary, as the direct fluorescence intensity comparison would allow algorithmic uncertainty estimation even if the mathematical form of the concentration-response curve was unknown, as deviations from logistic function may be common for different assay setups. In addition, the high correlation between the two different methods allows more easy transferability of the conclusions to different assay designs. On the other hand, the competition binding curve comparison approach is better at visualizing the context of the results, such as assessing if larger errors appear in the plateau or slope region. In addition, the difference in predicted IC_{50} values are easier to interpret in terms of the assay´s predictive ability. In cases where manual ground truth is not available, it is also possible to optimize for the maximum agreement between the data and the expected general functional form of the data. Excluding trivial solutions, this approach is likely to converge towards not only the optimal shape of the curve but the real expected curve. This kind of approach was for example taken for optimization of algorithmic parameters for spot detection with SPOTNIC module in **Chapter 4.5.2** (**Paper III**), assessment of the quality of anomaly removal algorithm (**Paper VII**) and also in comparing the real impact of quality difference between random forest algorithm and U-Net in for M_4R live cell microscopy assay development, as described in **Chapter 4.5.1.1** and **Paper VI**.

Overall, the proposed approach of focusing on the down-stream assay level metrics has several practical applications essentially indicating the sensitivity and robustness of the assay in terms of image analysis related aspects and helping to guide the assay optimization and validation process. For example, in case of the optimistic scenario the technically complicated process of algorithmic uncertainty determination of the ML model can be skipped during assay development as the uncertainty contribution would be negligible in any case. Conversely, the pessimistic case indicates the need for better models or direct estimation of the algorithmic uncertainty. Finally, the biased ground-truth case indicates the need to work on the model ground truth. It must be noted, that the different behaviors here are not the only possibilities and in some cases even a naive image analysis method e.g calculation of average intensity of the image may not contribute significantly to the assay uncertainty.

5. CONCLUSIONS

GPCRs signal transduction is a complex biological system and better understanding of it is crucial for drug design. Despite the importance of GPCRs and scientific effort invested into studying them, many GPCRs remain undrugged while many existing drugs have serious side effects or are not similarly effective for all population groups. Gaining deeper mechanistic knowledge about GPCRs remains difficult as no single method can answer all questions and there are methodological gaps stopping some questions from being answered. These include image analysis tools for microscopy image analysis, development of novel fluorescence probes for development of advanced fluorescence based assays and difficulties in applying systems biology approach to GPCRs and aspects related to data collection, standardization and sharing.

In this thesis a new software, Aparecium, was developed for measurement and experimental data standardization, image data analysis and data export to systems biology software. Aparecium allows integration of measurement data and experimental data into a single information unit, the MIDAS file, which can be shared according to FAIR principles and used for data storage during long and highly collaborative projects. Aparecium allows the conversion of plate-reader as well as image data into the MIDAS format as well as data export to different analysis platforms providing a single gateway for plate-reader based assay data analysis. Use of these features is exemplified during the development of several assays for measuring ligand binding to different GPCRs.

In total five fluorescence anisotropy based assays using budded baculovirus particles for muscarinic M_1, M_2 and M_4 receptors, dopamine D_3 receptors and neuropeptide Y Y1 receptors are covered using the meta analysis approach. The kinetic fluorescence anisotropy data of M_2 receptor is used for deeper mechanistic exploration of ligand binding to this receptor going through a typical quantitative global analysis process using an ODE system based model. In this case, the kinetic data suggests that muscarinic M_2 receptors exist as dimers in BBV particles with allosteric modulation between the binding sites on monomers following the tandemly arranged two-site model.

Next, general principles of developing high content screening compatible live-cell based assays and total internal reflection microscopy based assays using immobilized budded baculovirus particles are covered. Both types of assays are suitable for different purposes. Live-cells contain similar signalling systems to live tissues making these a somewhat closer system to physiological conditions while total internal reflection microscopy assay using immobilized baculoviruses allows the measurement of extremely high affinity interactions, potentially down to single fluorescent molecule detection.

Finally, as imaging based assays rely on advanced image analysis algorithms, machine learning models and software, a closer look is taken at the role of machine learning model properties in the context of bioimage analysis pipeline quality. The analysis of the final uncertainty contribution of the image

analysis pipeline reveals that in different situations, the impact of using deep learning models over more classical machine learning models can vary widely. Using more advanced models can sometimes provide only negligible returns in terms of final assay quality while image level metrics would suggest otherwise. Conversely, in other situations using a machine learning model even with marginal image-level metrics can significantly increase the assay level quality. Therefore, during the development of imaging based assays, looking at the impact of algorithmic changes on the quality of final assay level metrics can guide the development of image based assay development and help focus on the most important sources of uncertainty.

Together, this thesis shows that the integration of assay systems, high performing machine learning and deep learning image analysis algorithms, Aparecium software and quantitative kinetic modeling allows more rigorous testing of holistic models and theories for GPCR ligand binding and signalling systems.

REFERENCES

Abdar, M., Pourpanah, F., Hussain, S., Rezazadegan, D., Liu, L., Ghavamzadeh, M., Fieguth, P., Cao, X., Khosravi, A., Acharya, U. R., Makarenkov, V., & Nahavandi, S. (2021). A review of uncertainty quantification in deep learning: Techniques, applications and challenges. *Information Fusion*, *76*, 243–297. https://doi.org/10.1016/j.inffus.2021.05.008

Aguet, F., Antonescu, C. N., Mettlen, M., Schmid, S. L., & Danuser, G. (2013). Advances in Analysis of Low Signal-to-Noise Images Link Dynamin and AP2 to the Functions of an Endocytic Checkpoint. *Developmental Cell*, *26*(3), 279–291. https://doi.org/10.1016/j.devcel.2013.06.019

Albrecht, T., Slabaugh, G., Alonso, E., & Al-Arif, S. M. R. (2017). Deep learning for single-molecule science. *Nanotechnology*, *28*(42), 423001. https://doi.org/10.1088/1361-6528/aa8334

Ali, M. A. S., Hollo, K., Laasfeld, T., Torp, J., Tahk, M.-J., Rinken, A., Palo, K., Parts, L., & Fishman, D. (2022). *ArtSeg-CHO-M4R: Artifact segmentation in microscopy of ligand binding to M4 muscarinic receptor in live CHO-K1-hM4 cells.* https://doi.org/10.23673/re-307

Allan, C., Burel, J.-M., Moore, J., Blackburn, C., Linkert, M., Loynton, S., MacDonald, D., Moore, W. J., Neves, C., Patterson, A., Porter, M., Tarkowska, A., Loranger, B., Avondo, J., Lagerstedt, I., Lianas, L., Leo, S., Hands, K., Hay, R. T., … Swedlow, J. R. (2012). OMERO: Flexible, model-driven data management for experimental biology. *Nature Methods*, *9*(3), Article 3. https://doi.org/10.1038/nmeth.1896

Allikalt, A., Laasfeld, T., Ilisson, M., Kopanchuk, S., & Rinken, A. (2021). Quantitative analysis of fluorescent ligand binding to dopamine D3 receptors using live-cell microscopy. *The FEBS Journal*, *288*(5), 1514–1532. https://doi.org/10.1111/febs.15519

Angermueller, C., Pärnamaa, T., Parts, L., & Stegle, O. (2016). Deep learning for computational biology. *Molecular Systems Biology*, *12*(7), 878. https://doi.org/10.15252/msb.20156651

Anton, S. E., Kayser, C., Maiellaro, I., Nemec, K., Möller, J., Koschinski, A., Zaccolo, M., Annibale, P., Falcke, M., Lohse, M. J., & Bock, A. (2022). Receptor-associated independent cAMP nanodomains mediate spatiotemporal specificity of GPCR signaling. *Cell*, *185*(7), 1130–1142.e11. https://doi.org/10.1016/j.cell.2022.02.011

Avet, C., Mancini, A., Breton, B., Le Gouill, C., Hauser, A. S., Normand, C., Kobayashi, H., Gross, F., Hogue, M., Lukasheva, V., St-Onge, S., Carrier, M., Héroux, M., Morissette, S., Fauman, E. B., Fortin, J.-P., Schann, S., Leroy, X., Gloriam, D. E., & Bouvier, M. (2022). Effector membrane translocation biosensors reveal G protein and βarrestin coupling profiles of 100 therapeutically relevant GPCRs. *ELife*, *11*, e74101. https://doi.org/10.7554/eLife.74101

Berg, S., Kutra, D., Kroeger, T., Straehle, C. N., Kausler, B. X., Haubold, C., Schiegg, M., Ales, J., Beier, T., Rudy, M., Eren, K., Cervantes, J. I., Xu, B., Beuttenmueller, F., Wolny, A., Zhang, C., Koethe, U., Hamprecht, F. A., & Kreshuk, A. (2019). ilastik: Interactive machine learning for (bio)image analysis. *Nature Methods*, *16*(12), Article 12. https://doi.org/10.1038/s41592-019-0582-9

Black, J. W., & Leff, P. (1997). Operational models of pharmacological agonism. *Proceedings of the Royal Society of London. Series B. Biological Sciences*, *220*(1219), 141–162. https://doi.org/10.1098/rspb.1983.0093

Brothers, S. P., & Wahlestedt, C. (2010). Therapeutic potential of neuropeptide Y (NPY) receptor ligands. *EMBO Molecular Medicine*, *2*(11), 429–439. https://doi.org/10 1002/emmm.201000100

Bush, A., Vasen, G., Constantinou, A., Dunayevich, P., Patop, I. L., Blaustein, M., & Colman-Lerner, A. (2016). Yeast GPCR signaling reflects the fraction of occupied receptors, not the number. *Molecular Systems Biology*, *12*(12), 898. https://doi.org/10.15252/msb.20166910

Caroli, J., Mamyrbekov, A., Harpsøe, K., Gardizi, S., Dörries, L., Ghosh, E., Hauser, A. S., Kooistra, A. J., & Gloriam, D. E. (2023). A community Biased Signaling Atlas. *Nature Chemical Biology*, *19*(5), Article 5. https://doi.org/10.1038/s41589-023-01292-8

Carvalho, S., Pearce, A., & Ladds, G. (2021). Novel mathematical and computational models of G protein–coupled receptor signalling. *Current Opinion in Endocrine and Metabolic Research*, *16*, 28–36. https://doi.org/10.1016/j.coemr.2020.07.002

Cheng, Y.-C., & Prusoff, W. H. (1973). Relationship between the inhibition constant (KI) and the concentration of inhibitor which causes 50 per cent inhibition (I50) of an enzymatic reaction. *Biochemical Pharmacology*, *22*(23), 3099–3108. https://doi.org/10.1016/0006-2952(73)90196-2

Clark, A. J. (1926). The reaction between acetyl choline and muscle cells. *The Journal of Physiology*, *61*(4), 530–546.

Colquhoun, D. (1998). Binding, gating, affinity and efficacy: The interpretation of structure-activity relationships for agonists and of the effects of mutating receptors. *British Journal of Pharmacology*, *125*(5), 923–947. https://doi.org/10.1038/sj.bjp.0702164

Danková, H. (2020). *Characterization of ligand binding to M1 muscarinic acetylcholine receptor using fluorescence anisotropy method*. https://dspace.cuni.cz/handle/20.500.11956/117938

Dautzenberg, F. M., & Neysari, S. (2005). Irreversible Binding Kinetics of Neuropeptide Y Ligands to Y2 but Not to Y1 and Y5 Receptors. *Pharmacology*, *75*(1), 21–29. https://doi.org/10.1159/000085897

de Ligt, R. A. F., Kourounakis, A. P., & IJzerman, A. P. (2000). Inverse agonism at G protein-coupled receptors: (Patho)physiological relevance and implications for drug discovery. *British Journal of Pharmacology*, *130*(1), 1–12. https://doi.org/10.1038/sj.bjp.0703311

de Mendoza, A., Sebé-Pedrós, A., & Ruiz-Trillo, I. (2014). The Evolution of the GPCR Signaling System in Eukaryotes: Modularity, Conservation, and the Transition to Metazoan Multicellularity. *Genome Biology and Evolution*, *6*(3), 606–619. https://doi.org/10.1093/gbe/evu038

Drevon, D., Fursa, S. R., & Malcolm, A. L. (2017). Intercoder Reliability and Validity of WebPlotDigitizer in Extracting Graphed Data. *Behavior Modification*, *41*(2), 323–339. https://doi.org/10.1177/0145445516673998

Eglen, R. M. (2005). Muscarinic Receptor Subtype Pharmacology and Physiology. In F. D. King & G. Lawton (Eds.), *Progress in Medicinal Chemistry* (Vol. 43, pp. 105–136). Elsevier. https://doi.org/10.1016/S0079-6468(05)43004-0

Falk, T., Mai, D., Bensch, R., Çiçek, Ö., Abdulkadir, A., Marrakchi, Y., Böhm, A., Deubner, J., Jäckel, Z., Seiwald, K., Dovzhenko, A., Tietz, O., Dal Bosco, C., Walsh, S., Saltukoglu, D., Tay, T. L., Prinz, M., Palme, K., Simons, M., … Ronneberger, O. (2019). U-Net: Deep learning for cell counting, detection, and morphometry. *Nature Methods*, *16*(1), 67–70. https://doi.org/10.1038/s41592-018-0261-2

Fishman, D., Salumaa, S.-O., Majoral, D., Laasfeld, T., Peel, S., Wildenhain, J., Schreiner, A., Palo, K., & Parts, L. (2021). Practical segmentation of nuclei in brightfield cell images with neural networks trained on fluorescently labelled samples. *Journal of Microscopy*, *284*(1), 12–24. https://doi.org/10.1111/jmi.13038

Fraser, A. S. (1957). Simulation of Genetic Systems by Automatic Digital Computers I. Introduction. *Australian Journal of Biological Sciences*, *10*(4), 484–491. https://doi.org/10.1071/bi9570484

Gesztelyi, R., Zsuga, J., Kemeny-Beke, A., Varga, B., Juhasz, B., & Tosaki, A. (2012). The Hill equation and the origin of quantitative pharmacology. *Archive for History of Exact Sciences*, *66*(4), 427–438. https://doi.org/10.1007/s00407-012-0098-5

Gherbi, K., May, L. T., Baker, J. G., Briddon, S. J., & Hill, S. J. (2015). Negative cooperativity across β1-adrenoceptor homodimers provides insights into the nature of the secondary low-affinity CGP 12177 β1-adrenoceptor binding conformation. *The FASEB Journal*, *29*(7), 2859–2871. https://doi.org/10.1096/fj.14-265199

Grätz, L., Laasfeld, T., Allikalt, A., Gruber, C. G., Pegoli, A., Tahk, M.-J., Tsernant, M.-L., Keller, M., & Rinken, A. (2021). BRET- and fluorescence anisotropy-based assays for real-time monitoring of ligand binding to M_2 muscarinic acetylcholine receptors. *Biochimica et Biophysica Acta (BBA) – Molecular Cell Research*, *1868*(3), 118930. https://doi.org/10.1016/j.bbamcr.2020.118930

Gupta, G. K., Sacks-Davis, R., & Tescher, P. E. (1985). A review of recent developments in solving ODEs. *ACM Computing Surveys*, *17*(1), 5–47. https://doi.org/10.1145/4078.4079

Gurevich, V. V., & Gurevich, E. V. (2020). Biased GPCR signaling: Possible mechanisms and inherent limitations. *Pharmacology & Therapeutics*, *211*, 107540. https://doi.org/10.1016/j.pharmthera.2020.107540

Han, J., Jentzen, A., & E, W. (2018). Solving high-dimensional partial differential equations using deep learning. *Proceedings of the National Academy of Sciences*, *115*(34), 8505–8510. https://doi.org/10.1073/pnas.1718942115

Hauser, A. S., Avet, C., Normand, C., Mancini, A., Inoue, A., Bouvier, M., & Gloriam, D. E. (2022). Common coupling map advances GPCR-G protein selectivity. *ELife*, *11*, e74107. https://doi.org/10.7554/eLife.74107

Heitzler, D., Crépieux, P., Poupon, A., Clément, F., Fages, F., & Reiter, E. (2009). Towards a systems biology approach of G protein-coupled receptor signalling: Challenges and expectations. *Comptes Rendus Biologies*, *332*(11), 947–957. https://doi.org/10.1016/j.crvi.2009.09.002

Hill, A. V. (1910). The possible effects of the aggregation of the molecules of hemoglobin on its dissociation curves. *J. Physiol.*, *40*, iv–vii.

Hoare, S. R. J., Pierre, N., Moya, A. G., & Larson, B. (2018). Kinetic operational models of agonism for G-protein-coupled receptors. *Journal of Theoretical Biology*, *446*, 168–204. https://doi.org/10.1016/j.jtbi.2018.02.014

Hoare, S. R. J., Tewson, P. H., Quinn, A. M., & Hughes, T. E. (2020). A kinetic method for measuring agonist efficacy and ligand bias using high resolution biosensors and a kinetic data analysis framework. *Scientific Reports*, *10*(1), Article 1. https://doi.org/10.1038/s41598-020-58421-9

Hoffmann, C., Castro, M., Rinken, A., Leurs, R., Hill, S. J., & Vischer, H. F. (2015). Ligand residence time at G-protein–coupled receptors—Why we should take our time to study it. *Molecular Pharmacology*, *88*(3), 552–560. https://doi.org/10.1124/mol.115.099671

Hucka, M., Bergmann, F. T., Chaouiya, C., Dräger, A., Hoops, S., Keating, S. M., König, M., Novère, N. L., Myers, C. J., Olivier, B. G., Sahle, S., Schaff, J. C., Sheriff, R., Smith, L. P., Waltemath, D., Wilkinson, D. J., & Zhang, F. (2019). The Systems Biology Markup Language (SBML): Language Specification for Level 3 Version 2 Core Release 2. *Journal of Integrative Bioinformatics*, *16*(2). https://doi.org/10.1515/jib-2019-0021

Hucka, M., Finney, A., Sauro, H. M., Bolouri, H., Doyle, J. C., Kitano, H., Arkin, A. P., Bornstein, B. J., Bray, D., Cornish-Bowden, A., Cuellar, A. A., Dronov, S., Gilles, E. D., Ginkel, M., Gor, V., Goryanin, I. I., Hedley, W. J., Hodgman, T. C., Hofmeyr, J.-H., … and the rest of the SBML Forum: (2003). The systems biology markup language (SBML): A medium for representation and exchange of biochemical network models. *Bioinformatics*, *19*(4), 524–531. https://doi.org/10.1093/bioinformatics/btg015

Hucka, M., Hoops, S., Keating, S., Le Novère, N., Sahle, S., & Wilkinson, D. (2008). Systems Biology Markup Language (SBML) Level 2: Structures and Facilities for Model Definitions. *Nature Precedings*, 1–1. https://doi.org/10.1038/npre.2008.2715.1

Ilien, B., Glasser, N., Clamme, J.-P., Didier, P., Piemont, E., Chinnappan, R., Daval, S. B., Galzi, J.-L., & Mely, Y. (2009). Pirenzepine Promotes the Dimerization of Muscarinic M1 Receptors through a Three-step Binding Process *. *Journal of Biological Chemistry*, *284*(29), 19533–19543. https://doi.org/10.1074/jbc.M109.017145

Inoue, A., Raimondi, F., Kadji, F. M. N., Singh, G., Kishi, T., Uwamizu, A., Ono, Y., Shinjo, Y., Ishida, S., Arang, N., Kawakami, K., Gutkind, J. S., Aoki, J., & Russell, R. B. (2019). Illuminating G-Protein-Coupling Selectivity of GPCRs. *Cell*, *177*(7), 1933–1947.e25. https://doi.org/10.1016/j.cell.2019.04.044

Iversen, L., Mathiasen, S., Larsen, J. B., & Stamou, D. (2015). Membrane curvature bends the laws of physics and chemistry. *Nature Chemical Biology*, *11*(11), Article 11. https://doi.org/10.1038/nchembio.1941

Jakubík, J., & El-Fakahany, E. E. (2010). Allosteric Modulation of Muscarinic Acetylcholine Receptors. *Pharmaceuticals*, *3*(9), 2838–2860. https://doi.org/10.3390/ph3092838

Jakubík, J., El-Fakahany, E. E., & Tuček, S. (2000). Evidence for a Tandem Two-site Model of Ligand Binding to Muscarinic Acetylcholine Receptors*. *Journal of Biological Chemistry*, *275*(25), 18836–18844. https://doi.org/10.1074/jbc.M000112200

Jeffrey Conn, P., Christopoulos, A., & Lindsley, C. W. (2009). Allosteric modulators of GPCRs: A novel approach for the treatment of CNS disorders. *Nature Reviews Drug Discovery*, *8*(1), Article 1. https://doi.org/10.1038/nrd2760

Kairys, V., Baranauskiene, L., Kazlauskiene, M., Matulis, D., & Kazlauskas, E. (2019). Binding affinity in drug design: Experimental and computational techniques. *Expert Opinion on Drug Discovery*, *14*(8), 755–768. https://doi.org/10.1080/17460441.2019.1623202

Keating, S. M., Waltemath, D., König, M., Zhang, F., Dräger, A., Chaouiya, C., Bergmann, F. T., Finney, A., Gillespie, C. S., Helikar, T., Hoops, S., Malik-Sheriff, R. S., Moodie, S. L., Moraru, I. I., Myers, C. J., Naldi, A., Olivier, B. G., Sahle, S., Schaff, J. C., … Sbml, L. 3 C. members. (2020). SBML Level 3: An extensible format for the exchange and reuse of biological models. *Molecular Systems Biology*, *16*(8), e9110. https://doi.org/10.15252/msb.20199110

Kelly, E., Bailey, C. P., & Henderson, G. (2008). Agonist-selective mechanisms of GPCR desensitization. *British Journal of Pharmacology*, *153*(S1), S379–S388. https://doi.org/10.1038/sj.bjp.0707604

Kennedy, J., & Eberhart, R. (1995). Particle swarm optimization. *Proceedings of ICNN'95 – International Conference on Neural Networks*, *4*, 1942–1948 vol.4. https://doi.org/10.1109/ICNN.1995.488968

Kirkpatrick, S., Gelatt, C. D., & Vecchi, M. P. (1983). Optimization by Simulated Annealing. *Science*, *220*(4598), 671–680. https://doi.org/10.1126/science.220.4598.671

Kohl, P., Crampin, E. J., Quinn, T. A., & Noble, D. (2010). Systems Biology: An Approach. *Clinical Pharmacology & Therapeutics*, *88*(1), 25–33. https://doi.org/10.1038/clpt.2010.92

Kolb, P., Kenakin, T., Alexander, S. P. H., Bermudez, M., Bohn, L. M., Breinholt, C. S., Bouvier, M., Hill, S. J., Kostenis, E., Martemyanov, K. A., Neubig, R. R., Onaran, H. O., Rajagopal, S., Roth, B. L., Selent, J., Shukla, A. K., Sommer, M. E., & Gloriam, D. E. (2022). Community guidelines for GPCR ligand bias: IUPHAR review 32. *British Journal of Pharmacology*, *179*(14), 3651–3674. https://doi.org/10.1111/bph.15811

Kopanchuk, S., Veiksina, S., Mutulis, F., Mutule, I., Yahorava, S., Mandrika, I., Petrovska, R., Rinken, A., & Wikberg, J. E. S. (2006). Kinetic evidence for tandemly arranged ligand binding sites in melanocortin 4 receptor complexes. *Neurochemistry International*, *49*(5), 533–542. https://doi.org/10.1016/j.neuint.2006.04.006

Krizhevsky, A., Sutskever, I., & Hinton, G. E. (2017). ImageNet classification with deep convolutional neural networks. *Communications of the ACM*, *60*(6), 84–90. https://doi.org/10.1145/3065386

Kudlak, M., & Tadi, P. (2023). Physiology, Muscarinic Receptor. In *StatPearls*. StatPearls Publishing. http://www.ncbi.nlm.nih.gov/books/NBK555909/

Kukkonen, J. P. (2021). Allosteric interactions via the orthosteric ligand binding sites in a constitutive G-protein-coupled receptor homodimer. *Pharmacological Research*, *166*, 105116. https://doi.org/10.1016/j.phrs.2020.105116

Kyoda, K., Ho, K. H. L., Tohsato, Y., Itoga, H., & Onami, S. (2020). BD5: An open HDF5-based data format to represent quantitative biological dynamics data. *PLOS ONE*, *15*(8), e0237468. https://doi.org/10.1371/journal.pone.0237468

Kyoda, K., Tohsato, Y., Ho, K. H. L., & Onami, S. (2015). Biological Dynamics Markup Language (BDML): An open format for representing quantitative biological dynamics data. *Bioinformatics*, *31*(7), 1044–1052. https://doi.org/10.1093/bioinformatics/btu767

Laasfeld, T., Ehrminger, R., Tahk, M.-J., Veiksina, S., Rene Kõlvart, K., Min, M., Kopanchuk, S., & Rinken, A. (2021). Budded baculoviruses as a receptor display system to quantify ligand binding with TIRF microscopy. *Nanoscale*, *13*(4), 2436–2447. https://doi.org/10.1039/D0NR06737G

Laasfeld, T., Kopanchuk, S., & Rinken, A. (2017). Image-based cell-size estimation for baculovirus quantification. *BioTechniques*, *63*(4), 161–168. https://doi.org/10.2144/000114595

Laine, R. F., Arganda-Carreras, I., Henriques, R., & Jacquemet, G. (2021). Avoiding a replication crisis in deep-learning-based bioimage analysis. *Nature Methods*, *18*(10), Article 10. https://doi.org/10.1038/s41592-021-01284-3

Li, S., Besson, S., Blackburn, C., Carroll, M., Ferguson, R. K., Flynn, H., Gillen, K., Leigh, R., Lindner, D., Linkert, M., Moore, W. J., Ramalingam, B., Rozbicki, E.,

Rustici, G., Tarkowska, A., Walczysko, P., Williams, E., Allan, C., Burel, J.-M., … Swedlow, J. R. (2016). Metadata management for high content screening in OME-RO. *Methods*, *96*, 27–32. https://doi.org/10.1016/j.ymeth.2015.10.006

Lienen, M., & Günnemann, S. (2023). *torchode: A Parallel ODE Solver for PyTorch* (arXiv:2210.12375). arXiv. https://doi.org/10.48550/arXiv.2210.12375

Lin, H.-H., Ng, K.-F., Chen, T.-C., & Tseng, W.-Y. (2022). Ligands and Beyond: Mechanosensitive Adhesion GPCRs. *Pharmaceuticals*, *15*(2), 219. https://doi.org/10.3390/ph15020219

Link, R., Veiksina, S., Tahk, M.-J., Laasfeld, T., Paiste, P., Kopanchuk, S., & Rinken, A. (2020). The constitutive activity of melanocortin-4 receptors in cAMP pathway is allosterically modulated by zinc and copper ions. *Journal of Neurochemistry*, *153*(3), 346–361. https://doi.org/10.1111/jnc.14933

Lohse, M. J., Benovic, J. L., Codina, J., Caron, M. G., & Lefkowitz, R. J. (1990). β-Arrestin: A Protein that Regulates β-adrenergic Receptor Function. *Science*, *248*(4962), 1547–1550. https://doi.org/10.1126/science.2163110

Lohse, M. J., Maiellaro, I., & Calebiro, D. (2014). Kinetics and mechanism of G protein-coupled receptor activation. *Current Opinion in Cell Biology*, *27*, 87–93. https://doi.org/10.1016/j.ceb.2013.11.009

Lu, L., Meng, X., Mao, Z., & Karniadakis, G. E. (2021). DeepXDE: A Deep Learning Library for Solving Differential Equations. *SIAM Review*, *63*(1), 208–228. https://doi.org/10.1137/19M1274067

Marsango, S., Jenkins, L., Pediani, J. D., Bradley, S. J., Ward, R. J., Hesse, S., Biener, G., Stoneman, M. R., Tobin, A. B., Raicu, V., & Milligan, G. (2022). The M1 muscarinic receptor is present in situ as a ligand-regulated mixture of monomers and oligomeric complexes. *Proceedings of the National Academy of Sciences of the United States of America*, *119*(24), e2201103119. https://doi.org/10.1073/pnas.2201103119

Marsango, S., Ward, R. J., Alvarez-Curto, E., & Milligan, G. (2018). Muscarinic receptor oligomerization. *Neuropharmacology*, *136*, 401–410. https://doi.org/10.1016/j.neuropharm.2017.11.023

Martinez, V. J., Asico, L. D., Jose, P. A., & Tiu, A. C. (2020). Lipid Rafts and Dopamine Receptor Signaling. *International Journal of Molecular Sciences*, *21*(23), Article 23. https://doi.org/10.3390/ijms21238909

Marullo, S., Doly, S., Saha, K., Enslen, H., Scott, M. G. H., & Coureuil, M. (2020). Mechanical GPCR Activation by Traction Forces Exerted on Receptor N-Glycans. *ACS Pharmacology & Translational Science*, *3*(2), 171–178. https://doi.org/10.1021/acsptsci.9b00106

Mashanov, G. I., & Molloy, J. E. (2007). Automatic Detection of Single Fluorophores in Live Cells. *Biophysical Journal*, *92*(6), 2199–2211. https://doi.org/10.1529/biophysj.106.081117

Medina, A., Reintsch, W., & Steinbeisser, H. (2000). Xenopus frizzled 7 can act in canonical and non-canonical Wnt signaling pathways: Implications on early patterning and morphogenesis. *Mechanisms of Development*, *92*(2), 227–237. https://doi.org/10.1016/S0925-4773(00)00240-9

Millard, B. L., Niepel, M., Menden, M. P., Muhlich, J. L., & Sorger, P. K. (2011). Adaptive informatics for multifactorial and high-content biological data. *Nature Methods*, *8*(6), Article 6. https://doi.org/10.1038/nmeth.1600

Milligan, G. (2003). Constitutive Activity and Inverse Agonists of G Protein-Coupled Receptors: A Current Perspective. *Molecular Pharmacology*, *64*(6), 1271–1276. https://doi.org/10.1124/mol.64.6.1271

Müller, C., Gleixner, J., Tahk, M.-J., Kopanchuk, S., Laasfeld, T., Weinhart, M., Schollmeyer, D., Betschart, M. U., Lüdeke, S., Koch, P., Rinken, A., & Keller, M. (2022). Structure-Based Design of High-Affinity Fluorescent Probes for the Neuropeptide Y Y1 Receptor. *Journal of Medicinal Chemistry*, *65*(6), 4832–4853. https://doi.org/10.1021/acs.jmedchem.1c02033

Nagiri, C., Shihoya, W., Inoue, A., Kadji, F. M. N., Aoki, J., & Nureki, O. (2019). Crystal structure of human endothelin ETB receptor in complex with peptide inverse agonist IRL2500. *Communications Biology*, *2*(1), Article 1. https://doi.org/10.1038/s42003-019-0482-7

Napier, T. C., Kirby, A., & Persons, A. L. (2020). The role of dopamine pharmacotherapy and addiction-like behaviors in Parkinson's disease. *Progress in Neuro-Psychopharmacology and Biological Psychiatry*, *102*, 109942. https://doi.org/10.1016/j.pnpbp.2020.109942

Nelder, J. A., & Mead, R. (1965). A Simplex Method for Function Minimization. *The Computer Journal*, *7*(4), 308–313. https://doi.org/10.1093/comjnl/7.4.308

Nonga, O. E., Lavogina, D., Enkvist, E., Kestav, K., Chaikuad, A., Dixon-Clarke, S. E., Bullock, A. N., Kopanchuk, S., Ivan, T., Ekambaram, R., Viht, K., Knapp, S., & Uri, A. (2021). Crystal Structure-Guided Design of Bisubstrate Inhibitors and Photoluminescent Probes for Protein Kinases of the PIM Family. *Molecules*, *26*(14), Article 14. https://doi.org/10.3390/molecules26144353

Pachitariu, M., & Stringer, C. (2022). Cellpose 2.0: How to train your own model. *Nature Methods*, *19*(12), Article 12. https://doi.org/10.1038/s41592-022-01663-4

Paolocci, E., & Zaccolo, M. (2023). Compartmentalised cAMP signalling in the primary cilium. *Frontiers in Physiology*, *14*. https://www.frontiersin.org/articles/10.3389/fphys.2023.1187134

Pepperkok, R., & Ellenberg, J. (2006). High-throughput fluorescence microscopy for systems biology. *Nature Reviews Molecular Cell Biology*, *7*(9), Article 9. https://doi.org/10.1038/nrm1979

Pozzi, M., Bertella, S., Gatti, E., Peeters, G. G. A. M., Carnovale, C., Zambrano, S., & Nobile, M. (2020). Emerging drugs for the treatment of attention-deficit hyperactivity disorder (ADHD). *Expert Opinion on Emerging Drugs*, *25*(4), 395–407. https://doi.org/10.1080/14728214.2020.1820481

Qin, J., Cai, Y., Xu, Z., Ming, Q., Ji, S.-Y., Wu, C., Zhang, H., Mao, C., Shen, D.-D., Hirata, K., Ma, Y., Yan, W., Zhang, Y., & Shao, Z. (2022). Molecular mechanism of agonism and inverse agonism in ghrelin receptor. *Nature Communications*, *13*(1), Article 1. https://doi.org/10.1038/s41467-022-27975-9

Rascol, E., Villette, S., Harté, E., & Alves, I. D. (2021). Plasmon Waveguide Resonance: Principles, Applications and Historical Perspectives on Instrument Development. *Molecules*, *26*(21), Article 21. https://doi.org/10.3390/molecules26216442

Raspopovic, J., Marcon, L., Russo, L., & Sharpe, J. (2014). Digit patterning is controlled by a Bmp-Sox9-Wnt Turing network modulated by morphogen gradients. *Science*, *345*(6196), 566–570. https://doi.org/10.1126/science.1252960

Raue, A., Steiert, B., Schelker, M., Kreutz, C., Maiwald, T., Hass, H., Vanlier, J., Tönsing, C., Adlung, L., Engesser, R., Mader, W., Heinemann, T., Hasenauer, J., Schilling, M., Höfer, T., Klipp, E., Theis, F., Klingmüller, U., Schöberl, B., & Timmer, J. (2015). Data2Dynamics: A modeling environment tailored to parameter

estimation in dynamical systems. *Bioinformatics*, *31*(21), 3558–3560. https://doi.org/10.1093/bioinformatics/btv405

Regazzoni, F., Dedè, L., & Quarteroni, A. (2019). Machine learning for fast and reliable solution of time-dependent differential equations. *Journal of Computational Physics*, *397*, 108852. https://doi.org/10.1016/j.jcp.2019.07.050

Reinart-Okugbeni, R., Ausmees, K., Kriis, K., Werner, F., Rinken, A., & Kanger, T. (2012). Chemoenzymatic synthesis and evaluation of 3-azabicyclo[3.2.0]heptane derivatives as dopaminergic ligands. *European Journal of Medicinal Chemistry*, *55*, 255–261. https://doi.org/10.1016/j.ejmech.2012.07.025

Rinken, A., Lavogina, D., & Kopanchuk, S. (2018). Assays with Detection of Fluorescence Anisotropy: Challenges and Possibilities for Characterizing Ligand Binding to GPCRs. *Trends in Pharmacological Sciences*, *39*(2), 187–199. https://doi.org/10.1016/j.tips.2017.10.004

Ronneberger, O., Fischer, P., & Brox, T. (2015). U-Net: Convolutional Networks for Biomedical Image Segmentation. In N. Navab, J. Hornegger, W. M. Wells, & A. F. Frangi (Eds.), *Medical Image Computing and Computer-Assisted Intervention – MICCAI 2015* (pp. 234–241). Springer International Publishing.

Rosholm, K. R., Leijnse, N., Mantsiou, A., Tkach, V., Pedersen, S. L., Wirth, V. F., Oddershede, L. B., Jensen, K. J., Martinez, K. L., Hatzakis, N. S., Bendix, P. M., Callan-Jones, A., & Stamou, D. (2017). Membrane curvature regulates ligand-specific membrane sorting of GPCRs in living cells. *Nature Chemical Biology*, *13*(7), Article 7. https://doi.org/10.1038/nchembio.2372

Roth, B. L., & Chuang, D.-M. (1987). Multiple mechanisms of serotonergic signal transduction. *Life Sciences*, *41*(9), 1051–1064. https://doi.org/10.1016/0024-3205(87)90621-7

Saez-Rodriguez, J., Goldsipe, A., Muhlich, J., Alexopoulos, L. G., Millard, B., Lauffenburger, D. A., & Sorger, P. K. (2008). Flexible informatics for linking experimental data to mathematical models via DataRail. *Bioinformatics*, *24*(6), 840–847. https://doi.org/10.1093/bioinformatics/btn018

Sansone, S.-A., McQuilton, P., Rocca-Serra, P., Gonzalez-Beltran, A., Izzo, M., Lister, A. L., & Thurston, M. (2019). FAIRsharing as a community approach to standards, repositories and policies. *Nature Biotechnology*, *37*(4), Article 4. https://doi.org/10.1038/s41587-019-0080-8

Schälte, Y., Fröhlich, F., Jost, P. J., Vanhoefer, J., Pathirana, D., Stapor, P., Lakrisenko, P., Wang, D., Raimúndez, E., Merkt, S., Schmiester, L., Städter, P., Grein, S., Dudkin, E., Doresic, D., Weindl, D., & Hasenauer, J. (2023). *pyPESTO: A modular and scalable tool for parameter estimation for dynamic models* (arXiv:2305.01821). arXiv. https://doi.org/10.48550/arXiv.2305.01821

Scheerer, P., & Sommer, M. E. (2017). Structural mechanism of arrestin activation. *Current Opinion in Structural Biology*, *45*, 160–169. https://doi.org/10.1016/j.sbi.2017.05.001

Schindelin, J., Arganda-Carreras, I., Frise, E., Kaynig, V., Longair, M., Pietzsch, T., Preibisch, S., Rueden, C., Saalfeld, S., Schmid, B., Tinevez, J.-Y., White, D. J., Hartenstein, V., Eliceiri, K., Tomancak, P., & Cardona, A. (2012). Fiji: An open-source platform for biological-image analysis. *Nature Methods*, *9*(7), Article 7. https://doi.org/10.1038/nmeth.2019

Schmidt, H., & Jirstrand, M. (2006). Systems Biology Toolbox for MATLAB: A computational platform for research in systems biology. *Bioinformatics*, *22*(4), 514–515. https://doi.org/10.1093/bioinformatics/bti799

Schmidt, U., Weigert, M., Broaddus, C., & Myers, G. (2018). Cell Detection with Star-Convex Polygons. In A. F. Frangi, J. A. Schnabel, C. Davatzikos, C. Alberola-López, & G. Fichtinger (Eds.), *Medical Image Computing and Computer Assisted Intervention – MICCAI 2018* (pp. 265–273). Springer International Publishing. https://doi.org/10.1007/978-3-030-00934-2_30

Segebarth, D., Griebel, M., Stein, N., von Collenberg, C. R., Martin, C., Fiedler, D., Comeras, L. B., Sah, A., Schoeffler, V., Lüffe, T., Dürr, A., Gupta, R., Sasi, M., Lillesaar, C., Lange, M. D., Tasan, R. O., Singewald, N., Pape, H.-C., Flath, C. M., & Blum, R. (2020). On the objectivity, reliability, and validity of deep learning enabled bioimage analyses. *ELife*, *9*, e59780. https://doi.org/10.7554/eLife.59780

Siddique, N., Paheding, S., Elkin, C. P., & Devabhaktuni, V. (2021). U-Net and Its Variants for Medical Image Segmentation: A Review of Theory and Applications. *IEEE Access*, *9*, 82031–82057. https://doi.org/10.1109/ACCESS.2021.3086020

Sio, S. W. S., Sun, W., Kumar, S., Bin, W. Z., Tan, S. S., Ong, S. H., Kikuchi, H., Oshima, Y., & Tan, K. S. W. (2007). MalariaCount: An image analysis-based program for the accurate determination of parasitemia. *Journal of Microbiological Methods*, *68*(1), 11–18. https://doi.org/10.1016/j.mimet.2006.05.017

Slosky, L. M., Caron, M. G., & Barak, L. S. (2021). Biased Allosteric Modulators: New Frontiers in GPCR Drug Discovery. *Trends in Pharmacological Sciences*, *42*(4), 283–299. https://doi.org/10.1016/j.tips.2020.12.005

Smith, J. S., Lefkowitz, R. J., & Rajagopal, S. (2018). Biased signalling: From simple switches to allosteric microprocessors. *Nature Reviews Drug Discovery*, *17*(4), Article 4. https://doi.org/10.1038/nrd.2017.229

Srinivasan, S., Lubrano-Berthelier, C., Govaerts, C., Picard, F., Santiago, P., Conklin, B. R., & Vaisse, C. (2004). Constitutive activity of the melanocortin-4 receptor is maintained by its N-terminal domain and plays a role in energy homeostasis in humans. *Journal of Clinical Investigation*, *114*(8), 1158–1164. https://doi.org/10.1172/JCI200421927

Stein, S. C., & Thiart, J. (2016). TrackNTrace: A simple and extendable open-source framework for developing single-molecule localization and tracking algorithms. *Scientific Reports*, *6*(1), Article 1. https://doi.org/10.1038/srep37947

Stephenson, R. P. (1956). A Modification of Receptor Theory. *British Journal of Pharmacology and Chemotherapy*, *11*(4), 379–393. https://doi.org/10.1111/j.1476-5381.1956.tb00006.x

Stoddart, L. A., Goulding, J., & Briddon, S. J. (2022). Advances in the application of fluorescence correlation spectroscopy to study detergent purified and encapsulated membrane proteins. *The International Journal of Biochemistry & Cell Biology*, *146*, 106210. https://doi.org/10.1016/j.biocel.2022.106210

Stoddart, L. A., Johnstone, E. K. M., Wheal, A. J., Goulding, J., Robers, M. B., Machleidt, T., Wood, K. V., Hill, S. J., & Pfleger, K. D. G. (2015). Application of BRET to monitor ligand binding to GPCRs. *Nature Methods*, *12*(7), 661–663. https://doi.org/10.1038/nmeth.3398

Stoddart, L. A., Vernall, A. J., Denman, J. L., Briddon, S. J., Kellam, B., & Hill, S. J. (2012). Fragment Screening at Adenosine-A3 Receptors in Living Cells Using a Fluorescence-Based Binding Assay. *Chemistry & Biology*, *19*(9), 1105–1115. https://doi.org/10.1016/j.chembiol.2012.07.014

Stoddart, L. A., White, C. W., Nguyen, K., Hill, S. J., & Pfleger, K. D. G. (2016). Fluorescence- and bioluminescence-based approaches to study GPCR ligand

binding. *British Journal of Pharmacology*, *173*(20), 3028–3037. https://doi.org/10.1111/bph.13316

Stringer, C., Wang, T., Michaelos, M., & Pachitariu, M. (2021). Cellpose: A generalist algorithm for cellular segmentation. *Nature Methods*, *18*(1), Article 1. https://doi.org/10.1038/s41592-020-01018-x

Sungkaworn, T., Jobin, M.-L., Burnecki, K., Weron, A., Lohse, M. J., & Calebiro, D. (2017). Single-molecule imaging reveals receptor–G protein interactions at cell surface hot spots. *Nature*, *550*(7677), Article 7677. https://doi.org/10.1038/nature24264

Syrovatkina, V., Alegre, K. O., Dey, R., & Huang, X.-Y. (2016). Regulation, Signaling, and Physiological Functions of G-Proteins. *Journal of Molecular Biology*, *428*(19), 3850–3868. https://doi.org/10.1016/j.jmb.2016.08.002

Tahk, M.-J., Laasfeld, T., Meriste, E., Brea, J., Loza, M. I., Majellaro, M., Contino, M., Sotelo, E., & Rinken, A. (2023). Fluorescence based HTS-compatible ligand binding assays for dopamine D3 receptors in baculovirus preparations and live cells. *Frontiers in Molecular Biosciences*, *10*, 1119157. https://doi.org/10.3389/fmolb.2023.1119157

Tahk, M.-J., Torp, J., Ali, M. A. S., Fishman, D., Parts, L., Grätz, L., Müller, C., Keller, M., Veikšina, S., Laasfeld, T., & Rinken, A. (2022). *UT-GPCR001 microscopy of ligand binding to M4 muscarinic receptor in live CHO-K1-hM4 cells*. https://doi.org/10.23673/re-306

Tahk, M.-J., Torp, J., Ali, M. A. S., Fishman, D., Parts, L., Grätz, L., Müller, C., Keller, M., Veiksina, S., Laasfeld, T., & Rinken, A. (2022a). *UT-GPCR002 Machine learning models for CHO-K1 cell segmentation from fluorescence and bright-field microscopy images*. https://doi.org/10.23673/re-304

Tahk, M.-J., Torp, J., Ali, M. A. S., Fishman, D., Parts, L., Grätz, L., Müller, C., Keller, M., Veiksina, S., Laasfeld, T., & Rinken, A. (2022b). *UT-GPCR003 Fluorescence anisotropy and microscopy measurements experimental metadata of ligand binding to M4 muscarinic receptors*. https://doi.org/10.23673/re-303

Tahk, M.-J., Torp, J., Ali, M. A. S., Fishman, D., Parts, L., Grätz, L., Müller, C., Keller, M., Veiksina, S., Laasfeld, T., & Rinken, A. (2022c). *UT-GPCR004 CHO-K1 cell line bright-field and fluorescence microscopy and corresponding segmentation ground truth*. https://doi.org/10.23673/re-305

Taylor, C. F., Field, D., Sansone, S.-A., Aerts, J., Apweiler, R., Ashburner, M., Ball, C. A., Binz, P.-A., Bogue, M., Booth, T., Brazma, A., Brinkman, R. R., Clark, A. M., Deutsch, E. W., Fiehn, O., Fostel, J., Ghazal, P., Gibson, F., Gray, T., … Wiemann, S. (2008). Promoting coherent minimum reporting guidelines for biological and biomedical investigations: The MIBBI project. *Nature Biotechnology*, *26*(8), 889–896. https://doi.org/10.1038/nbt.1411

Tinevez, J.-Y., Perry, N., Schindelin, J., Hoopes, G. M., Reynolds, G. D., Laplantine, E., Bednarek, S. Y., Shorte, S. L., & Eliceiri, K. W. (2017). TrackMate: An open and extensible platform for single-particle tracking. *Methods*, *115*, 80–90. https://doi.org/10.1016/j.ymeth.2016.09.016

Tolkovsky, A. M. (1983). The Elucidation of Some Aspects of Receptor Function by the Use of a Kinetic Approach. In A. Kleinzeller & B. R. Martin (Eds.), *Current Topics in Membranes and Transport* (Vol. 18, pp. 11–44). Academic Press. https://doi.org/10.1016/S0070-2161(08)60525-0

Tolkovsky, A. M., & Levitzki, A. (1981). Theories and predictions of models describing sequential interactions between the receptor, the GTP regulatory unit, and the

catalytic unit of hormone dependent adenylate cyclases. *Journal of Cyclic Nucleotide Research*, *7*(3), 139–150.

Toth A. D., Szalai B., Kovacs O. T., Garger D., Prokop S., Balla A., Inoue A., Varnai P., Turu G. & Hunyady L. (2023). *Receptor endocytosis orchestrates the spatio-temporal bias of β-arrestin signaling | bioRxiv.* https://doi.org/10.1101/2023.04.27.538587

Tõntson, L., Kopanchuk, S., & Rinken, A. (2014). Characterization of 5-HT1A receptors and their complexes with G-proteins in budded baculovirus particles using fluorescence anisotropy of Bodipy-FL-NAN-190. *Neurochemistry International*, *67*, 32–38. https://doi.org/10.1016/j.neuint.2014.01.012

Turing, A. M. (1952). The chemical basis of morphogenesis. *Philosophical Transactions of the Royal Society of London. Series B, Biological Sciences, Vol. 237, No. 641. pp. 37-72.*

Ullmann, T., Gienger, M., Budzinski, J., Hellmann, J., Hübner, H., Gmeiner, P., & Weikert, D. (2021). Homobivalent Dopamine D2 Receptor Ligands Modulate the Dynamic Equilibrium of D2 Monomers and Homo- and Heterodimers. *ACS Chemical Biology*, *16*(2), 371–379. https://doi.org/10.1021/acschembio.0c00895

Uri, A., & Nonga, O. E. (2020). What is the current value of fluorescence polarization assays in small molecule screening? *Expert Opinion on Drug Discovery*, *15*(2), 131–133. https://doi.org/10.1080/17460441.2020.1702966

Veiksina, S., Kopanchuk, S., Mazina, O., Link, R., Lille, A., & Rinken, A. (2015). Homogeneous Fluorescence Anisotropy-Based Assay for Characterization of Ligand Binding Dynamics to GPCRs in Budded Baculoviruses: The Case of Cy3B-NDP-α-MSH Binding to MC4 Receptors. In D. M. F. Prazeres & S. A. M. Martins (Eds.), *G Protein-Coupled Receptor Screening Assays: Methods and Protocols* (pp. 37–50). Springer New York. https://doi.org/10.1007/978-1-4939-2336-6_3

Veiksina, S., Tahk, M.-J., Laasfeld, T., Link, R., Kopanchuk, S., & Rinken, A. (2021). Fluorescence Anisotropy-Based Assay for Characterization of Ligand Binding Dynamics to GPCRs: The Case of Cy3B-Labeled Ligands Binding to MC4 Receptors in Budded Baculoviruses. In S. A. M. Martins & D. M. F. Prazeres (Eds.), *G Protein-Coupled Receptor Screening Assays: Methods and Protocols* (pp. 119–136). Springer US. https://doi.org/10.1007/978-1-0716-1221-7_8

Vilardaga, J.-P., Jean-Alphonse, F. G., & Gardella, T. J. (2014). Endosomal generation of cAMP in GPCR signaling. *Nature Chemical Biology*, *10*(9), Article 9. https://doi.org/10.1038/nchembio.1611

von Chamier, L., Laine, R. F., Jukkala, J., Spahn, C., Krentzel, D., Nehme, E., Lerche, M., Hernández-Pérez, S., Mattila, P. K., Karinou, E., Holden, S., Solak, A. C., Krull, A., Buchholz, T.-O., Jones, M. L., Royer, L. A., Leterrier, C., Shechtman, Y., Jug, F., … Henriques, R. (2021). Democratising deep learning for microscopy with ZeroCostDL4Mic. *Nature Communications*, *12*(1), 2276. https://doi.org/10.1038/s41467-021-22518-0

Walker, L. C., Berizzi, A. E., Chen, N. A., Rueda, P., Perreau, V. M., Huckstep, K., Srisontiyakul, J., Govitrapong, P., Xiaojian, J., Lindsley, C. W., Jones, C. K., Riddy, D. M., Christopoulos, A., Langmead, C. J., & Lawrence, A. J. (2020). Acetylcholine Muscarinic M4 Receptors as a Therapeutic Target for Alcohol Use Disorder: Converging Evidence From Humans and Rodents. *Biological Psychiatry*, *88*(12), 898–909. https://doi.org/10.1016/j.biopsych.2020.02.019

Walsh, I., Fishman, D., Garcia-Gasulla, D., Titma, T., Pollastri, G., Harrow, J., Psomopoulos, F. E., & Tosatto, S. C. E. (2021). DOME: Recommendations for super-

vised machine learning validation in biology. *Nature Methods*, *18*(10), Article 10. https://doi.org/10.1038/s41592-021-01205-4

Waltemath, D., Adams, R., Beard, D. A., Bergmann, F. T., Bhalla, U. S., Britten, R., Chelliah, V., Cooling, M. T., Cooper, J., Crampin, E. J., Garny, A., Hoops, S., Hucka, M., Hunter, P., Klipp, E., Laibe, C., Miller, A. K., Moraru, I., Nickerson, D., … Novère, N. L. (2011). Minimum Information About a Simulation Experiment (MIASE). *PLOS Computational Biology*, *7*(4), e1001122. https://doi.org/10.1371/journal.pcbi.1001122

Wang, H., Wang, Z., Du, M., Yang, F., Zhang, Z., Ding, S., Mardziel, P., & Hu, X. (2020). *Score-CAM: Score-Weighted Visual Explanations for Convolutional Neural Networks*. 111–119. https://doi.org/10.1109/CVPRW50498.2020.00020

Wilhelmy, L. (1850). *Ueber das Gesetz, nach welchem die Enwirkung der Säuren auf den Rohrzucker stattfindet*. *81*, 413–433.

Wise, R. A., & Robble, M. A. (2020). Dopamine and Addiction. *Annual Review of Psychology*, *71*(1), 79–106. https://doi.org/10.1146/annurev-psych-010418-103337

Wolpert, D. H., & Macready, W. G. (1997). No free lunch theorems for optimization. *IEEE Transactions on Evolutionary Computation*, *1*(1), 67–82. https://doi.org/10.1109/4235.585893

Wyman Jr., J., & Allen, D. W. (1951). The problem of the heme interactions in hemoglobin and the basis of the bohr effect. *Journal of Polymer Science*, *7*(5), 499–518. https://doi.org/10.1002/pol.1951.120070506

Xu, J., Hu, Y., Kaindl, J., Risel, P., Hübner, H., Maeda, S., Niu, X., Li, H., Gmeiner, P., Jin, C., & Kobilka, B. K. (2019). Conformational Complexity and Dynamics in a Muscarinic Receptor Revealed by NMR Spectroscopy. *Molecular Cell*, *75*(1), 53-65.e7. https://doi.org/10.1016/j.molcel.2019.04.028

Zhang, C., Huber, F., Knop, M., & Hamprecht, F. A. (2014). Yeast cell detection and segmentation in bright field microscopy. *2014 IEEE 11th International Symposium on Biomedical Imaging (ISBI)*, 1267–1270. https://doi.org/10.1109/ISBI.2014.6868107

Zhuang, F., Qi, Z., Duan, K., Xi, D., Zhu, Y., Zhu, H., Xiong, H., & He, Q. (2021). A Comprehensive Survey on Transfer Learning. *Proceedings of the IEEE*, *109*(1), 43–76. https://doi.org/10.1109/JPROC.2020.3004555

SUMMARY IN ESTONIAN

Pildianalüüsi ja tervikliku modelleerimise ühendamine retseptor-ligand kompleksi kineetika kirjeldamiseks

G-valk seotud retseptorid (GPCR) on olulised ravimimärklauad. Samas on ligikaudu 800st inimese GPCRst vähemalt ühe ravimi märklauaks vähem kui 150 GPCRi, kuid ravimiametite poolt kinnitatud ravimi olemasolu ei tähenda, et patoloogia oleks leidnud täieliku ravi. Näiteks võivad ravimite hulka kuuluda ained, mis kõigest leevendavad kuid ei kaota sümptomeid, pidurdavad haiguse levikut, ravivad ainult haiguse teatud vorme või haigust teatud geenivariantidega populatsioonis või kaasneb ravikuuriga mõni tõsine kõrvalmõju. Vajadus uute ja paremate GPCR-i sihtmärgina kasutatavate ravimite järele on endiselt suur, kuid uute ravimite loomist on takistanud mitmed teaduslikud ja tehnoloogilised lüngad. Näiteks on avastatud, et GPCR-id võivad paralleelselt aktiveerida mitut signaalrada, moodustada nii homo- kui ka heterodimeere või oligomeere ja jätkata signaliseerimist raku seest. Lisaks sellele koonduvad pea kõikide 800 GPCR-i aktivatsiooni signaalrajad vähemasti suurusjärgu võrra väiksemale sekundaarsete virgatsainete hulgale, mille tõttu põimuvad mitmed signaalrajad omavahel vähemasti näiliselt läbi. Täit selgust, kuidas rakul õnnestub signaali õigesti tõlgendada, ei ole.

Käesolev doktoritöö loob raamistiku, mille abil on võimalik välja töötada, valideerida ja kasutada uusi spektroskoopilisi ja pildianalüüsil põhinevaid mõõtemetoodikaid GPCR-ide uurimiseks kvantitatiivse kineetilise modelleerimisega. Loodud raamistik hõlmab endas Aparecium tarkvara katseandmete standardiseerimiseks ning halduseks ja üldisi printsiipe, mida tuleks silmas pidada spektroskoopiliste ja mikroskoopiameetodite eksperimentaaldisainis, masinõppemudelite treenimisel ja kasutamisel biopiltide analüüsiks, mõõteandmete ja metaandmete haldamisel ning nende andmete põhjal mudelite loomisel. Väljatoodud printsiipide näitlikustamiseks loodi ja võrreldi erinevaid GPCRi ligandi sidumise meetodeid musakriinsete, dopaminergiliste ning neuropeptiid Y retseptorite näitel.

Loodud meetodid hõlmavad fluorestsentsanisotroopiat, elusrakkude fluorestsentsmikroskoopiat ning täieliku sisepeegelduse mikroskoopiat, kusjuures igal meetodil on spetsiifilised piirangud ja eelised, kuid kokku suudavad katta laia vajaduste spektri erinevate retseptorite ja kasutusjuhtude jaoks. Loodud mikroskoopiameetodite arendamise käigus loodi ja valideeriti masinõppemudelid ja pildianalüüsitarkvara vajalike ülesannete täitmiseks, näiteks rakke, fluorestsentsnanoosakesi ja mikroskoopiapiltidel erinevaid segajaid liigendavad mudelid. Viimaks vaadeldi kuidas erinevad algoritmide kvaliteedi mõõtmiseks kasutatavad pildipõhised mõõdikud võivad paljudel juhtudel nii üle- kui ka alahinnata pildianalüüsi kvaliteedi mõju lõplikule mõõtetulemusele ning võimalusi algoritmide kvaliteeti erapooletumalt hinnata.

ACKNOWLEDGEMENTS

Many people have contributed their time and effort to plan and carry out the experiments and analysis this thesis relies on. Firstly, I would like to thank my supervisors prof. Ago Rinken and Dr. Leopold Parts for supporting this inter-disciplinary thesis idea and all the useful discussions and practical tips over the years covering many topics. Secondly, I would like to thank Dr. Anni Allikalt for all the support, kindly sharing all the experimental data and willingness to discuss all kinds of hypotheses and ideas for Aparecium software which led to many interesting publications. Next, I want to thank Dr. Sergei Kopantšuk for helping me gain a solid ground in the scientific method especially during bachelor and master studies which has helped tremendously. I also want to thank my colleagues Dr. Reet Link, Dr. Mihkel Ilisson, Dr. Darja Lavõgina, Dr. Santa Veikšina, Dr. Olga Kukk, Dr. Edijs Vavers, Dr. Asko Uri, Dr. Kaido Viht Dr. Erki Enkvist, Dr. Tanel Sõrmus, Karl-Rene Kõlvart, Elen Laaneväli and all other current and former members of the Chair of Bioorganic Chemistry from the Institute of Chemistry for all the practical help especially helping to debug Aparecium software and interesting discussions related and unrelated to the topic of this thesis. I´m very grateful to Dr. Max Keller, Dr. Lukas Grätz and Dr. Christoph Müller from the University of Regensburg and Dr. Maria Majellaro and prof. Eddy Sotelo for a tight collaboration and constantly providing us with extraordinarily interesting fluorescence ligands and great ideas. Similarly, but completely differently I thank colleagues Dr. Dmytro Fishman, Dr. Kaupo Palo, Mohammed Ali, Kaspar Hollo, Sten-Oliver Salumaa, Mikhail Papkov and other current and former members of the Biomedical Computer Vision Lab and partners from Revvity for all the discussions, ideas and help related to machine learning and data science – you have immensely broadened my scientific world view. Next in line, I thank my current and former students Jane Torp, Hana Danková, Lakshmi Thoondee, Karl Suurkaev and Elo Meriste who have carried out many of the experiments presented in this thesis, have generated unique ideas and given me one of the best opportunities to learn – through teaching. I also want to thank Martin Saar, Ott Kekišev, Dr. Anneli Kruve and Dr. Uno Mäeorg, Dr. Vladislav Ivaništšev and everyone else connected to the science olympiads for sparking my original interest in chemistry and science. I'm grateful to my colleagues from Proekspert for interesting discussions, especially about quality assurance of image analysis pipelines and enabling flexible time schedules. Finally, my deepest gratitude goes to Dr. Maris-Johanna Tahk who has always supported me with absolutely everything inside and outside of the lab and has always been the first one ready to listen and discuss the wildest of ideas and without whom this work would have been impossible.

The thesis at hand was financed by the Estonian Ministry of Education and Science (IUT20-17 and PSG230), the University of Tartu ASTRA Project PER ASPERA, NATO (SPS 985261), the European Union through the European Regional Development Fund (EU48695), the Enterprise Estonia Applied research

programme 2021 and Ustus Agur stipend by Republic of Estonia Education and Youth Board and Estonian Association of Information Technology and Telecommunications. Furthermore, a large part of this work was made possible by the COST actions CM1207 GLISTEN, CA15124 NEUBIAS and CA18133 ERNEST.

PUBLICATIONS

CURRICULUM VITAE

Name: Tõnis Laasfeld
Date of birth: June 14, 1994
Citizenship: Estonian
Address: University of Tartu, Institute of Chemistry
Ravila 14a, 50411, Tartu, Estonia
E-mail: laasfeld@ut.ee

Education:

2019–…	University of Tartu, PhD student in chemistry
2017–2019	University of Tartu, MSc in chemistry, *cum laude*
2013–2016	University of Tartu, BSc in chemistry, *cum laude*
2001–2013	Gustav Adolf Grammar School

Professional employment:

2020–	Proekspert AS, Senior Data Scientist
2016, 2019	University of Tartu, Institute of Chemistry, Chemist

Professional organization:

2021–…	ERNEST COST Action, workgroup leader
2017–…	University of Tartu Chemistry Master's degree program committee, committee member
2013–2021	Member of the Jury of Estonian Chemistry Olympiad

Scientific publications:

1. Allikalt, A., **Laasfeld, T.**, Ilisson, M., Kopanchuk, S. and Rinken, A., 2021. Quantitative analysis of fluorescent ligand binding to dopamine D3 receptors using live-cell microscopy. *The FEBS Journal*, *288*(5), pp.1514–1532.
2. **Laasfeld, T.**, Ehrminger, R., Tahk, M.J., Veiksina, S., Kolvart, K.R., Min, M., Kopanchuk, S. and Rinken, A., 2021. Budded baculoviruses as a receptor display system to quantify ligand binding with TIRF microscopy. *Nanoscale*, *13*(4), pp.2436–2447.
3. Grätz, L., **Laasfeld, T.**, Allikalt, A., Gruber, C.G., Pegoli, A., Tahk, M.J., Tsernant, M.L., Keller, M. and Rinken, A., 2021. BRET-and fluorescence anisotropy-based assays for real-time monitoring of ligand binding to M2 muscarinic acetylcholine receptors. *Biochimica et Biophysica Acta (BBA)-Molecular Cell Research*, *1868*(3), p.118930.
4. Fishman, D., Salumaa, S.O., Majoral, D., **Laasfeld, T.**, Peel, S., Wildenhain, J., Schreiner, A., Palo, K. and Parts, L., 2021. Practical segmentation of nuclei in brightfield cell images with neural networks trained on fluorescently labelled samples. *Journal of Microscopy*, *284*(1), pp.12–24.

5. Müller, C., Gleixner, J., Tahk, M.J., Kopanchuk, S., **Laasfeld, T.**, Weinhart, M., Schollmeyer, D., Betschart, M.U., Lüdeke, S., Koch, P. and Rinken, A., 2022. Structure-Based Design of High-Affinity Fluorescent Probes for the Neuropeptide Y Y1 Receptor. *Journal of Medicinal Chemistry*, *65*(6), pp. 4832–4853.
6. **Laasfeld, T.**, Kopanchuk, S. and Rinken, A., 2017. Image-based cell-size estimation for baculovirus quantification. *Biotechniques*, *63*(4), pp.161–168.
7. Lavogina, D., Lust, H., Tahk, M.J., **Laasfeld, T.**, Vellama, H., Nasirova, N., Vardja, M., Eskla, K.L., Salumets, A., Rinken, A. and Jaal, J., 2022. Revisiting the Resazurin-Based Sensing of Cellular Viability: Widening the Application Horizon. *Biosensors*, *12*(4), p.196.
8. Link, R., Veiksina, S., Tahk, M.J., **Laasfeld, T.**, Paiste, P., Kopanchuk, S. and Rinken, A., 2020. The constitutive activity of melanocortin-4 receptors in cAMP pathway is allosterically modulated by zinc and copper ions. *Journal of neurochemistry*, *153*(3), pp.346–361.
9. Lavogina, D., **Laasfeld, T.**, Vardja, M., Lust, H. and Jaal, J., 2021. Viability fingerprint of glioblastoma cell lines: roles of mitotic, proliferative, and epigenetic targets. *Scientific Reports*, *11*(1), pp.1–14.
10. Ali, M.A., Hollo, K., **Laasfeld, T.**, Torp, J., Tahk, M.J., Rinken, A., Palo, K., Parts, L. and Fishman, D., 2022. ArtSeg—Artifact segmentation and removal in brightfield cell microscopy images without manual pixel-level annotations. *Scientific Reports*, *12*(1), p.11404.
11. Tahk, M.J., Torp, J., Ali, M.A., Fishman, D., Parts, L., Grätz, L., Müller, C., Keller, M., Veiksina, S., **Laasfeld, T.** and Rinken, A., 2022. Live-cell microscopy or fluorescence anisotropy with budded baculoviruses—which way to go with measuring ligand binding to M4 muscarinic receptors?. *Open Biology*, *12*(6), p.220019.
12. Tahk, M.J., **Laasfeld, T.**, Meriste, E., Brea, J., Loza, M.I., Majellaro, M., Contino, M., Sotelo, E. and Rinken, A., 2023. Fluorescence based HTS-compatible ligand binding assays for dopamine D3 receptors in baculovirus preparations and live cells. *Frontiers in Molecular Biosciences*, *10*.
13. Saar, M., Jaal, J., Meltsov, A., **Laasfeld, T.**, Lust, H., Kasvandik, S. and Lavogina, D., 2023. Exploring the Molecular Players behind the Potentiation of Chemotherapy Effects by Durvalumab in Lung Adenocarcinoma Cell Lines. *Pharmaceutics*, *15*(5), p.1485.
14. Sinijarv, H., Wu, S., Ivan, T., **Laasfeld, T.**, Viht, K. and Uri, A., 2017. Binding assay for characterization of protein kinase inhibitors possessing sub-picomolar to sub-millimolar affinity. *Analytical Biochemistry*, *531*, pp.67–77.
15. Veiksina, S., Tahk, M.J., **Laasfeld, T.**, Link, R., Kopanchuk, S. and Rinken, A., 2021. Fluorescence Anisotropy-Based Assay for Characterization of Ligand Binding Dynamics to GPCRs: The Case of Cy3B-Labeled Ligands Binding to MC 4 Receptors in Budded Baculoviruses. *G protein-coupled receptor screening assays: methods and protocols*, pp.119–136.

16. Lavogina, D., **Laasfeld, T.**, Tahk, M.J., Kukk, O., Allikalt, A., Kopanchuk, S. and Rinken, A., 2021. cAMP Biosensor Assay Using BacMam Expression System: Studying the Downstream Signaling of LH/hCG Receptor Activation. *G Protein-Coupled Receptor Screening Assays: Methods and Protocols*, pp.179–192.

Patents and patent applications:

1. Invention: Gelatin-based nanofibrous non-woven material; Owners: Gelatex Technologies OÜ; Authors: Märt-Erik Martens, Mihkel Ilisson, **Tõnis Laasfeld**, Jörgen Metsik, Uno Mäeorg; Priority number: USP201962941168; Priority date: 27.11.2019.

ELULOOKIRJELDUS

Nimi: Tõnis Laasfeld
Sünniaeg: 14. juuni 1994
Kodakondsus: Eesti
Aadress: Tartu Ülikool, Keemia instituut
Ravila 14a, 50411, Tartu, Estonia
E-post: laasfeld@ut.ee

Haridus:

2019–…	Tartu Ülikool, doktoriõpe keemias
2017–2019	Tartu Ülikool, MSc keemias, *cum laude*
2013–2016	Tartu Ülikool, BSc keemias, *cum laude*
2001–2013	Gustav Adolfi gümnaasium

Erialane teenistuskäik:

2020–…	Proekspert AS, Vanem Andmeteadlane
2016, 2019	Tartu Ülikooli Keemia instituut, Keemik

Teadusorganisatsioonid:

2021–…	ERNEST COST võrgustiku töörühmajuht
2017–…	Tartu Ülikooli Keemia magistriõppekava programmikomisjoni liige
2013–2021	Eesti Keemiaolümpiaadi žürii liige

Teaduspublikatsioonid:

1. Allikalt, A., **Laasfeld, T.**, Ilisson, M., Kopanchuk, S. and Rinken, A., 2021. Quantitative analysis of fluorescent ligand binding to dopamine D3 receptors using live-cell microscopy. *The FEBS Journal*, *288*(5), pp.1514–1532.
2. **Laasfeld, T.**, Ehrminger, R., Tahk, M.J., Veiksina, S., Kolvart, K.R., Min, M., Kopanchuk, S. and Rinken, A., 2021. Budded baculoviruses as a receptor display system to quantify ligand binding with TIRF microscopy. *Nanoscale*, *13*(4), pp. 2436–2447.
3. Grätz, L., **Laasfeld, T.**, Allikalt, A., Gruber, C.G., Pegoli, A., Tahk, M.J., Tsernant, M.L., Keller, M. and Rinken, A., 2021. BRET-and fluorescence anisotropy-based assays for real-time monitoring of ligand binding to M2 muscarinic acetylcholine receptors. *Biochimica et Biophysica Acta (BBA)-Molecular Cell Research*, *1868*(3), p.118930.
4. Fishman, D., Salumaa, S.O., Majoral, D., **Laasfeld, T.**, Peel, S., Wildenhain, J., Schreiner, A., Palo, K. and Parts, L., 2021. Practical segmentation of nuclei in brightfield cell images with neural networks trained on fluorescently labelled samples. *Journal of Microscopy*, *284*(1), pp.12–24.

5. Müller, C., Gleixner, J., Tahk, M.J., Kopanchuk, S., **Laasfeld, T.**, Weinhart, M., Schollmeyer, D., Betschart, M.U., Lüdeke, S., Koch, P. and Rinken, A., 2022. Structure-Based Design of High-Affinity Fluorescent Probes for the Neuropeptide Y Y1 Receptor. *Journal of Medicinal Chemistry*, *65*(6), pp. 4832–4853.
6. **Laasfeld, T.**, Kopanchuk, S. and Rinken, A., 2017. Image-based cell-size estimation for baculovirus quantification. *Biotechniques*, *63*(4), pp. 161–168.
7. Lavogina, D., Lust, H., Tahk, M.J., **Laasfeld, T.**, Vellama, H., Nasirova, N., Vardja, M., Eskla, K.L., Salumets, A., Rinken, A. and Jaal, J., 2022. Revisiting the Resazurin-Based Sensing of Cellular Viability: Widening the Application Horizon. *Biosensors*, *12*(4), p.196.
8. Link, R., Veiksina, S., Tahk, M.J., **Laasfeld, T.**, Paiste, P., Kopanchuk, S. and Rinken, A., 2020. The constitutive activity of melanocortin-4 receptors in cAMP pathway is allosterically modulated by zinc and copper ions. *Journal of neurochemistry*, *153*(3), pp.346–361.
9. Lavogina, D., **Laasfeld, T.**, Vardja, M., Lust, H. and Jaal, J., 2021. Viability fingerprint of glioblastoma cell lines: roles of mitotic, proliferative, and epigenetic targets. *Scientific Reports*, *11*(1), pp.1–14.
10. Ali, M.A., Hollo, K., **Laasfeld, T.**, Torp, J., Tahk, M.J., Rinken, A., Palo, K., Parts, L. and Fishman, D., 2022. ArtSeg—Artifact segmentation and removal in brightfield cell microscopy images without manual pixel-level annotations. *Scientific Reports*, *12*(1), p.11404.
11. Tahk, M.J., Torp, J., Ali, M.A., Fishman, D., Parts, L., Grätz, L., Müller, C., Keller, M., Veiksina, S., **Laasfeld, T.** and Rinken, A., 2022. Live-cell microscopy or fluorescence anisotropy with budded baculoviruses—which way to go with measuring ligand binding to M4 muscarinic receptors?. *Open Biology*, *12*(6), p.220019.
12. Tahk, M.J., **Laasfeld, T.**, Meriste, E., Brea, J., Loza, M.I., Majellaro, M., Contino, M., Sotelo, E. and Rinken, A., 2023. Fluorescence based HTS-compatible ligand binding assays for dopamine D3 receptors in baculovirus preparations and live cells. *Frontiers in Molecular Biosciences*, *10*.
13. Saar, M., Jaal, J., Meltsov, A., **Laasfeld, T.**, Lust, H., Kasvandik, S. and Lavogina, D., 2023. Exploring the Molecular Players behind the Potentiation of Chemotherapy Effects by Durvalumab in Lung Adenocarcinoma Cell Lines. *Pharmaceutics*, *15*(5), p.1485.
14. Sinijarv, H., Wu, S., Ivan, T., **Laasfeld, T.**, Viht, K. and Uri, A., 2017. Binding assay for characterization of protein kinase inhibitors possessing sub-picomolar to sub-millimolar affinity. *Analytical Biochemistry*, *531*, pp.67-77.
15. Veiksina, S., Tahk, M.J., **Laasfeld, T.**, Link, R., Kopanchuk, S. and Rinken, A., 2021. Fluorescence Anisotropy-Based Assay for Characterization of Ligand Binding Dynamics to GPCRs: The Case of Cy3B-Labeled Ligands Binding to MC 4 Receptors in Budded Baculoviruses. *G protein-coupled receptor screening assays: methods and protocols*, pp.119–136.

16. Lavogina, D., **Laasfeld, T.**, Tahk, M.J., Kukk, O., Allikalt, A., Kopanchuk, S. and Rinken, A., 2021. cAMP Biosensor Assay Using BacMam Expression System: Studying the Downstream Signaling of LH/hCG Receptor Activation. *G Protein-Coupled Receptor Screening Assays: Methods and Protocols*, pp. 179–192.

Patendid ja patenditaotlused:

1. Patenditaotlus: Gelatin-based nanofibrous non-woven material; Owners: Gelatex Technologies OÜ; Authors: Märt-Erik Martens, Mihkel Ilisson, **Tõnis Laasfeld**, Jörgen Metsik, Uno Mäeorg; Priority number: USP201962941168; Priority date: 27.11.2019.

DISSERTATIONES CHIMICAE UNIVERSITATIS TARTUENSIS

1. **Toomas Tamm.** Quantum-chemical simulation of solvent effects. Tartu, 1993, 110 p.
2. **Peeter Burk.** Theoretical study of gas-phase acid-base equilibria. Tartu, 1994, 96 p.
3. **Victor Lobanov.** Quantitative structure-property relationships in large descriptor spaces. Tartu, 1995, 135 p.
4. **Vahur Mäemets.** The ^{17}O and ^{1}H nuclear magnetic resonance study of H_2O in individual solvents and its charged clusters in aqueous solutions of electrolytes. Tartu, 1997, 140 p.
5. **Andrus Metsala.** Microcanonical rate constant in nonequilibrium distribution of vibrational energy and in restricted intramolecular vibrational energy redistribution on the basis of slater's theory of unimolecular reactions. Tartu, 1997, 150 p.
6. **Uko Maran.** Quantum-mechanical study of potential energy surfaces in different environments. Tartu, 1997, 137 p.
7. **Alar Jänes.** Adsorption of organic compounds on antimony, bismuth and cadmium electrodes. Tartu, 1998, 219 p.
8. **Kaido Tammeveski.** Oxygen electroreduction on thin platinum films and the electrochemical detection of superoxide anion. Tartu, 1998, 139 p.
9. **Ivo Leito.** Studies of Brønsted acid-base equilibria in water and non-aqueous media. Tartu, 1998, 101 p.
10. **Jaan Leis.** Conformational dynamics and equilibria in amides. Tartu, 1998, 131 p.
11. **Toonika Rinken.** The modelling of amperometric biosensors based on oxidoreductases. Tartu, 2000, 108 p.
12. **Dmitri Panov.** Partially solvated Grignard reagents. Tartu, 2000, 64 p.
13. **Kaja Orupõld.** Treatment and analysis of phenolic wastewater with microorganisms. Tartu, 2000, 123 p.
14. **Jüri Ivask.** Ion Chromatographic determination of major anions and cations in polar ice core. Tartu, 2000, 85 p.
15. **Lauri Vares.** Stereoselective Synthesis of Tetrahydrofuran and Tetrahydropyran Derivatives by Use of Asymmetric Horner-Wadsworth-Emmons and Ring Closure Reactions. Tartu, 2000, 184 p.
16. **Martin Lepiku.** Kinetic aspects of dopamine D_2 receptor interactions with specific ligands. Tartu, 2000, 81 p.
17. **Katrin Sak.** Some aspects of ligand specificity of P2Y receptors. Tartu, 2000, 106 p.
18. **Vello Pällin.** The role of solvation in the formation of iotsitch complexes. Tartu, 2001, 95 p.
19. **Katrin Kollist.** Interactions between polycyclic aromatic compounds and humic substances. Tartu, 2001, 93 p.

20. **Ivar Koppel.** Quantum chemical study of acidity of strong and superstrong Brønsted acids. Tartu, 2001, 104 p.
21. **Viljar Pihl.** The study of the substituent and solvent effects on the acidity of OH and CH acids. Tartu, 2001, 132 p.
22. **Natalia Palm.** Specification of the minimum, sufficient and significant set of descriptors for general description of solvent effects. Tartu, 2001, 134 p.
23. **Sulev Sild.** QSPR/QSAR approaches for complex molecular systems. Tartu, 2001, 134 p.
24. **Ruslan Petrukhin.** Industrial applications of the quantitative structure-property relationships. Tartu, 2001, 162 p.
25. **Boris V. Rogovoy.** Synthesis of (benzotriazolyl)carboximidamides and their application in relations with *N*- and *S*-nucleophyles. Tartu, 2002, 84 p.
26. **Koit Herodes.** Solvent effects on UV-vis absorption spectra of some solvatochromic substances in binary solvent mixtures: the preferential solvation model. Tartu, 2002, 102 p.
27. **Anti Perkson.** Synthesis and characterisation of nanostructured carbon. Tartu, 2002, 152 p.
28. **Ivari Kaljurand.** Self-consistent acidity scales of neutral and cationic Brønsted acids in acetonitrile and tetrahydrofuran. Tartu, 2003, 108 p.
29. **Karmen Lust.** Adsorption of anions on bismuth single crystal electrodes. Tartu, 2003, 128 p.
30. **Mare Piirsalu.** Substituent, temperature and solvent effects on the alkaline hydrolysis of substituted phenyl and alkyl esters of benzoic acid. Tartu, 2003, 156 p.
31. **Meeri Sassian.** Reactions of partially solvated Grignard reagents. Tartu, 2003, 78 p.
32. **Tarmo Tamm.** Quantum chemical modelling of polypyrrole. Tartu, 2003. 100 p.
33. **Erik Teinemaa.** The environmental fate of the particulate matter and organic pollutants from an oil shale power plant. Tartu, 2003. 102 p.
34. **Jaana Tammiku-Taul.** Quantum chemical study of the properties of Grignard reagents. Tartu, 2003. 120 p.
35. **Andre Lomaka.** Biomedical applications of predictive computational chemistry. Tartu, 2003. 132 p.
36. **Kostyantyn Kirichenko.** Benzotriazole – Mediated Carbon–Carbon Bond Formation. Tartu, 2003. 132 p.
37. **Gunnar Nurk.** Adsorption kinetics of some organic compounds on bismuth single crystal electrodes. Tartu, 2003, 170 p.
38. **Mati Arulepp.** Electrochemical characteristics of porous carbon materials and electrical double layer capacitors. Tartu, 2003, 196 p.
39. **Dan Cornel Fara.** QSPR modeling of complexation and distribution of organic compounds. Tartu, 2004, 126 p.
40. **Riina Mahlapuu.** Signalling of galanin and amyloid precursor protein through adenylate cyclase. Tartu, 2004, 124 p.

41. **Mihkel Kerikmäe.** Some luminescent materials for dosimetric applications and physical research. Tartu, 2004, 143 p.
42. **Jaanus Kruusma.** Determination of some important trace metal ions in human blood. Tartu, 2004, 115 p.
43. **Urmas Johanson.** Investigations of the electrochemical properties of polypyrrole modified electrodes. Tartu, 2004, 91 p.
44. **Kaido Sillar.** Computational study of the acid sites in zeolite ZSM-5. Tartu, 2004, 80 p.
45. **Aldo Oras.** Kinetic aspects of dATPαS interaction with $P2Y_1$ receptor. Tartu, 2004, 75 p.
46. **Erik Mölder.** Measurement of the oxygen mass transfer through the air-water interface. Tartu, 2005, 73 p.
47. **Thomas Thomberg.** The kinetics of electroreduction of peroxodisulfate anion on cadmium (0001) single crystal electrode. Tartu, 2005, 95 p.
48. **Olavi Loog.** Aspects of condensations of carbonyl compounds and their imine analogues. Tartu, 2005, 83 p.
49. **Siim Salmar.** Effect of ultrasound on ester hydrolysis in aqueous ethanol. Tartu, 2006, 73 p.
50. **Ain Uustare.** Modulation of signal transduction of heptahelical receptors by other receptors and G proteins. Tartu, 2006, 121 p.
51. **Sergei Yurchenko.** Determination of some carcinogenic contaminants in food. Tartu, 2006, 143 p.
52. **Kaido Tämm.** QSPR modeling of some properties of organic compounds. Tartu, 2006, 67 p.
53. **Olga Tšubrik.** New methods in the synthesis of multisubstituted hydrazines. Tartu. 2006, 183 p.
54. **Lilli Sooväli.** Spectrophotometric measurements and their uncertainty in chemical analysis and dissociation constant measurements. Tartu, 2006, 125 p.
55. **Eve Koort.** Uncertainty estimation of potentiometrically measured ph and pK_a values. Tartu, 2006, 139 p.
56. **Sergei Kopanchuk.** Regulation of ligand binding to melanocortin receptor subtypes. Tartu, 2006, 119 p.
57. **Silvar Kallip.** Surface structure of some bismuth and antimony single crystal electrodes. Tartu, 2006, 107 p.
58. **Kristjan Saal.** Surface silanization and its application in biomolecule coupling. Tartu, 2006, 77 p.
59. **Tanel Tätte.** High viscosity $Sn(OBu)_4$ oligomeric concentrates and their applications in technology. Tartu, 2006, 91 p.
60. **Dimitar Atanasov Dobchev**. Robust QSAR methods for the prediction of properties from molecular structure. Tartu, 2006, 118 p.
61. **Hannes Hagu**. Impact of ultrasound on hydrophobic interactions in solutions. Tartu, 2007, 81 p.
62. **Rutha Jäger.** Electroreduction of peroxodisulfate anion on bismuth electrodes. Tartu, 2007, 142 p.

63. **Kaido Viht.** Immobilizable bisubstrate-analogue inhibitors of basophilic protein kinases: development and application in biosensors. Tartu, 2007, 88 p.
64. **Eva-Ingrid Rõõm.** Acid-base equilibria in nonpolar media. Tartu, 2007, 156 p.
65. **Sven Tamp.** DFT study of the cesium cation containing complexes relevant to the cesium cation binding by the humic acids. Tartu, 2007, 102 p.
66. **Jaak Nerut.** Electroreduction of hexacyanoferrate(III) anion on Cadmium (0001) single crystal electrode. Tartu, 2007, 180 p.
67. **Lauri Jalukse.** Measurement uncertainty estimation in amperometric dissolved oxygen concentration measurement. Tartu, 2007, 112 p.
68. **Aime Lust.** Charge state of dopants and ordered clusters formation in CaF_2:Mn and CaF_2:Eu luminophors. Tartu, 2007, 100 p.
69. **Iiris Kahn**. Quantitative Structure-Activity Relationships of environmentally relevant properties. Tartu, 2007, 98 p.
70. **Mari Reinik.** Nitrates, nitrites, N-nitrosamines and polycyclic aromatic hydrocarbons in food: analytical methods, occurrence and dietary intake. Tartu, 2007, 172 p.
71. **Heili Kasuk.** Thermodynamic parameters and adsorption kinetics of organic compounds forming the compact adsorption layer at Bi single crystal electrodes. Tartu, 2007, 212 p.
72. **Erki Enkvist.** Synthesis of adenosine-peptide conjugates for biological applications. Tartu, 2007, 114 p.
73. **Svetoslav Hristov Slavov**. Biomedical applications of the QSAR approach. Tartu, 2007, 146 p.
74. **Eneli Härk.** Electroreduction of complex cations on electrochemically polished Bi(*hkl*) single crystal electrodes. Tartu, 2008, 158 p.
75. **Priit Möller.** Electrochemical characteristics of some cathodes for medium temperature solid oxide fuel cells, synthesized by solid state reaction technique. Tartu, 2008, 90 p.
76. **Signe Viggor.** Impact of biochemical parameters of genetically different pseudomonads at the degradation of phenolic compounds. Tartu, 2008, 122 p.
77. **Ave Sarapuu.** Electrochemical reduction of oxygen on quinone-modified carbon electrodes and on thin films of platinum and gold. Tartu, 2008, 134 p.
78. **Agnes Kütt.** Studies of acid-base equilibria in non-aqueous media. Tartu, 2008, 198 p.
79. **Rouvim Kadis.** Evaluation of measurement uncertainty in analytical chemistry: related concepts and some points of misinterpretation. Tartu, 2008, 118 p.
80. **Valter Reedo.** Elaboration of IVB group metal oxide structures and their possible applications. Tartu, 2008, 98 p.
81. **Aleksei Kuznetsov.** Allosteric effects in reactions catalyzed by the cAMP-dependent protein kinase catalytic subunit. Tartu, 2009, 133 p.

82. **Aleksei Bredihhin.** Use of mono- and polyanions in the synthesis of multisubstituted hydrazine derivatives. Tartu, 2009, 105 p.
83. **Anu Ploom.** Quantitative structure-reactivity analysis in organosilicon chemistry. Tartu, 2009, 99 p.
84. **Argo Vonk.** Determination of adenosine A_{2A}- and dopamine D_1 receptor-specific modulation of adenylate cyclase activity in rat striatum. Tartu, 2009, 129 p.
85. **Indrek Kivi.** Synthesis and electrochemical characterization of porous cathode materials for intermediate temperature solid oxide fuel cells. Tartu, 2009, 177 p.
86. **Jaanus Eskusson.** Synthesis and characterisation of diamond-like carbon thin films prepared by pulsed laser deposition method. Tartu, 2009, 117 p.
87. **Marko Lätt.** Carbide derived microporous carbon and electrical double layer capacitors. Tartu, 2009, 107 p.
88. **Vladimir Stepanov.** Slow conformational changes in dopamine transporter interaction with its ligands. Tartu, 2009, 103 p.
89. **Aleksander Trummal.** Computational Study of Structural and Solvent Effects on Acidities of Some Brønsted Acids. Tartu, 2009, 103 p.
90. **Eerold Vellemäe.** Applications of mischmetal in organic synthesis. Tartu, 2009, 93 p.
91. **Sven Parkel.** Ligand binding to 5-HT_{1A} receptors and its regulation by Mg^{2+} and Mn^{2+}. Tartu, 2010, 99 p.
92. **Signe Vahur.** Expanding the possibilities of ATR-FT-IR spectroscopy in determination of inorganic pigments. Tartu, 2010, 184 p.
93. **Tavo Romann**. Preparation and surface modification of bismuth thin film, porous, and microelectrodes. Tartu, 2010, 155 p.
94. **Nadežda Aleksejeva.** Electrocatalytic reduction of oxygen on carbon nanotube-based nanocomposite materials. Tartu, 2010, 147 p.
95. **Marko Kullapere.** Electrochemical properties of glassy carbon, nickel and gold electrodes modified with aryl groups. Tartu, 2010, 233 p.
96. **Liis Siinor.** Adsorption kinetics of ions at Bi single crystal planes from aqueous electrolyte solutions and room-temperature ionic liquids. Tartu, 2010, 101 p.
97. **Angela Vaasa.** Development of fluorescence-based kinetic and binding assays for characterization of protein kinases and their inhibitors. Tartu 2010, 101 p.
98. **Indrek Tulp.** Multivariate analysis of chemical and biological properties. Tartu 2010, 105 p.
99. **Aare Selberg.** Evaluation of environmental quality in Northern Estonia by the analysis of leachate. Tartu 2010, 117 p.
100. **Darja Lavõgina.** Development of protein kinase inhibitors based on adenosine analogue-oligoarginine conjugates. Tartu 2010, 248 p.
101. **Laura Herm.** Biochemistry of dopamine D_2 receptors and its association with motivated behaviour. Tartu 2010, 156 p.

102. **Terje Raudsepp.** Influence of dopant anions on the electrochemical properties of polypyrrole films. Tartu 2010, 112 p.
103. **Margus Marandi.** Electroformation of Polypyrrole Films: *In-situ* AFM and STM Study. Tartu 2011, 116 p.
104. **Kairi Kivirand.** Diamine oxidase-based biosensors: construction and working principles. Tartu, 2011, 140 p.
105. **Anneli Kruve.** Matrix effects in liquid-chromatography electrospray mass-spectrometry. Tartu, 2011, 156 p.
106. **Gary Urb.** Assessment of environmental impact of oil shale fly ash from PF and CFB combustion. Tartu, 2011, 108 p.
107. **Nikita Oskolkov.** A novel strategy for peptide-mediated cellular delivery and induction of endosomal escape. Tartu, 2011, 106 p.
108. **Dana Martin.** The QSPR/QSAR approach for the prediction of properties of fullerene derivatives. Tartu, 2011, 98 p.
109. **Säde Viirlaid.** Novel glutathione analogues and their antioxidant activity. Tartu, 2011, 106 p.
110. **Ülis Sõukand.** Simultaneous adsorption of Cd^{2+}, Ni^{2+}, and Pb^{2+} on peat. Tartu, 2011, 124 p.
111. **Lauri Lipping.** The acidity of strong and superstrong Brønsted acids, an outreach for the "limits of growth": a quantum chemical study. Tartu, 2011, 124 p.
112. **Heisi Kurig.** Electrical double-layer capacitors based on ionic liquids as electrolytes. Tartu, 2011, 146 p.
113. **Marje Kasari.** Bisubstrate luminescent probes, optical sensors and affinity adsorbents for measurement of active protein kinases in biological samples. Tartu, 2012, 126 p.
114. **Kalev Takkis.** Virtual screening of chemical databases for bioactive molecules. Tartu, 2012, 122 p.
115. **Ksenija Kisseljova**. Synthesis of aza-β^3-amino acid containing peptides and kinetic study of their phosphorylation by protein kinase A. Tartu, 2012, 104 p.
116. **Riin Rebane.** Advanced method development strategy for derivatization LC/ESI/MS. Tartu, 2012, 184 p.
117. **Vladislav Ivaništšev.** Double layer structure and adsorption kinetics of ions at metal electrodes in room temperature ionic liquids. Tartu, 2012, 128 p.
118. **Irja Helm.** High accuracy gravimetric Winkler method for determination of dissolved oxygen. Tartu, 2012, 139 p.
119. **Karin Kipper.** Fluoroalcohols as Components of LC-ESI-MS Eluents: Usage and Applications. Tartu, 2012, 164 p.
120. **Arno Ratas.** Energy storage and transfer in dosimetric luminescent materials. Tartu, 2012, 163 p.
121. **Reet Reinart-Okugbeni**. Assay systems for characterisation of subtype-selective binding and functional activity of ligands on dopamine receptors. Tartu, 2012, 159 p.

122. **Lauri Sikk.** Computational study of the Sonogashira cross-coupling reaction. Tartu, 2012, 81 p.
123. **Karita Raudkivi.** Neurochemical studies on inter-individual differences in affect-related behaviour of the laboratory rat. Tartu, 2012, 161 p.
124. **Indrek Saar.** Design of GalR2 subtype specific ligands: their role in depression-like behavior and feeding regulation. Tartu, 2013, 126 p.
125. **Ann Laheäär.** Electrochemical characterization of alkali metal salt based non-aqueous electrolytes for supercapacitors. Tartu, 2013, 127 p.
126. **Kerli Tõnurist.** Influence of electrospun separator materials properties on electrochemical performance of electrical double-layer capacitors. Tartu, 2013, 147 p.
127. **Kaija Põhako-Esko.** Novel organic and inorganic ionogels: preparation and characterization. Tartu, 2013, 124 p.
128. **Ivar Kruusenberg.** Electroreduction of oxygen on carbon nanomaterial-based catalysts. Tartu, 2013, 191 p.
129. **Sander Piiskop.** Kinetic effects of ultrasound in aqueous acetonitrile solutions. Tartu, 2013, 95 p.
130. **Ilona Faustova**. Regulatory role of L-type pyruvate kinase N-terminal domain. Tartu, 2013, 109 p.
131. **Kadi Tamm.** Synthesis and characterization of the micro-mesoporous anode materials and testing of the medium temperature solid oxide fuel cell single cells. Tartu, 2013, 138 p.
132. **Iva Bozhidarova Stoyanova-Slavova.** Validation of QSAR/QSPR for regulatory purposes. Tartu, 2013, 109 p.
133. **Vitali Grozovski**. Adsorption of organic molecules at single crystal electrodes studied by *in situ* STM method. Tartu, 2014, 146 p.
134. **Santa Veikšina**. Development of assay systems for characterisation of ligand binding properties to melanocortin 4 receptors. Tartu, 2014, 151 p.
135. **Jüri Liiv.** PVDF (polyvinylidene difluoride) as material for active element of twisting-ball displays. Tartu, 2014, 111 p.
136. **Kersti Vaarmets.** Electrochemical and physical characterization of pristine and activated molybdenum carbide-derived carbon electrodes for the oxygen electroreduction reaction. Tartu, 2014, 131 p.
137. **Lauri Tõntson**. Regulation of G-protein subtypes by receptors, guanine nucleotides and Mn^{2+}. Tartu, 2014, 105 p.
138. **Aiko Adamson.** Properties of amine-boranes and phosphorus analogues in the gas phase. Tartu, 2014, 78 p.
139. **Elo Kibena**. Electrochemical grafting of glassy carbon, gold, highly oriented pyrolytic graphite and chemical vapour deposition-grown graphene electrodes by diazonium reduction method. Tartu, 2014, 184 p.
140. **Teemu Näykki.** Novel Tools for Water Quality Monitoring – From Field to Laboratory. Tartu, 2014, 202 p.
141. **Karl Kaupmees.** Acidity and basicity in non-aqueous media: importance of solvent properties and purity. Tartu, 2014, 128 p.

142. **Oleg Lebedev**. Hydrazine polyanions: different strategies in the synthesis of heterocycles. Tartu, 2015, 118 p.
143. **Geven Piir.** Environmental risk assessment of chemicals using QSAR methods. Tartu, 2015, 123 p.
144. **Olga Mazina.** Development and application of the biosensor assay for measurements of cyclic adenosine monophosphate in studies of G protein-coupled receptor signalinga. Tartu, 2015, 116 p.
145. **Sandip Ashokrao Kadam.** Anion receptors: synthesis and accurate binding measurements. Tartu, 2015, 116 p.
146. **Indrek Tallo.** Synthesis and characterization of new micro-mesoporous carbide derived carbon materials for high energy and power density electrical double layer capacitors. Tartu, 2015, 148 p.
147. **Heiki Erikson.** Electrochemical reduction of oxygen on nanostructured palladium and gold catalysts. Tartu, 2015, 204 p.
148. **Erik Anderson.** *In situ* Scanning Tunnelling Microscopy studies of the interfacial structure between Bi(111) electrode and a room temperature ionic liquid. Tartu, 2015, 118 p.
149. **Girinath G. Pillai.** Computational Modelling of Diverse Chemical, Biochemical and Biomedical Properties. Tartu, 2015, 140 p.
150. **Piret Pikma.** Interfacial structure and adsorption of organic compounds at Cd(0001) and Sb(111) electrodes from ionic liquid and aqueous electrolytes: an *in situ* STM study. Tartu, 2015, 126 p.
151. **Ganesh babu Manoharan.** Combining chemical and genetic approaches for photoluminescence assays of protein kinases. Tartu, 2016, 126 p.
152. **Carolin Siimenson**. Electrochemical characterization of halide ion adsorption from liquid mixtures at Bi(111) and pyrolytic graphite electrode surface. Tartu, 2016, 110 p.
153. **Asko Laaniste.** Comparison and optimisation of novel mass spectrometry ionisation sources. Tartu, 2016, 156 p.
154. **Hanno Evard.** Estimating limit of detection for mass spectrometric analysis methods. Tartu, 2016, 224 p.
155. **Kadri Ligi.** Characterization and application of protein kinase-responsive organic probes with triplet-singlet energy transfer. Tartu, 2016, 122 p.
156. **Margarita Kagan.** Biosensing penicillins' residues in milk flows. Tartu, 2016, 130 p.
157. **Marie Kriisa.** Development of protein kinase-responsive photoluminescent probes and cellular regulators of protein phosphorylation. Tartu, 2016, 106 p.
158. **Mihkel Vestli.** Ultrasonic spray pyrolysis deposited electrolyte layers for intermediate temperature solid oxide fuel cells. Tartu, 2016, 156 p.
159. **Silver Sepp**. Influence of porosity of the carbide-derived carbon on the properties of the composite electrocatalysts and characteristics of polymer electrolyte fuel cells. Tartu, 2016, 137 p.
160. **Kristjan Haav**. Quantitative relative equilibrium constant measurements in supramolecular chemistry. Tartu, 2017, 158 p.

161. **Anu Teearu**. Development of MALDI-FT-ICR-MS methodology for the analysis of resinous materials. Tartu, 2017, 205 p.
162. **Taavi Ivan**. Bifunctional inhibitors and photoluminescent probes for studies on protein complexes. Tartu, 2017, 140 p.
163. **Maarja-Liisa Oldekop**. Characterization of amino acid derivatization reagents for LC-MS analysis. Tartu, 2017, 147 p.
164. **Kristel Jukk**. Electrochemical reduction of oxygen on platinum- and palladium-based nanocatalysts. Tartu, 2017, 250 p.
165. **Siim Kukk**. Kinetic aspects of interaction between dopamine transporter and *N*-substituted nortropane derivatives. Tartu, 2017, 107 p.
166. **Birgit Viira**. Design and modelling in early drug development in targeting HIV-1 reverse transcriptase and Malaria. Tartu, 2017, 172 p.
167. **Rait Kivi**. Allostery in cAMP dependent protein kinase catalytic subunit. Tartu, 2017, 115 p.
168. **Agnes Heering**. Experimental realization and applications of the unified acidity scale. Tartu, 2017, 123 p.
169. **Delia Juronen**. Biosensing system for the rapid multiplex detection of mastitis-causing pathogens in milk. Tartu, 2018, 85 p.
170. **Hedi Rahnel.** ARC-inhibitors: from reliable biochemical assays to regulators of physiology of cells. Tartu, 2018, 176 p.
171. **Anton Ruzanov.** Computational investigation of the electrical double layer at metal–aqueous solution and metal–ionic liquid interfaces. Tartu, 2018, 129 p.
172. **Katrin Kestav.** Crystal Structure-Guided Development of Bisubstrate-Analogue Inhibitors of Mitotic Protein Kinase Haspin. Tartu, 2018, 166 p.
173. **Mihkel Ilisson.** Synthesis of novel heterocyclic hydrazine derivatives and their conjugates. Tartu, 2018, 101 p.
174. **Anni Allikalt.** Development of assay systems for studying ligand binding to dopamine receptors. Tartu, 2018, 160 p.
175. **Ove Oll.** Electrical double layer structure and energy storage characteristics of ionic liquid based capacitors. Tartu, 2018, 187 p.
176. **Rasmus Palm.** Carbon materials for energy storage applications. Tartu, 2018, 114 p.
177. **Jörgen Metsik.** Preparation and stability of poly(3,4-ethylenedioxythiophene) thin films for transparent electrode applications. Tartu, 2018, 111 p.
178. **Sofja Tšepelevitš.** Experimental studies and modeling of solute-solvent interactions. Tartu, 2018, 109 p.
179. **Märt Lõkov.** Basicity of some nitrogen, phosphorus and carbon bases in acetonitrile. Tartu, 2018, 104 p.
180. **Anton Mastitski**. Preparation of α-aza-amino acid precursors and related compounds by novel methods of reductive one-pot alkylation and direct alkylation. Tartu, 2018, 155 p.
181. **Jürgen Vahter**. Development of bisubstrate inhibitors for protein kinase CK2. Tartu, 2019, 186 p.

182. **Piia Liigand.** Expanding and improving methodology and applications of ionization efficiency measurements. Tartu, 2019, 189 p.
183. **Sigrid Selberg.** Synthesis and properties of lipophilic phosphazene-based indicator molecules. Tartu, 2019, 74 p.
184. **Jaanus Liigand.** Standard substance free quantification for LC/ESI/MS analysis based on the predicted ionization efficiencies. Tartu, 2019, 254 p.
185. **Marek Mooste.** Surface and electrochemical characterisation of aryl film and nanocomposite material modified carbon and metal-based electrodes. Tartu, 2019, 304 p.
186. **Mare Oja.** Experimental investigation and modelling of pH profiles for effective membrane permeability of drug substances. Tartu, 2019, 306 p.
187. **Sajid Hussain.** Electrochemical reduction of oxygen on supported Pt catalysts. Tartu, 2019, 220 p.
188. **Ronald Väli.** Glucose-derived hard carbon electrode materials for sodium-ion batteries. Tartu, 2019, 180 p.
189. **Ester Tee.** Analysis and development of selective synthesis methods of hierarchical micro- and mesoporous carbons. Tartu, 2019, 210 p.
190. **Martin Maide.** Influence of the microstructure and chemical composition of the fuel electrode on the electrochemical performance of reversible solid oxide fuel cell. Tartu, 2020, 144 p.
191. **Edith Viirlaid.** Biosensing Pesticides in Water Samples. Tartu, 2020, 102 p.
192. **Maike Käärik.** Nanoporous carbon: the controlled nanostructure, and structure-property relationships. Tartu, 2020, 162 p.
193. **Artur Gornischeff.** Study of ionization efficiencies for derivatized compounds in LC/ESI/MS and their application for targeted analysis. Tartu, 2020, 124 p.
194. **Reet Link.** Ligand binding, allosteric modulation and constitutive activity of melanocortin-4 receptors. Tartu, 2020, 108 p.
195. **Pilleriin Peets.** Development of instrumental methods for the analysis of textile fibres and dyes. Tartu, 2020, 150 p.
196. **Larisa Ivanova.** Design of active compounds against neurodegenerative diseases. Tartu, 2020, 152 p.
197. **Meelis Härmas.** Impact of activated carbon microstructure and porosity on electrochemical performance of electrical double-layer capacitors. Tartu, 2020, 122 p.
198. **Ruta Hecht.** Novel Eluent Additives for LC-MS Based Bioanalytical Methods. Tartu, 2020, 202 p.
199. **Max Hecht.** Advances in the Development of a Point-of-Care Mass Spectrometer Test. Tartu, 2020, 168 p.
200. **Ida Rahu.** Bromine formation in inorganic bromide/nitrate mixtures and its application for oxidative aromatic bromination. Tartu, 2020, 116 p.
201. **Sander Ratso**. Electrocatalysis of oxygen reduction on non-precious metal catalysts. Tartu, 2020, 371 p.
202. **Astrid Darnell.** Computational design of anion receptors and evaluation of host-guest binding. Tartu, 2021, 150 p.

203. **Ove Korjus.** The development of ceramic fuel electrode for solid oxide cells. Tartu, 2021, 150 p.
204. **Merit Oss.** Ionization efficiency in electrospray ionization source and its relations to compounds' physico-chemical properties. Tartu, 2021, 124 p.
205. **Madis Lüsi**. Electroreduction of oxygen on nanostructured palladium catalysts. Tartu, 2021, 180 p.
206. **Eliise Tammekivi.** Derivatization and quantitative gas-chromatographic analysis of oils. Tartu, 2021, 122 p.
207. **Simona Selberg.** Development of Small-Molecule Regulators of Epi-transcriptomic Processes. Tartu, 2021, 122 p.
208. **Olivier Etebe Nonga.** Inhibitors and photoluminescent probes for in vitro studies on protein kinases PKA and PIM. Tartu, 2021, 189 p.
209. **Riinu Härmas.** The structure and H2 diffusion in porous carbide-derived carbon particles. Tartu, 2022, 123 p.
210. **Maarja Paalo.** Synthesis and characterization of novel carbon electrodes for high power density electrochemical capacitors. Tartu, 2022, 144 p.
211. **Jinfeng Zhao.** Electrochemical characteristics of Bi(hkl) and micro-meso-porous carbon electrodes in ionic liquid based electrolytes. Tartu, 2022, 134 p.
212. **Alar Heinsaar.** Investigation of oxygen electrode materials for high-temperature solid oxide cells in natural conditions. Tartu, 2022, 120 p.
213. **Jaana Lilloja.** Transition metal and nitrogen doped nanocarbon cathode catalysts for anion exchange membrane fuel cells. Tartu, 2022, 202 p.
214. **Maris-Johanna Tahk.** Novel fluorescence-based methods for illuminating transmembrane signal transduction by G-protein coupled receptors. Tartu, 2022, 200 p.
215. **Eerik Jõgi.** Development and Applications of E. coli Immunosensor. Tartu, 2022, 103 p.
216. **Alo Rüütel.** Design principles of synthetic molecular receptors for anion-selective electrodes. Tartu, 2022, 109 p.
217. **Tanel Sõrmus.** Development of stimuli-responsive and covalent bisubstrate inhibitors of protein kinases. Tartu, 2022, 148 p.
218. **Oleg Artemchuk.** Autotrophic nitrogen removal processes for nutrient removal from sidestream and mainstream wastewater. Tartu, 2022, 115 p.
219. **Andre Leesment.** Quantitative studies of Brønsted acidity in biphasic systems and gas-phase. Tartu, 2023, 83 p.
220. **Meeli Arujõe-Sado.** Structural effects in aza-peptide bond formation reaction. Tartu, 2023, 83 p.
221. **Jonas Mart Linge.** Electrochemical reduction of oxygen on silver-based catalysts. Tartu, 2023, 269 p.